

**A Theoretical and Experimental Study on the Pyrolysis of Softwood
Sawmill Residues to Py-oil**

By

©Sadegh Papari

A thesis submitted to the school of Graduate Studies in partial fulfilment of
the requirements for the degree of

Doctor of Philosophy

Faculty of Engineering and Applied Science
Memorial University of Newfoundland

November, 2016

St. John's, Newfoundland
Canada

Abstract

Pyrolysis oil (py-oil) that is obtained from biomass, through thermochemical conversion in the absence of oxygen, is a possible sustainable source of renewable energy and for useful chemicals. Based on our existing infrastructure which is petroleum-based, py-oil can be an attractive alternative/blend for fossil fuel. The fuel application of py-oil can be limited by high water content, low heating value and high total acid number. Lab-scale and pilot-scale, pyrolysis experiments on forestry residues were performed to determine the impact of key parameters on py-oil yield and properties. The overall objectives of this study were to; determine the important operational factors and scale up of the pyrolysis of woody biomass, determine the range of conditions at lab scale for optimal py-oil yield and fuel properties, use these results to optimize the pilot scale auger unit, and develop a process model to simulate the process and be used as a design tool. In Chapter One, an overview on the first and the second generation of pyrolysis, the scopes, the objectives and the significance of this study along with a summary of the thesis chapters was outlined. In Chapter Two, the literature was reviewed to identify the impact of reactor operating conditions on py-oil yield and properties. The results indicated that the key parameters are a faster heating rate and a shorter vapour residence time which produce a higher py-oil yield (up to 75 wt.%) with a higher heating value (up to 22 kJ/kg). In addition, the published empirical and process models for pyrolysis of woody biomass were investigated in order to better understand the applied heat/mass transfer equations, assumptions, kinetic models, and the method of solution. The reported kinetic models in literature were compared with our experimental data obtained from the lab-scale reactor

in order to find the “best” model. In Chapter Three, the impact of three process parameters including temperature, N₂ flow rate, and biomass particle size were investigated on py-oil yield and water content using response surface methodology coupled with central composite design (RSM-CCD) in a lab-scale tube furnace reactor. The results indicated that a 500-550 °C temperature, a 500 mL/min N₂ flow rate, and a 0.1-0.5 mm particle size produced the optimum oil for the lab-scale reactor. The quadratic CCD model with factor interactions better predicted the experimental data compared to the quadratic model without parameter interactions. In addition, the results showed that the secondary tar cracking should be included in pyrolysis reactions at a temperature higher than 550 °C, since some condensable organics convert to non-condensable gases by these reactions. After finding the optimum conditions of the lab-scale tube furnace pyrolysis reactor in Chapter Three, the impact of feedstock quality (particle size, moisture content, and age of feedstock) on py-oil yield, higher heating value (HHV), total acid number (TAN), and water content was investigated in the lab-scale reactor (Chapter Four). The results illustrated that the initial moisture content has a little effect on the water chemically produced during pyrolysis. Particle size reduction did not have a significant effect on HHV. The aged feedstock produced a slightly lower py-oil yield and higher water content compared to the fresh feedstock. In addition, a qualitative assessment of the pyrolysis heat of reaction was performed in the lab-scale reactor. The results illustrate the overall endothermic nature of the pyrolysis of this type of biomass (balsam fir wood). This result was helpful in next Chapter (i.e. process modeling). In Chapter Five, a process model was developed for the 2-4 kg/h auger reactor with assuming plug flow model for both solid and gas phases. Process modeling is typically used as a tool in

process optimization, scale up, and reactor design to reduce the capital and operating cost of a pyrolysis system. The transport equations for each phase are combined with the kinetic model to predict py-oil, bio-char, and non-condensable gas yields. The process model was validated with the experimental data obtained from this reactor and showed good agreement (with approximately 10% average relative deviation). The model was used to predict py-oil yield as a function of temperature, feed flow rate and reactor pressure. In Chapter Six, the impact of process variables (temperature, feed flow rate, and vacuum fan speed) on py-oil yield, water content, and more importantly phase separation were investigated in the 2-4 kg/h auger reactor. In the optimum conditions (a 450-475 °C temperature, a 2415 rpm vacuum fan speed, and a 4 kg/h feed flow rate) a single phase softwood oil was obtained with 53 wt.% yield and 26 wt.% water content. A comparison between different sawmill residues (softwood shavings, hardwood sawdust, and softwood bark) at similar conditions showed that hardwood and softwood produced a single phase oil with a higher oil yield (53-55 wt.%) and a lower water content (25-26 wt.%) compared to bark (39 wt.% oil yield and a 33 wt.% water content).

Acknowledgment

This work could only have been accomplished by the mutual collaboration of many people.

Firstly, I would like to express my sincere gratitude to my supervisor Dr. Kelly Hawboldt for her excellent support of my PhD study, her patience, motivation, and enormous knowledge. Her guidance helped me in all the time of research and writing of this thesis. She was truly a tremendous mentor for me.

My sincere thanks also goes to Dr. Robert Helleur, who gave me access to his laboratory and research facilities. I have been extremely lucky to have a co-supervisor who cared so much about my work and it was a privilege and an honor for me to share of his exceptional scientific knowledge. Without his precious support it would not be possible to conduct this research.

Beside my supervisors, I would like to thank Dr. Peter Fransham, for his insightful comments, constructive suggestions and encouragement. He has a great knowledge, over than 30 years, on pyrolysis. Also, I would like to thank Dr. James as one of my supervisory committee.

I would also like to thank the Faculty of Engineering and Applied Science, Memorial University of Newfoundland, and acknowledge the funding provided by CFSI/ Department of Fisheries, Forestry and Agrifoods/ the Government of Newfoundland and Labrador, BioFuelNet Canada, the Canadian Foundation for Innovation, the Natural Science and Engineering Research Council of Canada and Memorial University of Newfoundland.

I would like to give special thanks to my wife, Mrs. Hanieh Bamdad, for supporting me spiritually throughout writing this thesis.

I want to express my appreciation to my father, my mother, my sisters, and my brothers for everything - too unfortunate my father cannot see me graduate and his memory will be with me for ever.

Table of Contents

Acknowledgment	v
List of Tables	xi
List of Figures	xiii
1. CHAPTER ONE	1
Introduction and Overview	1
2. CHAPTER TWO	11
Literature Review	11
2.1. Introduction	13
2.2. Pyrolysis Reactors	16
2.2.1. Fluidized-bed Reactor	16
2.2.2. Plasma Pyrolysis Reactor	18
2.2.3. Free-Fall Reactor	19
2.2.4. Fixed-bed Reactor	20
2.2.5. Rotating Cone Reactor	21
2.2.6. Microwave Reactor	22
2.2.7. Auger Reactor	23
2.2.8. Reactor Models	25
2.3. Kinetic Models	32
2.3.1. Global Kinetic Model	32
2.3.2. Three Parallel Reactions	35
2.3.3. Competitive Models	39
2.3.4. Models with Secondary Tar Cracking	40
2.3.5. Shafizadeh and Bradbury Model	41
2.3.6. Activation Energy Distribution Model (AEDM)	43
2.3.7. Chemical Percolation Devolatilization Model	45
2.4. Heat of pyrolysis	51
2.5. Comparing Different Kinetic Models	53
2.6. Conclusion	57
Acknowledgment	57
2.7. References	58
3. CHAPTER THREE	67

A Theoretical and Experimental Study on the Conversion of Softwood Sawmill residues to Pyrolysis Oil in a Lab-scale Reactor	67
Abstract	68
3.1. Introduction	69
3.2. Experimental Design	71
3.2.1. Statistical Analysis	71
3.3. Kinetic Model	72
3.4. Experimental	74
3.4.1. Feedstock	74
3.4.2. Semi-batch reactor	74
3.5. Results and Discussion	76
3.5.1. ANOVA analysis	76
3.6. Conclusions	86
Acknowledgment	87
3.7. References	88
4. CHAPTER FOUR	91
A Study of Quality of Woody Biomass Feedstock on the Yield and Quality of Py-oil with a Lab-Scale Reactor	91
Abstract	92
4.1. Introduction	93
4.2. Experimental Section	96
4.2.1. Feedstock Preparation	96
4.2.2. Reactor Description	97
4.2.3. Py-oil Properties	99
4.3. Results and Discussion	99
4.3.1. Pyrolysis Heat	99
4.3.2. Effect of Particle Size on Biomass Pyrolysis	101
4.2.3. Impact of Feedstock Moisture Content on Py-oil	103
4.2.4. Effect of Age of Feedstock on Biomass Pyrolysis	105
4.5. Conclusion	107
Acknowledgment	108
4.6. References	108
5. CHAPTER FIVE	111

Development and Validation of a Process Model to Describe Pyrolysis of Forestry Residues in an Auger Reactor	111
Abstract	112
5.1. Introduction	113
5.2. Experimental Section	115
5.2.1. Feedstock	118
5.2.2. Model Description	119
5.2.3. Solution Method.....	128
5.3. Results and Discussion	132
5.3.1. Kinetic model selection.....	132
5.3.2. Model validation	133
5.3.3. Heat transfer	134
5.4. Parametric investigation.....	136
5.4.1. Feed flow rate	136
5.4.2. Temperature	137
5.4.3. Pressure	138
5.5. Conclusion.....	139
Acknowledgment	140
5.6. References	141
6. CHAPTER SIX.....	144
Optimization of an Auger Reactor for the Production of Py-oil from Sawmill Residues	144
Abstract	145
6.1. Introduction	146
6.2. Experimental	147
6.2.1. Feedstock	147
6.2.2. Auger Reactor	148
6.2.3. Py-oil characterization testing protocols.....	150
6.3. Result and Discussion	151
6.3.1. Impact of reactor operating conditions on py-oil yield and quality	151
6.3.1.1. Temperature	151
6.3.1.2. Feed flow rate	152
6.3.1.3. Physical and Chemical py-oil properties	153
6.4. Conclusion	161

Acknowledgment	162
6.5. References	162
7. CHAPTER SEVEN	165
Summary and Recommendations for Future Work	165
7.1. Literature Review.....	166
7.2. Lab-Scale Reactor	167
7.3. Investigation on feedstock quality	168
7.4. Process modeling for auger reactor.....	169
7.5. Evaluation of auger oil yield and properties	169
7.6. Recommendations for Future Work.....	171
Appendix.....	174
Py-oil Procedures Manual.....	175
Higher Heating Value (HHV).....	175
Water Content (Karl Fischer Coulometric Titration).....	185
GC/MS	188
Dynamic Viscosity	195
Percent Suspended Solids (Bio-char) in Py-Oil.....	198
Acidity (Total Acid Number).....	201

List of Tables

Table 2-1: The chemical composition of different types of wood [7,8]	15
Table 2-2: Overall composition of softwoods as a function of species [10].....	15
Table 2-3: Comparison of the physical and chemical py-oil properties obtained from different pyrolysis reactors.....	25
Table 2-4: Common reactor mathematical models for the pyrolysis process.....	29
Table 2-5: Definition of the kinetic parameters for the CPD Model	45
Table 2-6: Different kinetic models for the pyrolysis of woody biomass	47
Table 2-7: Heat of pyrolysis	52
Table 2-8: Experimental conditions for the lab scale pyrolysis experiments	53
Table 2-9: Experimental conditions of published studies/models	54
Table 2-10: Average relative error for sawdust feedstock.....	56
Table 3-1: Proximate analysis of dried softwood feedstock.....	74
Table 3-2: ANOVA for response surface reduced quadratic model (py-oil).....	77
Table 3-3: ANOVA for response surface reduced quadratic model (bio-char).....	78
Table 3-4: Quadratic model: Py-oil and bio-char yields based on coded factors	79
Table 3-5: Fitted parameters for the quadratic and kinetic models.....	85
Table 4-1: Heat of pyrolysis	94
Table 5-1: Proximate analysis of balsam fir wood	118
Table 5-2: Composition of balsam fir in Newfoundland and Labrador [16].....	119
Table 5-3: Auger reactor dimensions.....	121
Table 5-4: Properties of steel shot and biomass.....	121

Table 5-5: Reaction rate constants for biomass pyrolysis, Chan et al. (primary) coupled with Morf (secondary) [9, 24].....	126
Table 5-6: Reaction kinetics for biomass pyrolysis, Miller et al [15].....	126
Table 5-7: Kinetic constants for woody biomass pyrolysis	127
Table 5-8: Experimental conditions from literature for kinetic models used in this study	127
Table 5-9: Organic components of py-oil [32]	128
Table 5-10: Comparison between two kinetic models.....	135
Table 6-1: Proximate analysis of hardwood, softwood, and softwood bark.....	148
Table 6-2: Methods for measuring physical and chemical properties of py-oil	151
Table 6-3: Impact of auger reactor parameters on py-oil yield and water content from SW	152
Table 6-4: Physicochemical properties of py-oil obtained from different auger reactors	156
Table 6-5: GC-MS results: most abundant components in py-oils obtained from soft/hard wood and bark.....	159

List of Figures

Figure 1-1: Biomass conversion processes [2]	3
Figure 1-2: Bio-based fuel production from biomass [2]	5
Figure 1-3: Thermo-chemical conversion processes [2].....	6
Figure 2-1: Process Flow Diagram (PFD) for Pyrolysis.....	14
Figure 2-2: Process flow diagram of fluidized bed reactor for the pyrolysis of biomass [20].....	18
Figure 2-3: Process flow diagram of pyrolysis plasma reactor [24].....	19
Figure 2-4: Process flow diagram of a free-fall reactor for the pyrolysis of biomass [25]	20
Figure 2-5: Process flow diagram of a fixed-bed reactor for the pyrolysis of biomass [27]	21
Figure 2-6: Process flow diagram of rotating reactor for the pyrolysis of biomass [29] ...	22
Figure 2-7: Lab-scale microwave reactor setup [31]	23
Figure 2-8: Process flow diagram of auger reactor for the pyrolysis of biomass	24
Figure 2-9: Flow diagram of plug flow reactor in series to a CSTR cross-flowing dead volume [48].....	28
Figure 2-10: TGA profile for proximate analysis of sawdust for a particle size of 250 μm [60].....	33
Figure 2-11: Comparison of activation energy as a function of feedstock conversion for three different models (FWO, KAS, and Kissinger) [61].....	34
Figure 2-12: Three parallel reactions mechanism. α , β , and γ are the mass fraction of cellulose, hemicellulose and lignin in biomass respectively and k is kinetic constant.....	35

Figure 2-13: Kinetic parameters predictions for different biomass feedstock (ln k ₀ , ln E, and n) as a function of solid residue yield (x) for biomass samples [64]	37
Figure 2-14: Relationship between solid residue yield (x) and lignin content (L) and between fixed-carbon yield (y _{fc}) and L [64]	38
Figure 2-15: Competitive mechanism of biomass pyrolysis; k ₁ , k ₂ , and k ₃ are kinetic constants.....	40
Figure 2-16: Secondary tar cracking mechanism for biomass pyrolysis k ₁ , k ₂ , k ₃ , k ₄ and k ₅ are kinetic constants [75]	40
Figure 2-17: Modeled proposed by Shafizadeh and Bradbury [80], Y is the formation ratio for the char component [37]	41
Figure 2-18: Comparison of model prediction to Thurner and Mann's (1981) data (a) T=354°C, (b) T=369°C and (c) T=392°C [75]	42
Figure 2-19: Experimental and calculated TG curves at a = 2, 5, and 10 K/min for cellulose, rice straw, rice husk, and corncob [82].....	44
Figure 2-20: Chemical bridge reaction pathways treated in the CPD model to describe pyrolysis [84]	45
Figure 2-21: Comparison of measured and modeled sawdust pyrolysis yields using the three parallel models at 1 atm and gas temperatures of 1163–1433 K [83]	46
Figure 2-22: Pyrolysis heat of spruce wood measured using a DSC [106]	51
Figure 2-23: Heat of pyrolysis for spruce and beech wood as a function of final char yield [106]. H _p stands for the heat of primary pyrolysis and m ₀ is initial weight of biomass ...	53
Figure 2-24: PY-Oil yield vs. temperature for sawmill residues: N ₂ flow rate 200 mL/min, sample load 2 g, and particle size 2 mm	55

Figure 2-25: Bio-char yield vs. temperature for sawmill residues feedstock: N ₂ flow rate 200 mL/min , sample load 2 g, and particle size 2mm	55
Figure 2-26: Non-condensable gas yield vs. temperature for sawmill residues feedstock: N ₂ flow rate 200 mL/min , sample load 2 g, and particle size 2 mm.....	56
Figure 3-1: Primary reactions for converting biomass to py-oil, bio-char and gas	73
Figure 3-2: Primary with secondary oil cracking kinetic mechanism	73
Figure 3-3: Schematic of lab-scale pyrolysis system.....	76
Figure 3-4: Effect of pyrolysis temperature and particle size on Py-oil yield of wood shaving feedstock; N ₂ flow rate = 500 mL/min	81
Figure 3-5: Effect of pyrolysis temperature and N ₂ flow rate on py-oil yield; average particle size = 0.75mm.....	82
Figure 3-6: Py-oil, bio-char, gas* and water yield vs. temperature at 0.75mm particle size, 500 ml/min sweep gas flow rate (dotted lines represent 95% confidence interval).* the gas yield was measured by difference	83
Figure 3-7: Py-oil, bio-char, gas*and water yield vs. temperature at 500°C temperature, 500 ml/min sweep gas flow rate (dotted lines represent 95% confidence interval).* gas yield was measured by difference	84
Figure 3-8: Py-oil, bio-char , gas* and water yield vs. temperature at 0.75mm particle size, 500°C temperature, (dotted lines represent 95% confidence interval).* gas yield was measured by difference	84
Figure 3-9: Comparison between experimental data and different models (Average particle size: 0.3 mm and sweep gas flow rate: 500 ml/min).....	86
Figure 4-1: Schematic of lab-scale pyrolysis system.....	99

Figure 4-2: Temperature detected by thermocouple vs. time of the thermocouple situated near the biomass at 200 (a), 500 (b), and 800 (c) mL/min nitrogen flow rates (number of replicates = 2).....	101
Figure 4-3: Impact of biomass particle size on the py-oil and bio-char yield, HHV, TAN, and water content at 500 °C and 500 mL/min (number of replicates = 2).....	103
Figure 4-4: Impact of initial moisture content on the py-oil and bio-char yield (a) , HHV, TAN, and water content (b) at 500 °C and 500 mL/min (number of replicates = 2).....	104
Figure 4-5: Impact of feedstock initial moisture content on the py-oil yield corrected for moisture, and water chemically produced at 500 °C and 500 mL/min.....	105
Figure 4-6: Impact of feedstock age on the py-oil and bio-char yield, HHV, TAN, and water content at 500 °C and 500 mL/min (number of replicates = 2)	106
Figure 5-1: Reaction pathways for the pyrolysis of biomass [3]	113
Figure 5-2: Process flow diagram for the auger reactor.....	117
Figure 5-3: A photo of the inside of auger pyrolysis system built by ABRI-Tech Inc....	118
Figure 5-4: Schematic of process flow of auger reactor and product collection system .	120
Figure 5-5: Auger reactor process model solution algorithm	131
Figure 5-6: Comparison of kinetic models with experimental data at 450 °C	132
Figure 5-7: Comparison of kinetic models with experimental data at 500 °C	133
Figure 5-8: Validation of model with experimental data using yields of products (feed rates = 1-3.5 kg/h, temperatures = 450-500 °C).....	134
Figure 5-9: Residence time for biomass particles require to reach the pyrolysis temperature of 450 °C (A) and of 500 °C (B)	135
Figure 5-10: Py-oil and bio-char yield vs. temperature at 3.5 kg/h feed flow rate.....	137

Figure 5-11: Py-oil (●) and bio-char (■) vs. reactor pressure at 450 °C temperature and 3.5 kg/h feed flow rate138

Figure 6-1: Process flow diagram for the auger reactor.....149

Figure 6-2: Photo (inside of the oven) of the auger pyrolysis system as built by ABRI-Tech Inc.....150

1.CHAPTER ONE

Introduction and Overview

Fossil fuels (e.g. crude oil, coal, and natural gas) are the major non-renewable and non-sustainable world energy sources. The emission of greenhouse gases (GHG), which causes global warming is the result of fossil fuel burning. The environmental impacts, limited availability of resources, price fluctuations, and increasing energy demand led researchers to offer bio-based chemical/fuels as an alternative to these non-renewable energy sources. Bio fuel/chemicals are obtained from biomass (i.e. all living and dead biological materials including agricultural waste, forest residues, sawmill residues, demolition wood, microalgae, municipal waste, and sewage sludge) by different conversion methods (Fig. 1-1). In contrast to fossil fuels, the utilization of biomass for energy contributes significant environmental advantages, since organic materials need carbon dioxide for growing. As such, the organic materials eliminate CO₂ that results from biofuel combustion [1]. The bio-based fuel is classified as “first generation” and “second generation” (Fig. 1-2). The first generation fuel (e.g. biodiesel, ethanol, and biogas) is obtained from feedstock, such as vegetable oils, residual oils, and fats, while second generation fuel is developed from non-food crops (e.g. lignocellulosic material) [2]. Biomass can be a good source of energy, since only 1.25% of the earth’ supply (100 billion tones organic dry matter) is currently being used for food, feed, or industrial raw materials, and the rest is unused or recycled into the earth [2].

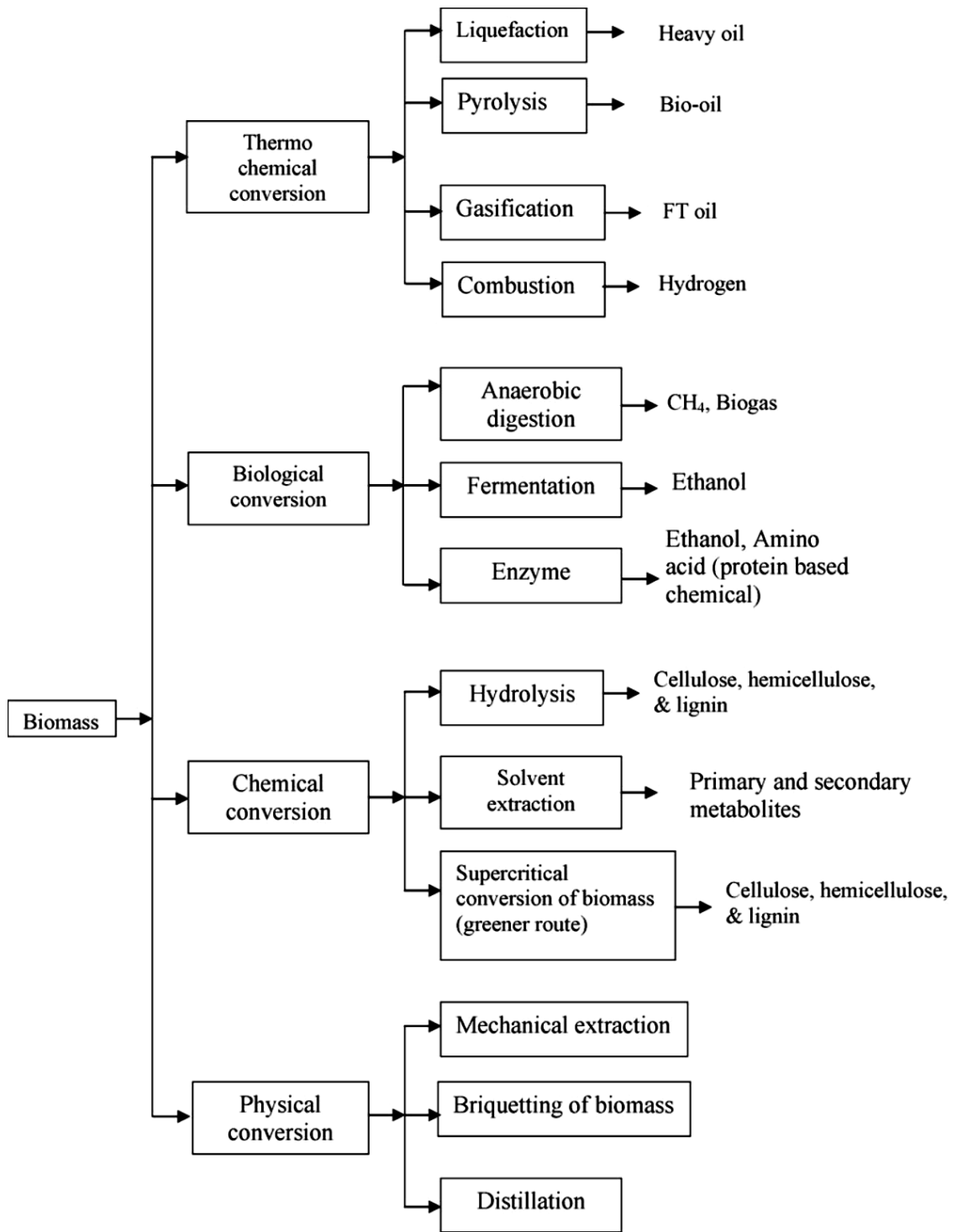


Figure 1-1: Biomass conversion processes [2] (without permission)

Woody biomass consists of cellulose, hemicellulose and lignin which are all bio polymers mostly composed of oxygen, carbon, and hydrogen. Several biomass conversion technologies are available in the literature which indicate how to convert biomass to bio-based fuel/chemicals (Fig. 1-1). Thermochemical and biochemical conversion technologies are usually used for converting lignocellulosic material to bio-based energy/chemicals [2]. Thermochemical conversion is preferred, due to its fast operation, and lower cost of pre-treatment. Although there are many thermochemical conversion methods, fast pyrolysis is a reasonable and promising technology conversion method that gives the highest liquid yield. This liquid can then be used as either fuel/blend or chemicals feedstock.

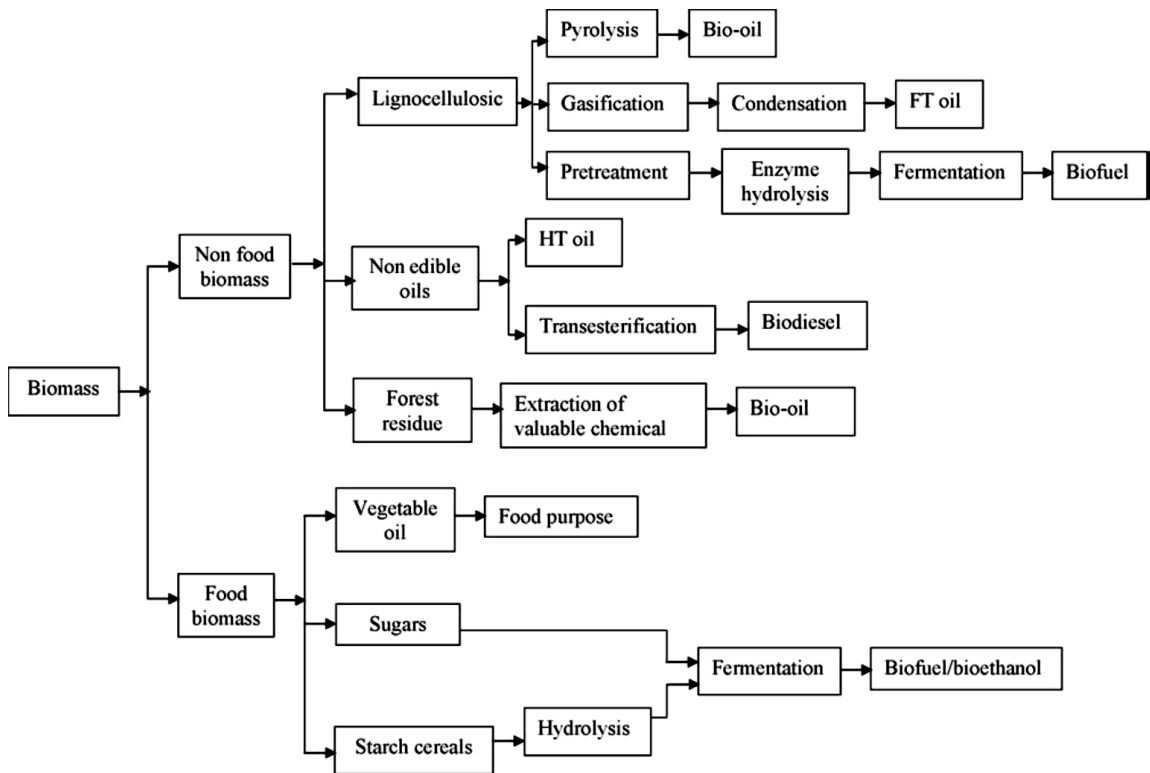


Figure 1-2: Bio-based fuel production from biomass [2] (without permission)

Pyrolysis converts 50-75% of woody biomass to py-oil in the absence of oxygen at a temperature near 400-600 °C (Fig. 1-3). Bio-char and non-condensable gas are the other pyrolysis products. Py-oil is a complex mixture of chemicals including acids, ketones, furans, phenols, hydro sugars and other oxygenates [3]. Py-oil can be limited to lower fuel quality applications due to its high acidity, oxygen/water content and low heating value. Optimizing of the pyrolysis reactor, and increasing the quality of feedstock can be two cost-effective methods for improving py-oil quality and yield.

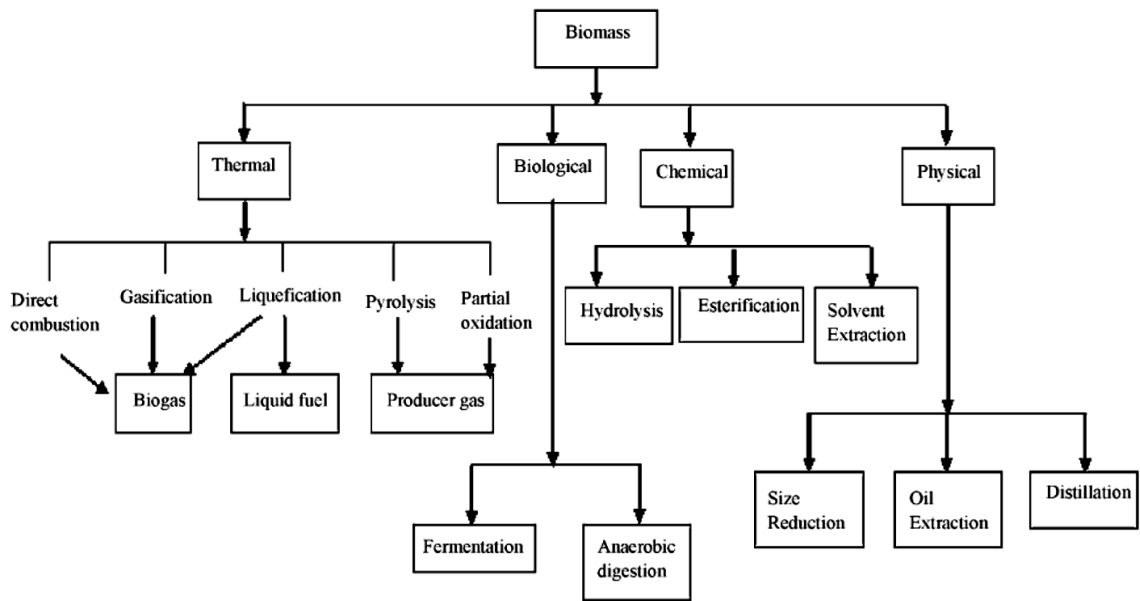


Figure 1-3: Thermo-chemical conversion processes [2] (without permission)

Biofuels or bio chemicals production can provide new job opportunities, especially in rural areas, and enhances the energy security. Canada has an ongoing plan to develop bio-based energy through the BioFuelNet project which will provide a portion of Canada’s energy needs from renewable biomass and waste over the next 20 years [4]. Canada has a wealth of biomass. BiofuelNet as a network integrates community of academic researchers, industry partners and government representatives to drive the commercialization of advanced biofuels and bioproducts. In Newfoundland and Labrador and other northern regions, sawmills and cutting operations lack the infrastructure to properly store forestry residue. This results in a biomass that is heterogeneous in terms of age, season, state of decomposition, moisture content, chemical stability and composition. The focus of this study is on the conversion of feedstock through pyrolysis, and the use of py-oil in remote regions. The development of on-site and/or regional biofuels from

forestry residue would benefit the industry and the region. However, significant research challenges still exist, such as pre-treatment requirement and py-oil quality.

The feedstock, sawmill residues, used in this study was a local biomass obtained from balsam fir wood. The results reported in the literature for the pyrolysis of this type of feedstock is rare. Two pyrolysis units (i.e. lab and pilot scale) were utilized during this research to convert the sawmill residues (shavings and bark) to py-oil. The preliminary experiments were conducted in the lab-scale tube furnace reactor in order to study the effects of temperature, residence time and other variables independently of the influence of transport phenomena. For instance, as the mass of the feedstock increases, heat transfer through the biomass will impact the temperature of the system. This makes it difficult to study the impact of temperature on the rate of reaction and yield as one must tease out the other effects. The information such as py-oil yield, water content and bio-char yield for this type of feedstock must be understood before running the pilot reactor. In Chapter Four, the heat of reactions during pyrolysis was investigated. In addition, the reported kinetic models in the literature were compared with the experimental data obtained from both the lab and pilot scale reactors to select the “best” kinetic model. Most kinetic models are generalized for many feedstock types. The auger reactor used in this study was a unique pyrolysis unit in terms of using steel shot as heat carrier and without sweep gas flow. The process modeling of this type of reactors with two phases (i.e. solid and gas) was challenging due to the lack of information in the literature. The process model was successfully developed and validated with the experimental data obtained from this reactor. Further experimental studies were conducted in the auger reactor to investigate

the quality and yield of py-oil for different feedstocks (softwood shaving, hardwood sawdust, and softwood bark). The results of this study are required for the future work, such as blending, distillation, and optimization of pyrolysis condensing system. In addition, the information generated in this study would be helpful for the design of new pyrolysis reactor. This thesis consists of a series of manuscripts either published, in review processes, or to be submitted for publication:

Chapter Two has been published in the Journal of Renewable and Sustainable Energy Reviews. The manuscript provides a literature review on the pyrolysis of woody biomass to py-oil. The focus is on the kinetic models.

Chapter Three has been published in the Journal of Industrial and Engineering Chemistry Research, and describes the analysis of pyrolysis of sawmill residues in a lab-scale pyrolysis unit. Response surface methodology coupled with central composite design is applied to optimize the significant pyrolysis parameters.

Chapter Four is divided into two sections: A qualitative assessment of the pyrolysis heat of reaction, and the impact of biomass quality (water content, age of feedstock and particle size) on py-oil yield and quality, such as higher heating value, total acid number, and water content.

Chapter Five is under review by the Journal of Fuel Processing Technology, and consists of the development of a process model for the pyrolysis of sawmill residues in auger reactor.

Chapter Six , is under review by the journal of Industrial and Engineering Chemistry Research, summarizes the experiments conducted in the 2-4 kg/h auger reactor in order to optimize py-oil yield and minimize water content. In addition, the impact of processing variables on py-oil phase separation is investigated.

Chapter Seven contains a summary, conclusions, and recommendations.

References

- [1] Mohan D, Pittman CU, Steele PH. Pyrolysis of wood/biomass for bio-oil: a critical review. *Energy & fuels*. 2006 May 17;20(3):848-89.
- [2] Naik SN, Goud VV, Rout PK, Dalai AK. Production of first and second generation biofuels: a comprehensive review. *Renewable and Sustainable Energy Reviews*. 2010 Feb 28;14(2):578-97.
- [3] Alsbou EM. *Pyrolysis bio-oil as a renewable fuel and source of chemicals: its production, characterization and stability* (Doctoral dissertation, Memorial University of Newfoundland).
- [4] Zhang L, Xu CC, Champagne P. Overview of recent advances in thermo-chemical conversion of biomass. *Energy Conversion and Management*. 2010 May 31;51(5):969-82.

2. CHAPTER TWO

Literature Review

This chapter has been **published**; Papari S, Hawboldt K. A review on the pyrolysis of woody biomass to py-oil: Focus on kinetic models. Renewable and Sustainable Energy Reviews. 2015 Dec 31;52:1580-95.

Abstract

The thermal decomposition of woody biomass in the absence of oxygen, or pyrolysis, is a series of complex reactions involving hundreds of compounds. The species of residue, form of residue (bark, sawdust, and other residues), age, storage conditions, among other factors, will impact the composition of the residue which in turn impacts the pyrolytic reactions. The reaction rates must be understood to optimize the pyrolysis reactor. However, the determination of intrinsic kinetics in this system is complex (both due to feedstock composition and the nature of reactions at pyrolysis temperatures) and as such the approach has been to use an overall reaction rate or series of simplified reactions. In this study, a review of pyrolysis process units, reactor mathematical models, mechanisms for conversion of woody biomass and overview of heat of pyrolysis is presented. In addition, the presented kinetic models have been compared to experimental data obtained from pyrolysis of different lignocellulosic biomass (i.e. sawdust, bark, and wood chips) in a lab-scale tube furnace reactor, to determine the “best” kinetic model for the fast pyrolysis of sawmill residues. The results show that the competitive model (Chan et al. *Fuel* 1985; 64:1505– 1513. doi:10.1016/0016-2361(85)90364-3) and chemical percolation devolatilization model (Lewis et al. *Energy Fuels* 2013; 27:942–953. doi:10.1021/ef3018783) show very good agreement with py-oil experimental data. Although the pyrolysis of biomass has been widely investigated in recent decades, the models have some limitations which could limit their application to a broad spectrum of feedstock and pyrolysis operating conditions.

Keywords: Pyrolysis reactor, Reactor model, Kinetic model, Woody biomass, Pyrolysis

2.1. Introduction

The environmental impacts associated with the extraction and use of fossil fuels have resulted in the rapid development of alternative energy sources. However, given that our existing infrastructure is petroleum-based, changes to this infrastructure will take time and therefore the complete elimination of fossil fuels in the near term is difficult. Bio-based fuels offer a partial solution to this problem, as with proper processing they can either be combined or used as an alternative to fossil fuels. The key is to develop processes that efficiently and sustainably convert biomass to biofuels and to ensure that these fuels meet current fuel quality standards. Although there are several ways to convert biomass to biofuel (i.e. fermentation, digestion, combustion, gasification, liquefaction, extraction, and chemical conversion), enzymatic conversion and pyrolysis are the most common methods for converting both soft and hard wood feedstock [1,2]. Pyrolysis offers the advantage of being a relatively fast process (seconds to minutes) compared to enzyme conversion (weeks) and does not require the level of pretreatment of the woody biomass required by enzyme conversion (e.g. steam explosion, hydrolysis etc.) [2]. Pyrolysis is a thermochemical process that occurs in the absence of oxygen. Pyrolysis is generally categorized as slow (slow heating rates, long solids residence times, and temperature less than 500°C), moderate (vapour residence times 10-20 s and temperature of 500°C), and fast (fast heating rates, short vapour residence times of less than 2 s, and 500°C). Fast pyrolysis has the highest py-oil yield of the three (50-75%) [3].

To determine how best to design a pyrolysis system (including pre-treatment), assess compatibility with traditional fossil fuels, and determine upgrading options, the reaction

rates and transport phenomena within the reactor are required. These are even more challenging tasks when the woody biomass is of low quality and therefore more complex in terms of composition than virgin wood. The reaction rates will clearly be impacted by mass and heat transfer effects. To study the kinetics independently of transport effects, the approach is to use small sample sizes and rapid heating. There are a number of studies on the pyrolysis of soft/hard wood residues, from studies of the different types of pyrolysis (e.g. fast) and product distribution [3–6] to the impact of different types of chemical reactors including fixed bed, moving bed, fluidized bed, and auger [4,6]. The Process Flow Diagram (PFD) for a typical pyrolysis process is shown in Fig. 2-1.

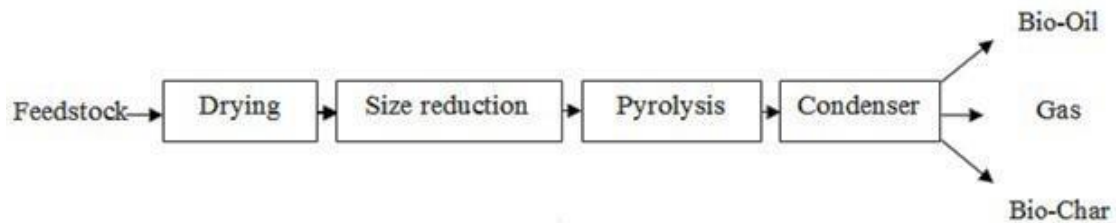


Figure 2-1: Process Flow Diagram (PFD) for Pyrolysis

In addition to the reactor type and operating conditions, the final product distribution depends on biomass properties. Bio-based feedstock can be sourced from agricultural waste (i.e. rice, wheat, sugar cane, straw, husks and shells), forestry residues (i.e. sawdust, bark, wood chips, shavings), and algae. The woody biomass is classified in three types of woods softwood, hardwood and eucalypt [7] and predominantly composed of three natural polymers: lignin (20-30%) [$C_9H_{10}O_3$], cellulose (40-45%) ($C_6H_{10}O_5$), and hemicelluloses (25-35%) (Table 2-1) [7,8].

Table 2-1: The chemical composition of different types of wood [7,8]

Feedstock type	Cellulose (%)	Hemicellulose (%)	Lignin (%)
Hardwood	40-45	25-30	25-30
Softwood	40-45	30-35	20-25
Eucalypt	45	20	30

Extractives, lipids, proteins, simple sugars, starches, water, hydrocarbons, and ash are present, but in much lower amounts [9]. Lignin has higher resistance to chemical degradation than other polymers [9,10]. Generally, woody biomass with lower lignin content and high cellulose/hemicellulose content is preferred for all conversion routes. Cellulose and hemicellulose are comprised of sugars such as C5-xylose and pentose [9,10]. A sample of chemical components of softwoods is listed in the Table 2-2.

Table 2-2: Overall composition of softwoods as a function of species [10]

Constituent	Scots pine (<i>Pinus sylvestris</i>)	Spruce (<i>Picea glauca</i>)	Eucalyptus (<i>Eucalyptus camaldulensis</i>)	Silver Birch (<i>Betula verrucosa</i>)
Cellulose	40	39.5	45	41
Hemicellulose				
-Glucomannan	16	17.2	3.1	2.3
-Glucuronoxylan	8.9	10.4	14.1	27.5
-Other polysaccharides	3.6	3.0	2.0	2.6
Lignin	27.7	27.5	31.3	22.0
Total extractives	3.5	2.1	2.8	3.0

.This review aims to integrate the information on kinetic mechanisms and models, pyrolysis heat, reactor models and types for the pyrolysis of woody biomass in one paper. The pyrolysis of sawmill residues (bark, sawdust, and wood chips) associated with the harvesting of softwoods was performed in a lab scale semi-batch system in order to focus on the reaction rates and yields without transport effects.

2.2. Pyrolysis Reactors

Selecting the type of reactors (heart of any chemical process) in pyrolysis of woody biomass is important as it has significant effects on py-oil composition and yield. py-oil yield and quality predictions are difficult because the dynamics of each pyrolysis reactor are different. Theoretically, short vapour residence time ($< 2s$), high heating rate (>100 °C/s) and temperature in the range of 400-600 °C are in favour of py-oil production. High vapour residence time and low heating rate are optimum for permanent gas and bio-char production, respectively [18]. A short review on different types of reactors is outlined below.

2.2.1. Fluidized-bed Reactor

The most common reactor type in the pilot scale for the pyrolysis of woody biomass is the bubbling fluidized bed reactor [13]. Fluidized bed reactors (FBR) are well-known reactors in the petrochemical industry and have a variety of applications (for instance, they are usually used to produce dimethyl ether from syngas or polypropylene from methanol). In this type of reactor, a gas flow fluidizes a bed of solid material (Fig. 2-2). In pyrolysis

of woody biomass, feedstock particles and hot sand are fluidized by circulating product gas. Fluidized reactors have a very good heat/mass transfer and subsequently rapid heating of feedstock particles takes place. High py-oil yield (i.e. 70~75) is typical [19]. Catalysts can be easily added to a fluidized bed reactor and the transport phenomena is well understood [5]. Although they have a good temperature control and efficient heat/mass transfer, the operating cost is high for this type of pyrolyzer. Heidari et al. [20] investigated the impact of pyrolysis temperature, nitrogen flow rate, biomass feed rate and biomass particle size on py-oil yield and composition in a lab-scale fluidized-bed reactor. The highest py-oil yield (71%) was obtained at a 450 °C temperature, a 90 g/h feed rate, a 12.6 L/min N₂ flow rate, and a 1.5 mm biomass particle size. There are several pilot and larger scale fluidized bed systems operating around the world (Dynamotive (400 kg/h), Wellman (250 kg/h), Ikerlan, RTI (20 kg/h)) [21].

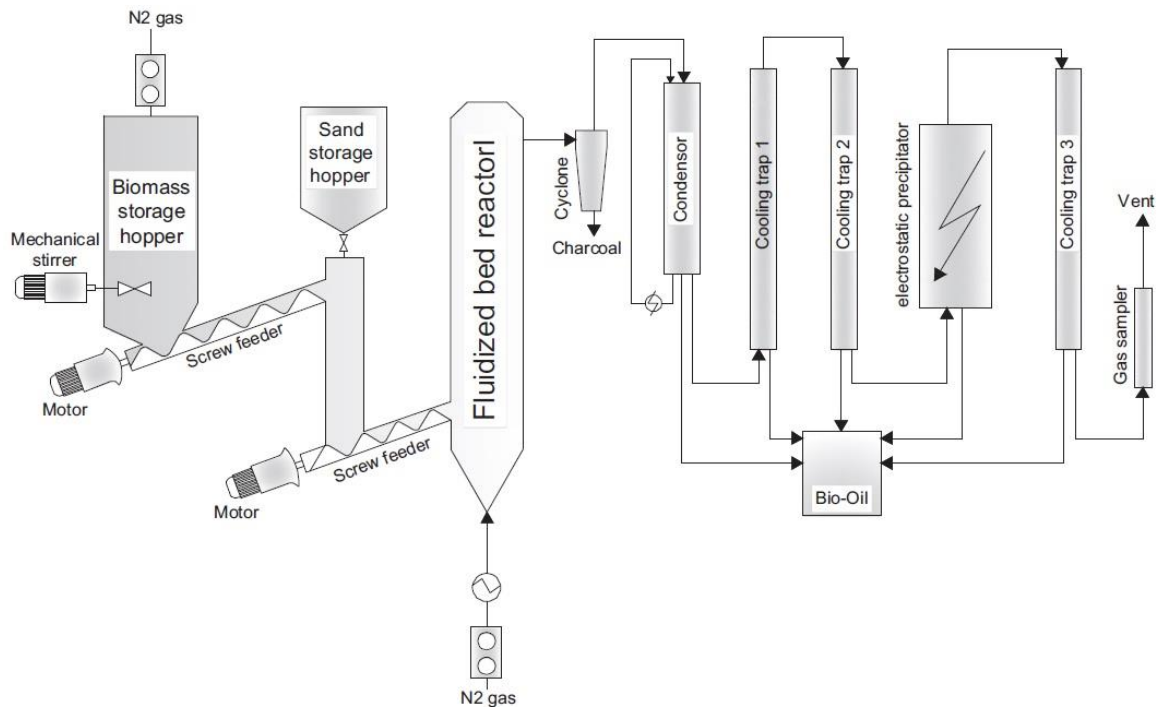


Figure 2-2: Process flow diagram of fluidized bed reactor for the pyrolysis of biomass [20] (without permission)

2.2.2. Plasma Pyrolysis Reactor

The external heating source is supplied by plasma in this type of reactor (Fig. 2-3). Plasma reactors are useful for the conventional pyrolysis (slow heating rate and low temperature) of biomass [22,23]. Although the plasma pyrolysis reactor method has been proposed for syngas and char production [22], the technology has very high energy requirements (the temperature initiated in thermal plasma is 2500–9500°C) [22,23]. Tang and Huang [22] used a radiofrequency (RF) coupled plasma pyrolysis reactor and the gas yield reached 66 % of the biomass feedstock. Further, they showed that the electrode geometry, input power and reactor pressure were the key parameters affecting the plasma characteristics such as plasma length, temperature, and energy transfer efficiency.

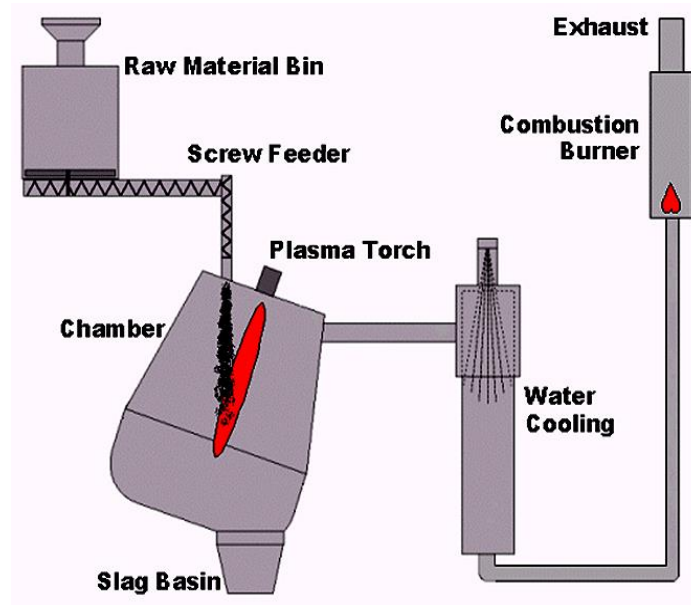


Figure 2-3: Process flow diagram of pyrolysis plasma reactor [24] (without permission)

2.2.3. Free-Fall Reactor

Free-fall or drop-tube reactors are in principle a simple technology. The particles fall through the length of the reactor. The flow of sweep gas is lower compared to other types of reactors due to the fact that biomass is fed from the top of the reactor. As Fig. 2-4 shows, char is captured in a collector and the volatile gas passes through a cyclone to remove solid particles before entering a condenser. py-oil is obtained by quenching volatile gases. These reactors operate at high heating rates and retention time can be varied from milliseconds to a few seconds [5]. Ellens and Brown [25] investigated the impact of heater set-point temperature, biomass (red oak) particle size, sweep gas flow rate and biomass feed rate in a free-fall reactor. Optimal operating conditions (a 575 °C temperature, a 300 μm particle size, a 2 kg/h feed rate) produced approximately 70%

py-oil yield. Sweep gas flow rate did not significantly impact py-oil yield over the 1–5 L/min range tested.

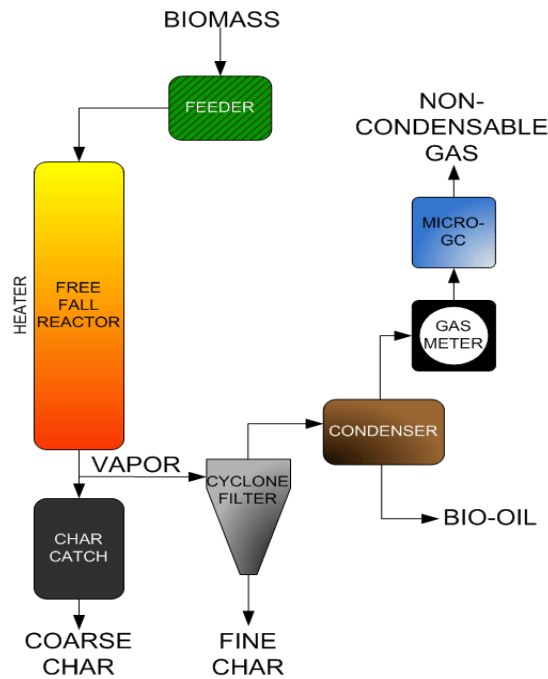


Figure 2-4: Process flow diagram of a free-fall reactor for the pyrolysis of biomass [25] (without permission)

2.2.4. Fixed-bed Reactor

Fixed bed pyrolyzers are usually used for slow pyrolysis to produce char [20]. The technology is simple, however, not flexible with respect to process changes (for instance, it is rarely used for fast pyrolysis due to a poor heat/mass transfer and a long vapour residence time). As shown in Fig. 2-5, a carrier gas enters the distributor and passes through the bed to carry both the condensable and non-condensable gases to the condenser. The fixed bed reactor is usually used in the laboratory or bench scale due to the simple structure [19]. Onay et al. [26] conducted a series of experiments on a sample

of rape seed to determine the optimum pyrolysis temperature, particle size, heating rate, and sweep gas flow rate on py-oil in a lab-scale reactor. The maximum py-oil yield of 68% was obtained at 550°C temperature, 0.6–0.85 mm particle size range, 300 °C/min heating rate, and 100 mL/min N₂ flow rate. A few 600 kg/h commercial units have been constructed in China [19].

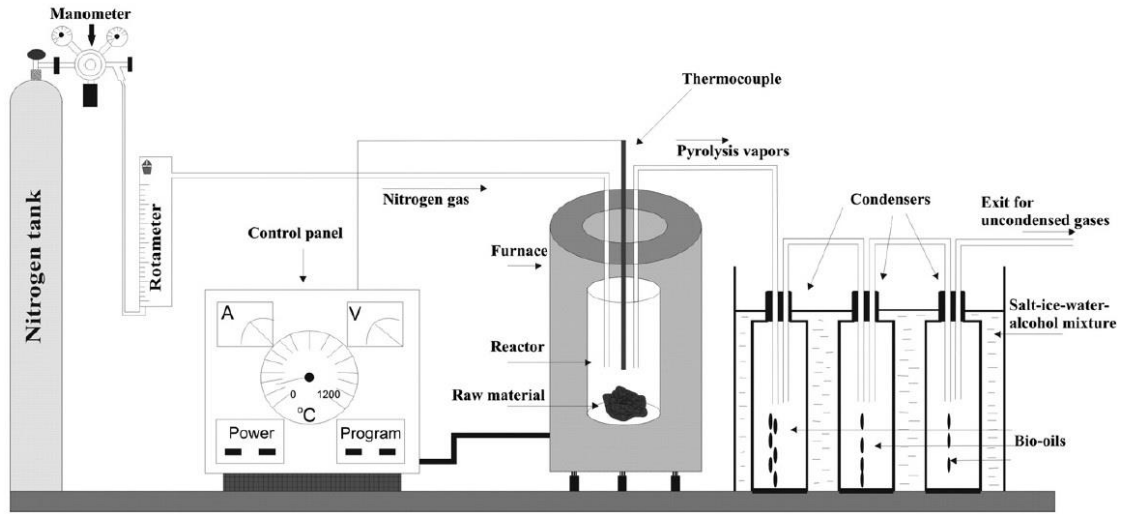


Figure 2-5: Process flow diagram of a fixed-bed reactor for the pyrolysis of biomass [27] (without permission)

2.2.5. Rotating Cone Reactor

The rapid heating rate and short residence time of this system (Fig. 2-6) make it ideal for flash pyrolysis. Compared to other units, the operating cost is lower due to the absence of carrier gas [19]. The high py-oil yields (60-70%) have increased interest in this type of reactor in recent years [13,19]. Junsheng et al. [28] optimized a 4 kg/h rotating cone reactor. The results indicated that a 550°C temperature, a 115 rpm rotating rate, and a 0.08 Mpa vacuum pressure are the optimum conditions that gives approximately 55% py-oil

from the sawdust. There are 2000 kg/h units operating in the Netherlands (BTG and BioEcon) and USA (Kior) [19,21].

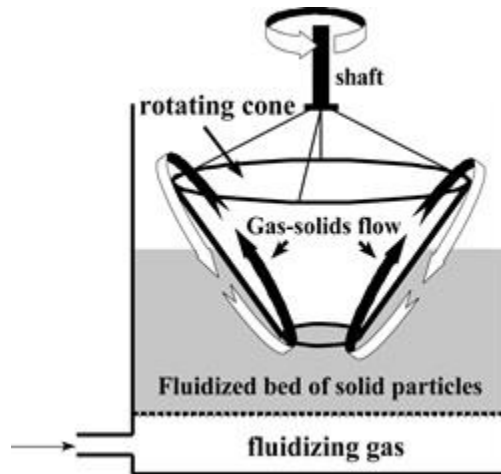


Figure 2-6: Process flow diagram of rotating reactor for the pyrolysis of biomass [29] (without permission)

2.2.6. Microwave Reactor

Microwave reactors (Fig. 2-7) differ from conventional pyrolysis units. These reactors operate without thermal gradients within the vessel [19,30]. However, there are challenges with respect to penetration of the microwaves. Lei et al. [31] propose that microwave reactors can be used for fast pyrolysis due to fast internal heating by microwave irradiation. They investigated the impact of reaction temperature and time, and particle size on the yields of py-oil and bio-char. A temperature of 650 °C and a 8 min reaction time were the optimum. The impact of particles was insignificant in the range studied (0.5-4 mm). Carbonscape in New Zealand and UK, and Bioenergy 2020 in Austria, are working on the commercial scale of microwave reactors [19].

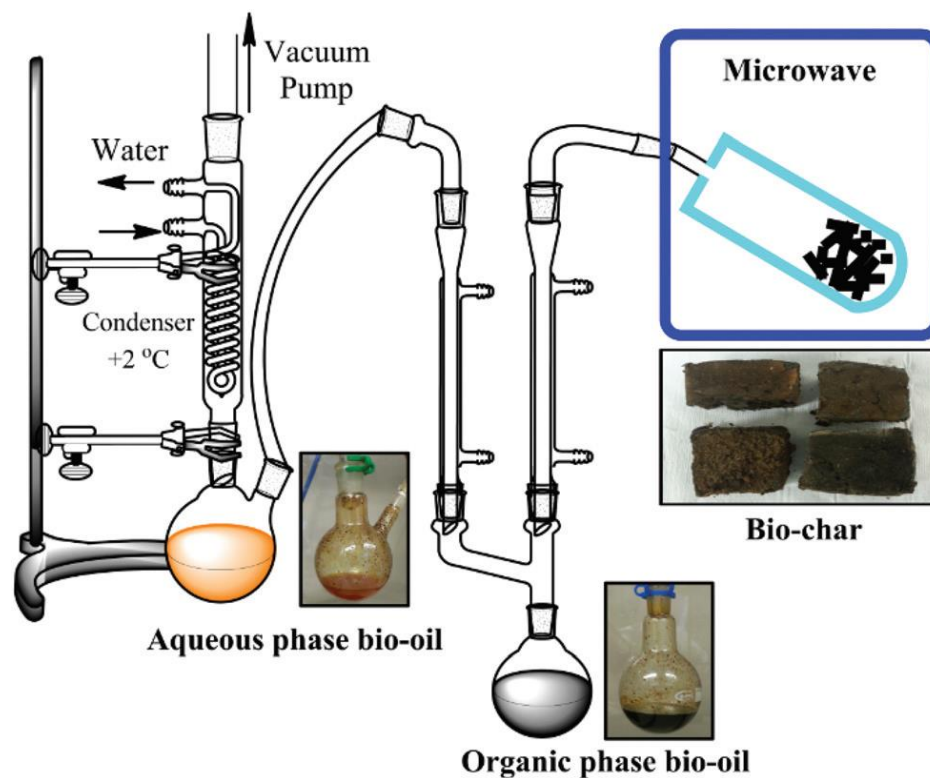


Figure 2-7: Lab-scale microwave reactor setup [32] (without permission)

2.2.7. Auger Reactor

Fluidized-bed and auger reactors (Fig. 2-8) are the most two common reactors used for the pyrolysis of woody biomass [33]. Although the fluidized-bed reactor has very good mass/heat transfer, the auger reactor can be less operationally complex which makes it ideal for mobile or remote locations. Auger pyrolysis can be modular and transported to the biomass. It has less energy loss than fluid bed or transport reactors and hence has a better energy conversion rate. In addition, auger pyrolysis is a viable pyrolysis technology that has not received the same theoretical treatment as other pyrolysis conversion technologies. Brown et al. [34] reached 75% py-oil yield in a 1 kg/h pilot plan auger

reactor. The feedstock, red oak biomass, was pyrolyzed at a sweep gas 3.5 standard L/min, a temperature of 600°C, an auger speeds of 63 rpm, and a heat carrier mass flow rates of 18 kg/h. Liaw et al. [35] investigated the effect of operating temperature on the quantity and quality of py-oil using an auger system on Douglas Fir wood. The results showed that compared to the fluidized bed, the auger reactor is able to reach yields achieved in fluidized beds for both py-oil and bio-char. ABRI-Tech in Canada (2083 kg/h), Lurgi-Ruhrgas process in Germany (500 kg/h), and Renewable Oil Intle in USA (200 kg/h) produce large scale augur reactors [19].

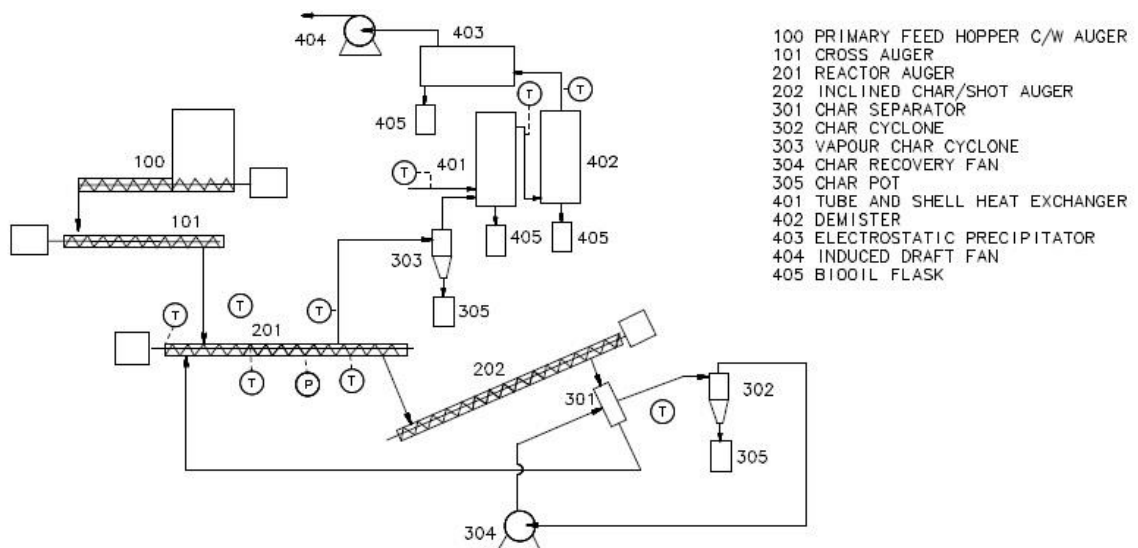


Figure 2-8: Process flow diagram of auger reactor for the pyrolysis of biomass

Fortum, VTT, and Ensyn design in Finland, Pyrovac in Canada, and PyTec in Germany are the other companies which work on the pyrolysis reactor design [21]. A summary of py-oil quality (i.e. psychochemical properties) and quantity (i.e. yield) as a function of pyrolysis unit is illustrated in Table 2-3.

Table 2-3: Comparison of the physical and chemical py-oil properties obtained from different pyrolysis reactors

Pyrolysis	Auger Reactor [33]	Fluidized-Bed Reactor [13]	Rotating Cone Reactor [28]	Free-Fall Reactor [36]
Scale	Bench	Bench	Bench	Bench
Feedstock	Oak	Oak	Pine	Red oak
Temperature °C	450	500	550	550
Py-oil yield	50–56	68	55	70
Bio-char yield	17–20	11	N/A	15
Water content	22	19	50	25
Solid content	0.8	N/A	0.09	1.2
pH	3.1	N/A	4.5	N/A
Total acid number	120	69	N/A	101
Viscosity (cP) at 40°C	N/A	57	47	N/A
Density (g/cm ³)	1.20	1.24	N/A	N/A
HHV (MJ/kg)	18.7	N/A	16.9	16.8

2.2.8. Reactor Models

To develop a process model for a reactor on a large scale the kinetic, heat and mass transfer models must be integrated through actual transport models. In addition to the process modeling, the empirical models, developed based on experimental data, are used

to mathematically demonstrate the impact of significant process variables on products [25,37–40]. Abnisa et al. [40] applied this type of model to optimize py-oil produced from palm shell waste using response surface methodology (RSM) in a fixed bed reactor. The py-oil yield was optimized at a temperature of 500 °C, a carrier gas (N₂) flow rate of 2 L/min, a particle size of 2 mm, and a reaction time of 60 min. Ngo et al. [39] developed an empirical model for py-oil production based on feed rate, temperature, and particle residence time. Brown et al. [34] used a quadratic model to optimize the operational parameters of an auger pyrolyzer with heat carrier using response surface methodology. Heat carrier, inlet temperature, mass flow rate, rotational speed of screws in the reactor, and volumetric flow rate of sweep gas were studied. The py-oil was maximized using a high heat carrier temperature (600 °C), high auger speeds (63 rpm) and high heat carrier mass flow rates (18 kg/h). As demonstrated above, although the optimal operating conditions fall in the same range, there is significant variation depending on reactor type and feedstock. As such, optimizing conditions where minimal transport resistances are present, allows one to isolate feedstock condition (fresh, moisture content etc.) and feedstock type impacts.

In the second approach, a process model is developed using basic concepts of transport phenomena (i.e. heat, mass, and momentum balance) and reaction rates. Computational Fluid Dynamic (CFD) software has been used to combine the kinetics and momentum/heat transport phenomena [37,41–44]. Xue et al. [45] modeled a fluidized bed reactor using Euler–Euler multiphase CFD. This model simulated fast pyrolysis of biomass in a fluidized-bed reactor. The velocity of produced gas, biomass density profile,

axial temperature of gases phase, partial density distribution, and the gas phase temperature in reactor outlet were predicted in the CFD model. The CFD model was not validated with experimental data. Haseli et al. [46] modeled the pyrolysis of a biomass particle with the temperature-dependent heat of reactions. Energy conservation was used to improve the simulation which has been neglected in past studies. The study demonstrated the importance of the heat of reaction released during the pyrolysis of woody biomass on the final results. The developed thermal/kinetic combined model (using primary reactions in the kinetic model) agreed well with experimental data; and a more complex model with secondary reactions was not required. Sadhukhan et al. [47] modeled the pyrolysis of wood particles with a transient mathematical model which included a kinetic model with both primary and secondary reactions. The conductive and internal convection within the particle and convective and radiative heat transfer between bulk and external surface were considered. The predictions showed good agreement with experimental data. Yeh et al. [48] developed a model based on an auger reactor. The reactor was divided into a plug flow zone in series with a continuous stirred tank with a stagnant dead volume. The model was based on the analysis of residence time distribution (RTD) (Fig. 2-9). They showed that the fraction of dead volume (d) varied from 0.04 to 0.16. In this figure, d is fraction of dead volume in the CSTR, C_d is tracer concentration in the dead volume (mg/cm³), C_{in} concentration of tracer entering the CSTR (mg/cm³), C_0 is tracer concentration in the effluent of the CSTR (mg/cm³), b is fraction of e , p is fraction of PFR, q is volumetric flow rate of food material (cm³/s), and V is total volume of the extruder (cm³).

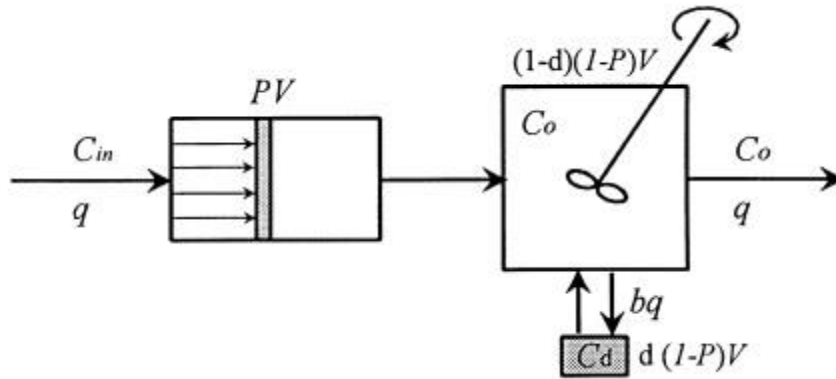


Figure 2-9: Flow diagram of plug flow reactor in series to a CSTR cross-flowing dead volume [48] (without permission)

To calculate mean residence time of biomass particles in the auger reactors, the following equation was proposed.

$$\bar{t} = 1316.76 - 142.79F_r - 3.07S_s + 0.17F_r \times S_s 5.35F_r^2 \quad (2-1)$$

Where F_r and S_s are feed rate (Kg/h) and auger speed (rpm) respectively.

The discussed models are summarized in Table 2-4.

Table 2-4: Common reactor mathematical models for the pyrolysis process

Reactor Model	Reactor type and scale	particle size (mm)	Reaction Mechanism	Heat transfer Mechanism	Assumptions	Solution method	Results
One dimensional steady-state, Eulerian fluid dynamics and heat transfer [49]	Circulating fluidized-bed (0.023 kg/s)	0.8	19 parallel reactions	All three heat transfer modes (conduction, convection and radiation) coexisted	Only the primary reactions were taken into account.	Solved by using the backward finite difference method with a constant step size of 0.05 m.	- Biomass particles were heated to pyrolysis temperature of 786 K in 0.3 s - Water yield was under predicted
Mass, momentum, energy and species balance coupled with chemical reactions [50]	Fluidized-bed reactor (2.22 kg/h)	N/A	Broido–Shafizadeh mechanism	Only convective heat transfer was accounted.	N/A	BIOTC (BIO mass Thermochemical Conversion) [51]	- The drag coefficient model significantly influenced the product yields - The same temperature profiles were predicted with different heat transfer models.
One dimensional model [43]	Entrained Flow Reactor (150 g/h)	250 μm	Primary with secondary tar cracking	The heat conduction along the radius of the particle, the	-The thermal conductivity and specific heat capacity of the particle vary	Lagrangian approach	-The temperature gradient inside the particle plays a significant role -The particle

				particle subjected to convective heat transfer	radially -Produced gas and tar immediately escapes from the particle -The spherical particle - No volume shrinkage		position in the reactor is highly dependent on the reaction mechanism
Response Surface Methodology (RSM) [34]	Auger Reactor (1 kg/h)	750 μm	N/A	N/A	N/A	Circumscribed central composite design of experiments	The reactor achieved liquid yields greater than 73 wt.%
Multi-scale model [52]	Fixed-bed and fluidized-bed	N/A	Primary with considering secondary tar cracking	Heat transfer occurs as conduction, convection and radiation	-The particle is spherical -The properties were considered one dimensional in space -Transport of mass occurred by convection and diffusion. -Ideal gases -Thermal equilibrium between the solid	Iterative method	Iterative method was the recommended method to solve particle models that were coupled to reactor models

and the gas							
Detailed mathematical model was coupled with a compressible Reynolds stress transport model [53]	Vortex pyrolysis reactor	5 mm	Shafizadeh and Bradbury	-The heat transfer into the particle was conduction. -The particle subjected to conductive, convective, and radiative.	It was assumed that the vortex reactor flow was nearly axisymmetric	Solved numerically on both 1D and 2D grids (Jacobi iteration procedure at each numerical time step)	The 1D particle model resulted in conservative estimates for total pyrolysis conversion times and tar collection.
A model incorporating heat and mass transfer, along with chemical reaction [54]	Vertical fixed-bed reactor	very small (-200 mesh)	Shafizadeh and Bradbury	N/A	No intraparticle heat and mass-transfer limitation was considered	Finite differences	Represented the transient behavior of the biomass pyrolyzer well.
A one dimensional steady state mathematical model [55]	Rotary kiln (bench-scale)	10 mm	Primary with secondary	Heat transfer was dominated by free convection flow patterns	-Pseudohomogeneous gas phase - Ideal gas - The axial diffusional was neglected	A fourth order Runge–Kutta algorithm	-The influence of the solids residence time was small. -The model described well the experimental data

2.3. Kinetic Models

2.3.1. Global Kinetic Model

In the previous section, the models were developed for the overall process. There has been significant work on focusing on the kinetics in pyrolysis process. Many researchers [56–59] have studied the pyrolysis of woody biomass and sawmill residue by thermogravimetry analysis (TGA). In TGA the weight loss as temperature is increased is used to determine decomposition reactions. The studies indicate the thermal decomposition of biomass occurs in three main stages: in the first stage (<200 °C), water, carbon monoxide, and carbon dioxide are released from the matrix. In the second stage (475 to 655 °C), the main decomposition occurs, and in the third stage (above 600 °C) the decomposition reaction slows down. The first decomposition takes place for cellulose and hemicelluloses under the temperature range of 475-655 °C (the second stage) while the decomposition of lignin initiates at the temperatures higher than 455 °C, as shown in Fig. 2-10.

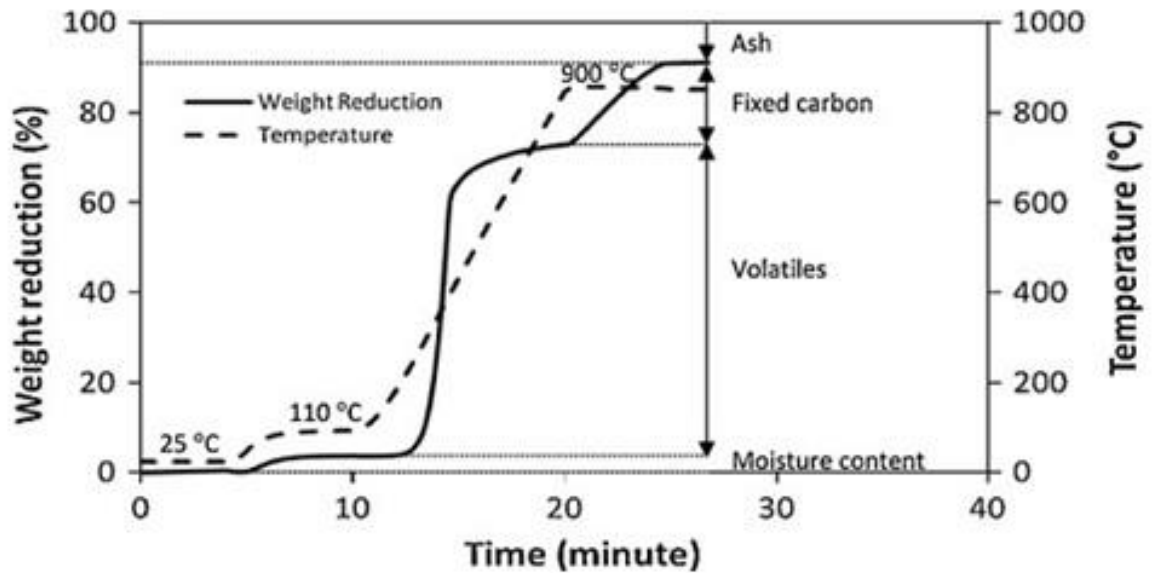


Figure 2-10: TGA profile for proximate analysis of sawdust for a particle size of 250 μm [60] (without permission)

In recent TGA analysis [57–59], an overall kinetic model of multicomponent has been developed to describe the mass loss or thermal degradation of woody biomass. The proposed model is shown below.



$$\frac{d\alpha}{dt} = kf(\alpha) \quad (2-2)$$

Sloepicka et al. [61] compared three methods for predicting kinetic parameters (Fig. 2-11): the Kissinger model [62], Kissinger–Akahira–Sunose (KAS), and Flynn–Wall–Ozawa (FWO) [38]. The Kissinger method is based on the following expression:

$$\ln\left(\frac{\beta}{T_m^2}\right) = \ln\left(\frac{AR}{E}\right) - \frac{E}{RT_m} \quad (2-3)$$

Where biomass conversion is defined as below:

$$\text{Conversion} = \alpha = \frac{M_t - M_\infty}{M_0 - M_\infty} \quad (2-4)$$

M_t is mass of feedstock at time t , M_0 and M_∞ are the masses of feedstock at the beginning and end of the reaction respectively, β is heating rate, and α is conversion.

The KAS method is outlined in equation 2-5.

$$\ln\left(\frac{\beta_i}{T_{\alpha i}^2}\right) = \ln\left(\frac{A\alpha R}{E_\alpha g \alpha}\right) - \frac{E_\alpha}{RT_{\alpha i}} \quad (2-5)$$

The FWO model is based on the following expression:

$$\ln(\beta_i) = \ln\left(\frac{A_\alpha E_\alpha}{R_g(\alpha)}\right) - 5.331 - 1.052 \frac{E_\alpha}{RT_{\alpha i}} \quad (2-6)$$

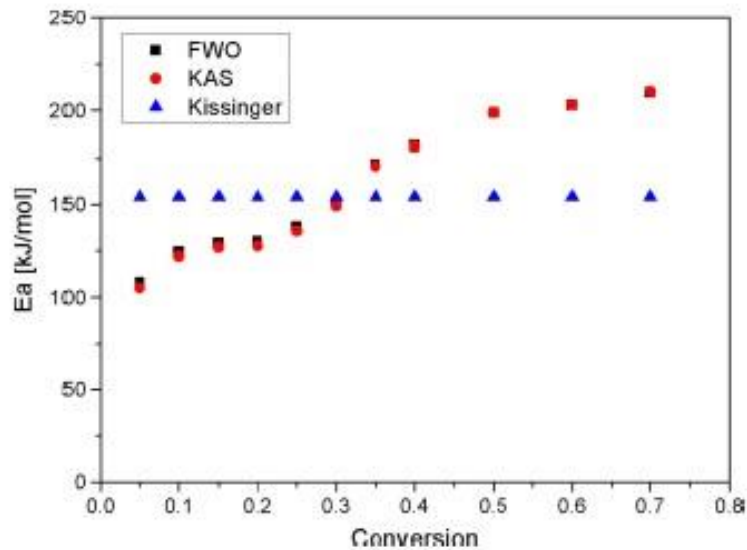


Figure 2-11: Comparison of activation energy as a function of feedstock conversion for three different models (FWO, KAS, and Kissinger) [61] (without permission)

The FWO and KAS models show a variation in the E_a , demonstrating the changing reaction mechanisms.

2.3.2. Three Parallel Reactions

In order to better predict products, researchers have proposed dividing the biomass feedstock into three main fractions (cellulose, hemicellulose, and lignin), (Fig. 2-12) [57,63].



Figure 2-12: Three parallel reactions mechanism. α , β , and γ are the mass fraction of cellulose, hemicellulose and lignin in biomass respectively and k is kinetic constant

Hashimoto et al. [64] performed a kinetic analysis of the pyrolysis of various types of biomass such as trunk, bark, leaf, shell, herbage, food dregs, and polysaccharide using TGA analysis data. A synthetic biomass mixture was composed of cellulose and lignin was studied with this model. Studies indicate the reaction rates can be characterized using a nth-order reaction kinetic model (equation 2-7). The rate parameters are correlated with the solid residue yield and the lignin content of woody biomass.

$$\frac{\beta}{T^2} = \frac{k_0 R}{EG(z)} e^{-E/RT} \quad (2-7)$$

$$n=1 : G(z) = -\ln z,$$

$$n \neq 1: G(z) = (1 - z^{1-n}) / (1 - n)$$

β is the heating rate, E is the activation energy, T is temperature, K_0 is the frequency factor, and R is the universal gas constants.

The kinetic parameters including k_0 , E and n are obtained using the TGA curve and equation 2-7. A nonlinear least squares estimation (NLE) calculates the optimum values for parameters. The reaction rate constant was correlated to frequency factor and activation energy in equation 2-8. Fifteen biomass samples were used to develop the correlation and the average error was 3.8%.

$$\ln k_0 = 2.42 \times 10^{-4}E - 7.04 \quad (2-8)$$

Hashimoto et al. concluded that pyrolysis of cellulose and hemicellulose is first order; however, lignin is higher order and developed the following correlation between solid residue yield and lignin content with 16.8% average error (Fig. 2-13).

$$\omega = 0.284L + 0.105 \quad (2-9)$$

ω is solid residue yield and L stands for lignin content (Fig. 2-14).

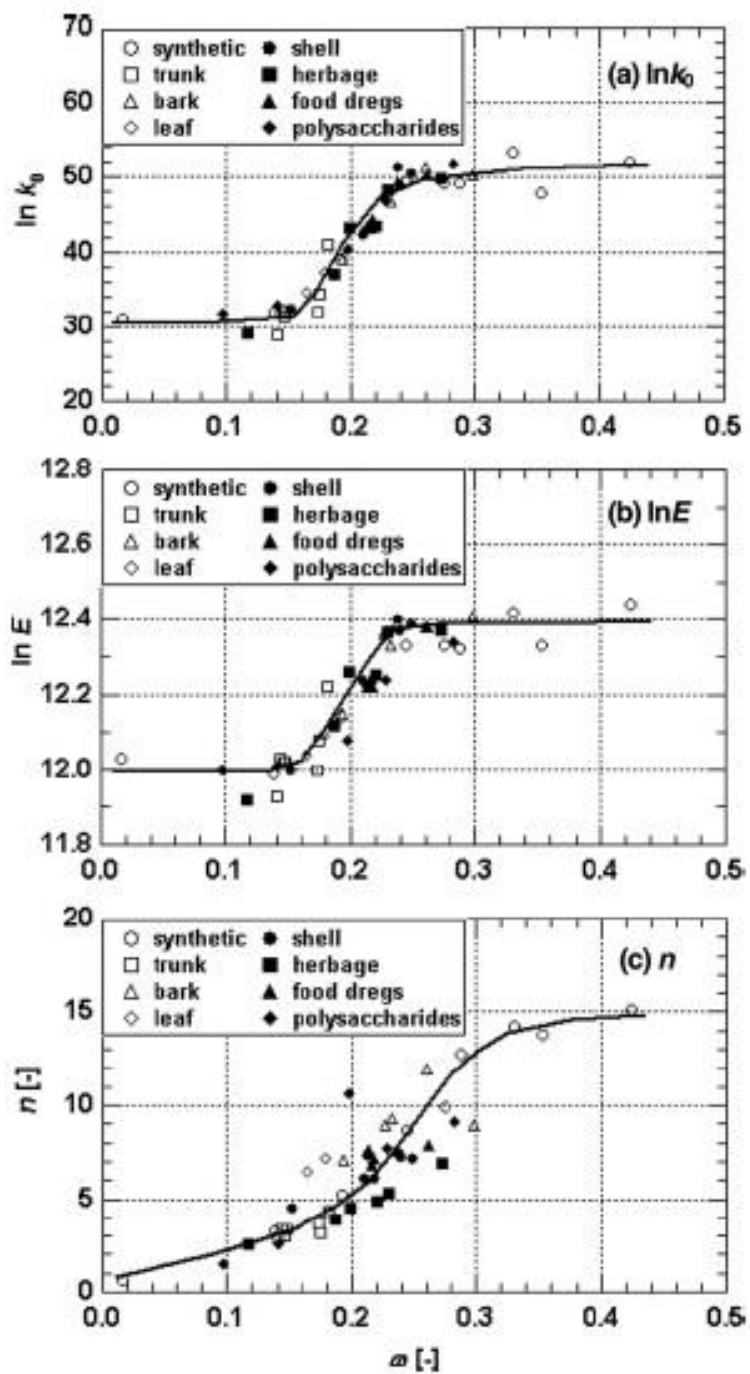


Figure 2-13: Kinetic parameters predictions for different biomass feedstock ($\ln k_0$, $\ln E$, and n) as a function of solid residue yield (x) for biomass samples [64] (without permission)

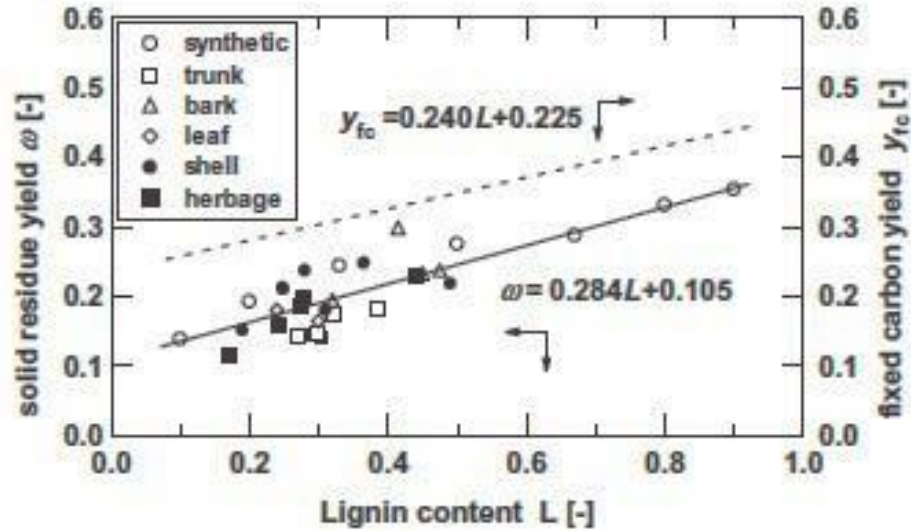


Figure 2-14: Relationship between solid residue yield (x) and lignin content (L) and between fixed-carbon yield (y_{fc}) and L [64] (without permission)

Cardoso et al [65] investigated the thermal decomposition of tobacco waste and sorghum bagasse using models by Ozawa [38] and Starink [66]. Based on these models, the pyrolysis reactions were correlated to residual mass and temperature, according to equation 2-10:

$$\frac{dX}{dt} = k_0 \exp\left(\frac{-E_a}{RT}\right) f(x) \quad (2-10)$$

t is time, T is temperature, E is activation energy, and X is converted biomass which is defined according to the following equation:

$$X = \frac{(m_0 - m_t)}{(m_0 - m_r)} \quad (2-11)$$

Where m_0 is the initial mass, and m_t and m_r are the masses at time, t , and residual mass respectively. In this model, it is proposed that the three main biomass components and other components including alkali, potassium, sodium, calcium, and chlorine react simultaneously. The proposed parallel reactions model is as follows:

$$\frac{dX}{dt} = - \sum_{i=1}^m c_i \left(\frac{dX_i}{dt} \right) \quad (2-12)$$

where m is the number of pseudo-components.

When this model is coupled with the heat and mass transport equations (in which transport resistances play a role) as well as the hydrodynamic of the system, the model may prove to be overly complex.

2.3.3. Competitive Models

A common approach to represent the components of pyrolysis is to simply lump them into different groups. The three parallel reactions scheme, which shows the production of gas, vapour, and char, has been widely used (Fig. 2-15) [67–69].

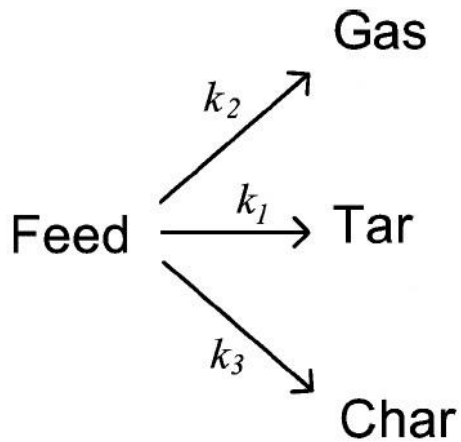


Figure 2-15: Competitive mechanism of biomass pyrolysis; k_1 , k_2 , and k_3 are kinetic constants

2.3.4. Models with Secondary Tar Cracking

A number of researchers proposed a secondary tar cracking model as outlined in Fig.2-16 [70–74].

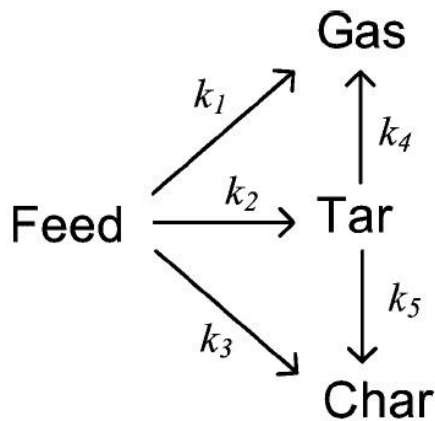


Figure 2-16: Secondary tar cracking mechanism for biomass pyrolysis k_1 , k_2 , k_3 , k_4 and k_5 are kinetic constants [75] (without permission)

In this model, the biomass is decomposed during primary reactions to produce non-condensable, py-oil and bio-char products. Subsequently, the gas/vapour phase is converted to char and light gas by using secondary reactions. All of the reactions are proposed as first order.

2.3.5. Shafizadeh and Bradbury Model

This mechanism (Fig. 2-17) includes both primary and secondary reactions; however, initially the feedstock is converted to activated biomass called intermediate and the activated particle participates in competitive and cracking reactions. Several researchers have determined in the fast pyrolysis of woody biomass, the biomass degrades and produces intermediate oil before forming volatile products [76–78]. The existence of intermediate liquids was verified using high speed photography during decomposition of the solid biomass. The reactions that take place in the intermediate phase may produce small-molecules as gas-phase product [73] or polymerize to form char. Boutin et al. [79] confirmed that a liquid-phase intermediate product exists in the fast pyrolysis of biomass. Kashual and Abedi [75] used the Shafizadeh and Bradbury model for pyrolysis of sawdust between 330°C, 350°C and 370 °C (Fig. 2-18).

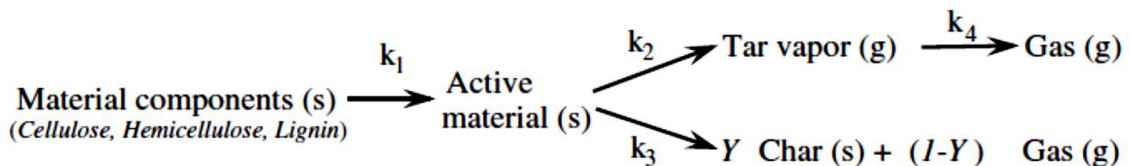


Figure 2-17: Modeled proposed by Shafizadeh and Bradbury [80], Y is the formation ratio for the char component [37] (without permission)

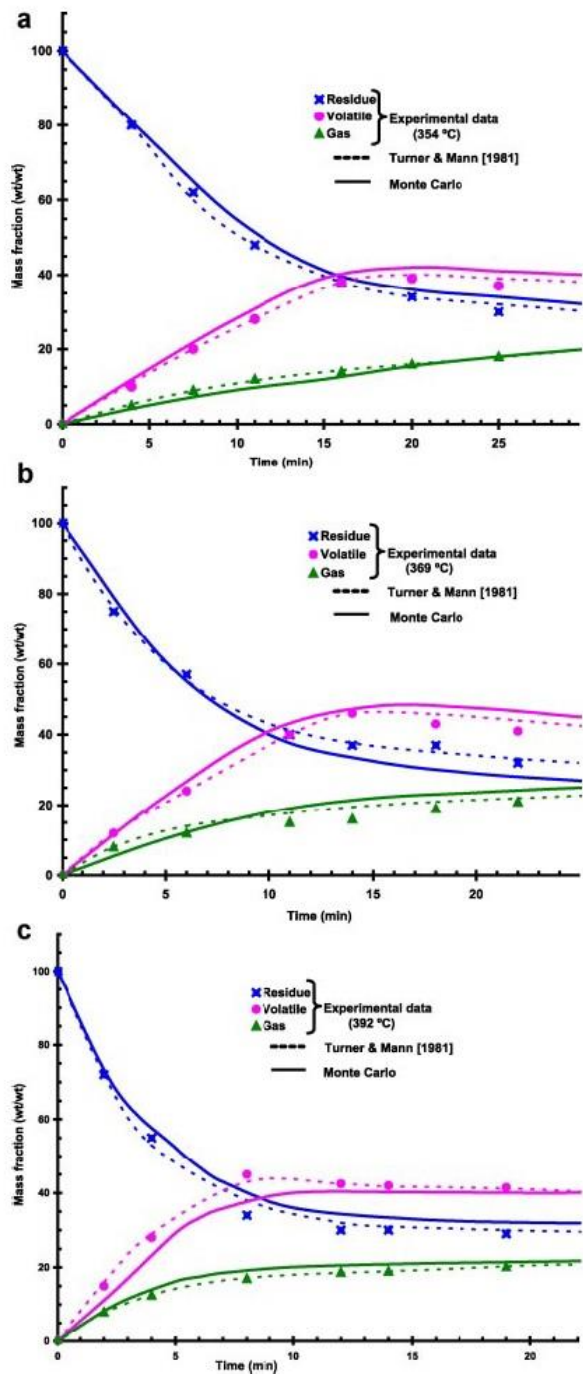


Figure 2-18: Comparison of model prediction to Thurner and Mann's(1981) data (a) T=354°C, (b) T=369°C) and (c) T=392°C [75] (without permission)

2.3.6. Activation Energy Distribution Model (AEDM)

In this model, an infinite number of irreversible first order parallel reactions with different activation energies are proposed and distribution function $f(E)$ is used to represent the range of activation energies. This model was proposed by Vand [81] for the first time. The activation energy (E) and frequency factor (k_0) can be experimentally obtained by TGA. Equations 2-13 and 2-14 are used to calculate both activation energy and frequency factor:

$$\ln\left(\frac{a}{T^2}\right) = \ln\left(\frac{k_0 R}{E}\right) + 0.6075 - \frac{E}{RT} \quad (2-13)$$

$$\frac{V}{V^*} = 1 - \int_{E_s}^{\infty} f(E) dE = \int_0^{E_s} f(E) dE \quad (2-14)$$

where V^* is the total volatile content of the biomass and V is the volatile produced as a function of time, “ a ” is the heating rate, T is temperature, R is gas constant, E is activation energy, and k_0 is frequency factor. $f(E)$ is determined by simply differentiating the V/V^* against E relation by resorting to equation 2-14.

In work by Sonobe et al [82], cellulose, rice straw and husk, and corn cobs were pyrolyzed under a variety of conditions and compared to predictions using distribution curve of activation energy. The calculated volatile production was compared to the experimental results (the pyrolysis experiments were performed in a sensitive thermo-balance at a heating rate of 10 °C/min up to a final temperature of 900 °C under the helium flow rate of 50 ml/min) (Fig. 2-19). The experimental results and the model predictions at the three different heating rates compare well. The activation energy of

biomass pyrolysis is widely distributed, from 120 kJ/mol to 250 kJ/mol, reflecting the different feedstock used.

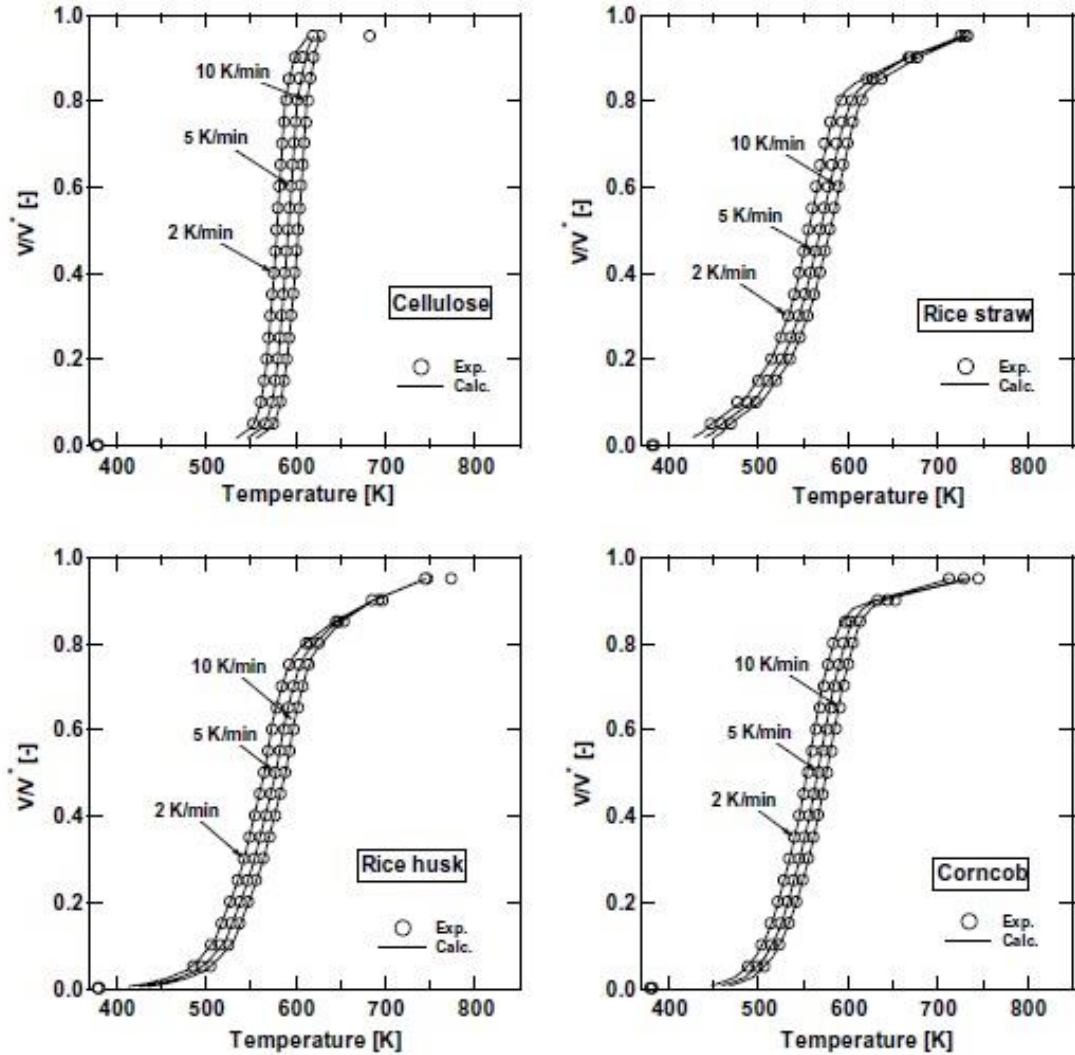


Figure 2-19: Experimental and aalculated TG curves at a = 2, 5, and 10 K/min for cellulose, rice straw, rice husk, and corncob [82] (without permission)

Where V^* is the total volatile content of the biomass and V is the volatile produced as a function of time. The value of k_0 for rice straw, rice husk, corncob and cellulose increased

from an order of 10^{11} to the order of 10^{18} s^{-1} , while E increased from 120 kJ/mol to 250 kJ/mol. This model is accurate for predicting experimental data, however, there is a limitation; the model is restricted to prediction of the volatile vapour.

2.3.7. Chemical Percolation Devolatilization Model

As Fig. 2-20 shows the Chemical Percolation Devolatilization (CPD) model can be a combination of the parallel, competitive and Shafizadeh and Bradbury models. The kinetic model is outlined in Fig. 2-20 and parameters definitions in Table 2-5 [83]. The CPD model uses a base structural unit, a sugar ring with attached side chains (L in figure 2-20) for biomass as proposed by Fletcher et al. [84]. The bridge then becomes activated (L^*) upon heating and subsequently breaks into side chains and char.

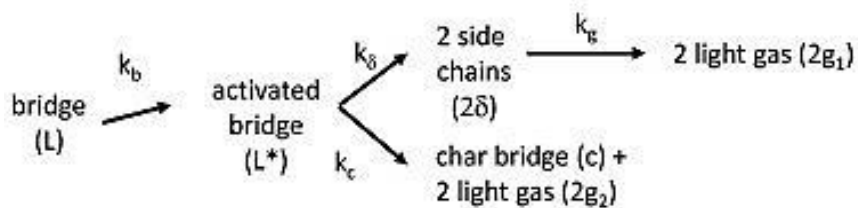


Figure 2-20: Chemical bridge reaction pathways treated in the CPD model to describe pyrolysis [84] (without permission)

Table 2-5: Definition of the kinetic parameters for the CPD Model [83]

Kinetic Parameters	Parameters Definitions
E_b , kcal/mol	Bridge breaking activation energy
A_b , s^{-1}	Bridge pre-experimental factor
σ_b , kcal/mol	Standard deviation of E_b
E_g , kcal/mol	Gas formation activation energy
A_g , s^{-1}	Gas pre-experimental factor
σ_g , kcal/mol	Standard deviation of E_g
ρ	Char-to-gas kinetic ratio

E_c , kcal/mol	Difference in activation energy between bridge breaking and char formation
E_{cross} , kcal/mol	Cluster cross-linking activation energy
A_{cross} , s^{-1}	Cluster pre-experimental factor

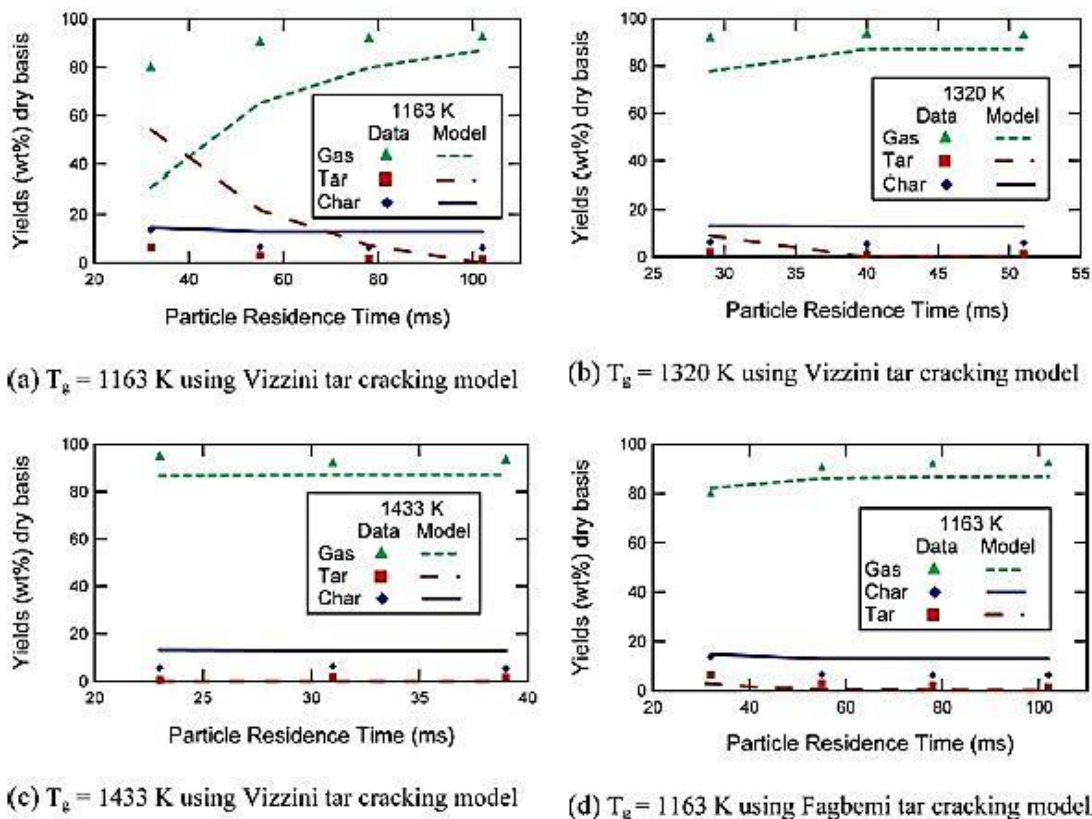


Figure 2-21: Comparison of measured and modeled sawdust pyrolysis yields using the three parallel models at 1 atm and gas temperatures of 1163–1433 K [83] (without permission)

The predictions match the experimental data (Fig. 2-21) at higher temperature and residence times but less so at lower temperatures and shorter particle residence times. This could be a result of the reaction to the side chains not being favoured at lower temperature or not having sufficient particle reaction time [84].

A summary of the discussed models is outlined in Table 2-6.

Table 2-6: Different kinetic models for the pyrolysis of woody biomass

Sample [reference]	Method of Analysis	Mechanism	Heating Rate (C/min)	Sample Load (mg)	Temperature Range	Particle Size (μm)	E (kJ/mol)	Frequency Factor (S^{-1})
Cellulose [85]	TG-MS, DTG	Global Model	2-80	2-3	250-400 °C	N/A	221	log k = 16.1
Beech wood, saw dust, rice husk [86]	TGA, DTG	Three Independent-Parallel Reactions	5-50	5-15	400-800 k	335-1000	Cellulose = 184-192 Hemicellulose = 129-133 Lignin = 64-87	Cellulose log k= 13.9 - 13.4, Hemicellulose log k= 10.2 - 9.9 Lignin log k = 3.1 -1.8
Rice husk, olive cake, cacao shells [56]	TG	Variable Activation Energy Model	5-100	5-6	400-800 k	90-125	Rice husk = 135.5 kJ/mol Olive cake = 119.1 Cacao shells = 127.7	N/A
Rice straw, empty fruits brunch, hesperaloe) [87]	TGA	Three Parallel Reaction	10	5	25-900 °C	160	Cellulose =204-208 Hemicellulose =86-90 Lignin =59-62	Cellulose = 34.7 Hemicellulose = 12.3 Lignin = 6.8
Cherry stones [88]	TGA	A four independent-parallel reactions	5-20	10-100	300-600 °C	320-2000	H ₂ = 92.5 CO= 42.8 CH ₄ = 58.1 CO ₂ = 21.9	H ₂ (1/min) = 7801.0 CO = 48.1 CH ₄ = 309.8 CO ₂ = 4.8

Cellulose [89]	TGA	Independent parallel reactions	0.1-60	N/A	N/A	N/A	210-280	N/A
Olive residue [90]	TGA	Activation Energy Distribution	2-50	20	300-900 °C	200	Hemicellulose=153-162 Cellulose= 204-215	N/A
Red algae (<i>P. yezoensis</i>) [91]	GC and TGA	(Popescu method, KAS method, FWO method)	10-50	10	25-800 °C	120	121.1-136.9	$\ln k = 20.9 - 26.9 (1/\text{min})$
Tobacco (Leaves) [92]	DTG/TGA	Global model (Two stages)	10	10	200-350 °C	250-380	17.48-25.36	$k = 1.45 - 2.994 (1/\text{min})$
Filter paper [93]	TGA	Global model	5	10	25-900 °C	40	226.54	$k = 4.8 \times 410^{16}$
Lignoboost and Acetocell [94]	TGA	Distributed reactivity models	5-40	12	25-900 °C	42.5	252.0-259.1	$k = 3.33 \times 10^{19} - 1.11 \times 10^{20}$
Corn stover [95]	TGA	Distributed activation energy model	10-30	N/A	25-1000 °C	180	77-79	N/A

Forest waste [96]	TGA	Global model (Two stages)	40	25	225-900 °C	N/A	112-232.77	$k = 3.12 \times 10^4 - 5.46 \times 10^{11}$
Sawdust [60]	TGA	Two Parallel reaction	5-50	10	25-900 °C	53-212	60.71-79.53	$k = 1.01 \times 10^3 - 1.90 \times 10^6$
Leaf of fir [97]	DTG	Global Kinetic Model (Moll Method)	10-30	10	25-700 °C	40	75.2-76.8	$\ln k = 13.6 - 16.9$
Metamorphic rice [98]	TG/DTG	Global Kinetic Model	5-20	5	25-700 °C	150-200	87.75-109.52	$k = 1.48 \times 10^7 - 5.30 \times 10^9$
Forest pinewood waste [99]	DTG	Three independent parallel reactions	100	10	15-800 °C	1000-2000	Hemicellulose=8.14 Cellulose= 15.96 Lignin= 0.25	Hemicellulose = 115 Cellulose =218 Lignin= 35
Wheat, Oat, Barley, and Brassica [100]	DTG/TGA	Distributed activation energy model	10-47	8	150-600	60	167.3- 225.7	$\log k = 12.91 - 18.71$
Cellulose, wood [67]	Pyrex reactor,	Three competitive reactions kinetic	N/A	N/A	500-1100 k	2000-6000	Gas =140 Tar=133 Char=121	Gas = 1.3×10^8 Tar= 2.0×10^8 Char= 1.07×10^7

spruce wood [101]	TGA	Primary with tar cracking	5	300	105-1050	500-1000	E, tar =117.0-320.2 E, cracking = 66.3	$k=8.20 \times 10^7$ - 3.02×10^{21} $k, \text{cracking} = 3.076 \times 10^3$
Cellulose Hemicellulose Lignin [102]	-	Shafizadeh and Bradbury	-	-	-	-	Cellulose=196.5 Hemicellulose=202.7 Lignin=143.8 Cracking=108.0	Cellulose= 3.28×10^{14} Hemicellulose= 2.6×10^{16} Lignin= 1.5×10^9 Cracking= 1.3×10^8
Pine wood [69]	Drop tube	Competitive	-	-	553-873	100-125	Gas =177 Tar=149 Char=125	Gas = 1.4×10^{11} Tar = 9.2×10^9 Char = 3.05×10^7
Beech [68]	Tube Furnace	Competitive	9	-	573-708	80	Gas =153 Tar =148 Char =112	Gas= 4.4×10^9 Tar= 1.1×10^{10} Char = 3.3×10^6
Cellulose Hemicellulose Lignin [83]	-	CPD	-	-	-	-	Cellulose=55.4* Hemicellulose =55.1 Lignin=55.4	Cellulose = 2×10^{16} Hemicellulose = 1.2×10^{20} Lignin = 7.0×10^{16}
Tar [103]	-	Tar cracking	-	-	-	-	$E=76.6$	$k=4.0 \times 10^4$

*kcal/mol

2.4. Heat of pyrolysis

In order to develop an overall process model, the heat of reaction must be combined with the rate of reaction and the other transport equations. There are two common theories regarding the heat associated with pyrolysis. One is that the pyrolysis of the woody biomass to non-condensable gases, volatiles, and char is assumed to be a series of endothermic reactions, while cracking of tar to the gas and char in the secondary reactions is considered exothermic [104]. In the second approach, the char formation process is exothermic, while the condensable and non-condensable gas formation process is endothermic [105]. Fig. 2-22 outlines the change from endothermic to exothermic at T_{shift} .

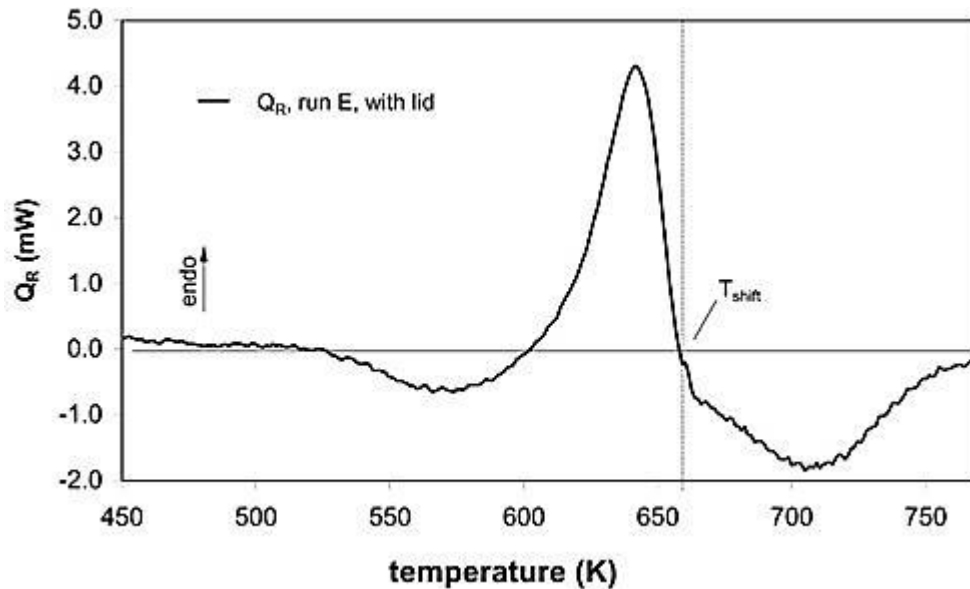


Figure 2-22: Pyrolysis heat of spruce wood measured using a DSC [106] (without permission)

Table 2-7 outlines enthalpy of pyrolysis from the literature. Differential Scanning Calorimetry (DSC) and TGA were used to measure the heat of reaction.

Table 2-7: Heat of pyrolysis

Heat of pyrolysis (kJ/kg)	Feedstock
538 (volatiles formation), -2000 (char formation)	cellulose [106]
64	Biomass [107]
274 (decomposition of cellulose and hemicellulose), -353 (decomposition of lignin)	Pinus Pinaster [105]
610 (at low heat flux), -1090 to -1725(at high heat fulx)	maple particles [104]
-255 (low conversion), 20 (high conversion)	Biomass [108]
600	wood pellets [109]
1464 (tar), -301(char and gas)	Fibrous Cellulose [110]
300	Wood slabs [111]
1256	Wood [112]
450 {150 (tar), 150 (char), 150 (gas)}	Sawdust [67]
203	Wood [113]
-420 - 0	Wood [114]

The results illustrate a large range of heats of pyrolysis, which is not unexpected given the variations in external heating rate, total heating time and type of feedstock [46]. Rath et al. [115] studied the heat of pyrolysis of beech and spruce wood based on a second theory (exothermic reaction) by using DSC. They showed that the heat of wood pyrolysis will be a function of final char yield and proposed two reaction steps, the primary reactions of volatile gases formation (endothermic) followed by primary char formation (exothermic) (Fig. 2-23). The following equation was proposed [116].

$$\Delta H_{pyrolysis} = \frac{\Delta H_{DSC}}{\ln(Y_c)} \quad (2-15)$$

In the equation 2-15, Y_c represents the final char yield at the end of pyrolysis process.

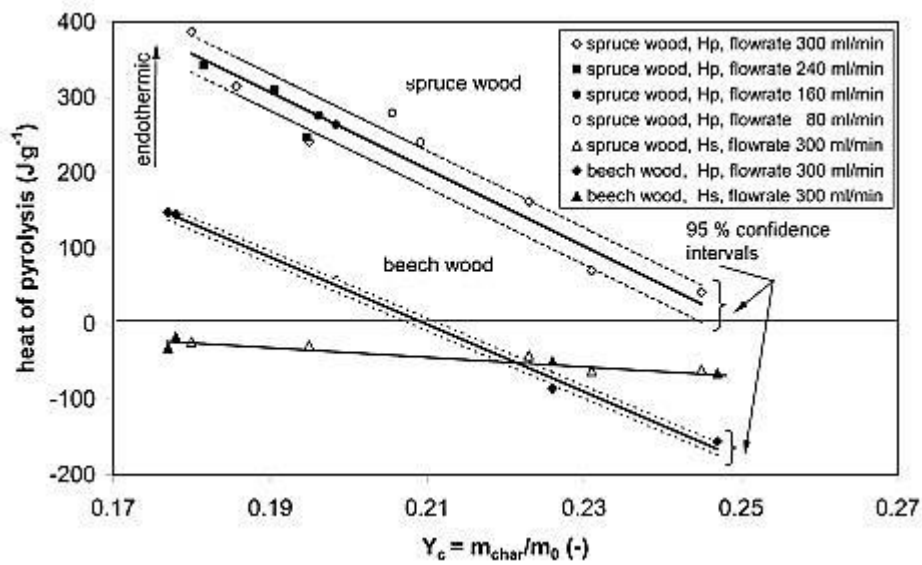


Figure 2-23: Heat of pyrolysis for spruce and beech wood as a function of final char yield [106]. Hp stands for the heat of primary pyrolysis and m_0 is initial weight of biomass (without permission)

2.5. Comparing Different Kinetic Models

The long term goal of this work is to develop an auger pyrolysis process model and use the review to determine which pyrolysis kinetic models were the most robust in terms of prediction of products as a function of fast pyrolysis operating conditions and feedstock. We performed a series of experiments in a batch tube pyrolysis system outlined elsewhere [117] using different types of softwood residues (bark, saw dust, saw chips) controlling moisture content of feedstock.

The operating conditions for our system and literature are listed in Table 2-8 and Table 2-9:

Table 2-8: Experimental conditions for the lab scale pyrolysis experiments

Feedstock	Temperature	Sample load	N ₂ flow rate	Particle size
-----------	-------------	-------------	--------------------------	---------------

	(°C)	(g)	(ml/min)	(mm)
Sawdust, wood chips, bark	400-600	2	200	2

Table 2-9: Experimental conditions of published studies/models

Author	Model	Feedstock (variety, size, mass)	Experimental System
Lewis et al. [83]	CPD	Sawdust	Burner reactor
Wagenaar et al. [69]	Primary	Sawdust	Drop tube reactor
Calonasi et al. [118]	Primary with secondary	Cellulose, Hemicellulose and lignin	Drop tube reactor
Chan et al. [67]	Competitive Reactions	Compressed Sawdust	Pyrex reactor

The experimental data were then compared with model predictions (Fig 2-24-26).

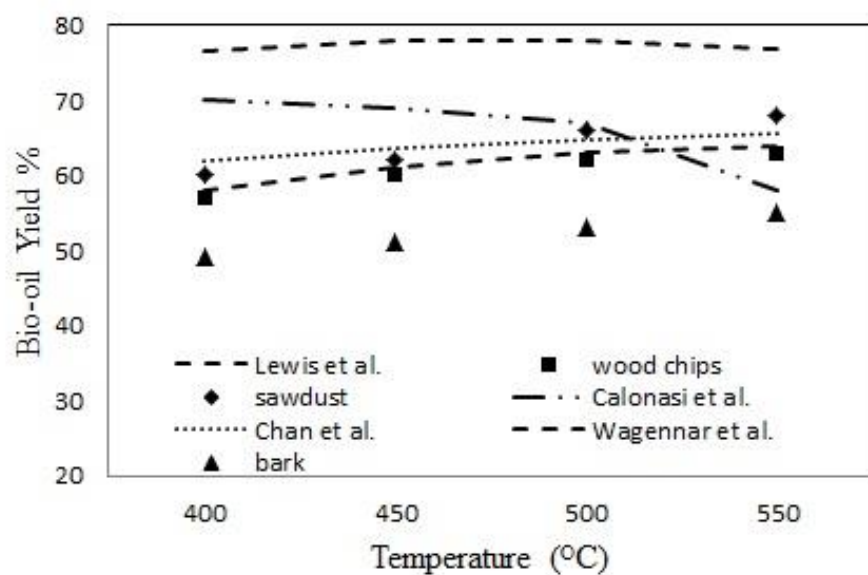


Figure 2-24: PY-Oil yield vs. temperature for sawmill residues: N₂ flow rate 200 mL/min, sample load 2 g, and particle size 2 mm

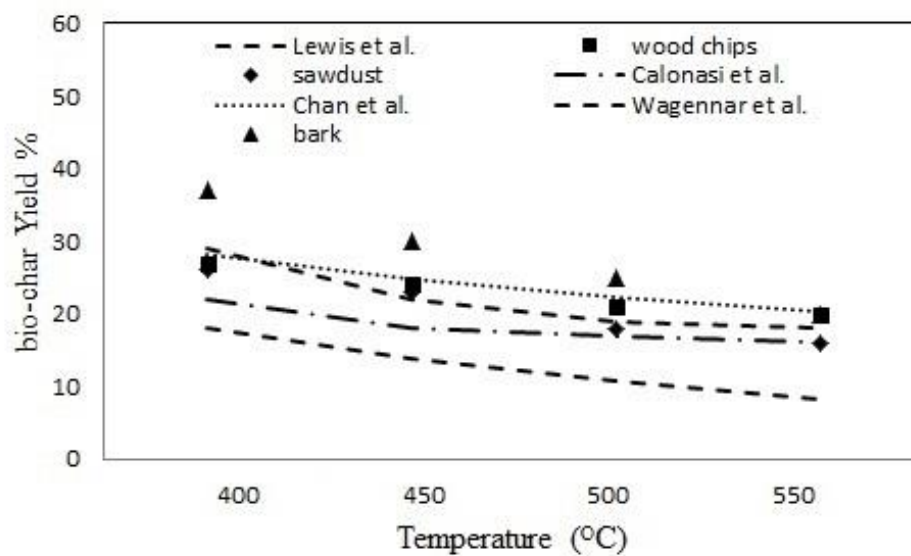


Figure 2-25: Bio-char yield vs. temperature for sawmill residues feedstock: N₂ flow rate 200 mL/min, sample load 2 g, and particle size 2 mm

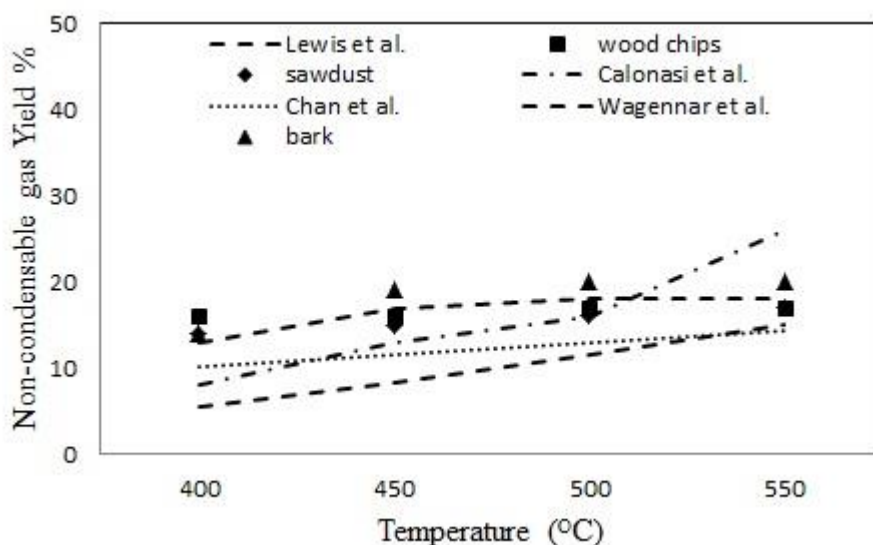


Figure 2-26: Non-condensable gas yield vs. temperature for sawmill residues feedstock: N₂ flow rate 200 mL/min , sample load 2 g, and particle size 2 mm

Table 2-10 shows the Average Relative Deviation (ARD) of experimental data from model predictions for sawdust feedstock. The Chan et al. model [67] and Lewis et al. model [83] show very good agreement with py-oil experimental data. These models have been explained in the kinetic models section and Tables 2-6 and 2-9. The different

Table 2-10: Average relative error for sawdust feedstock

Average Relative Deviation (AVE)	Lewis et al.	Wagennar et al.	Calonasi et al.	Chan et al.
Py-oil	3.8	21	11	2.8
Bio-char	4.6	41.7	14	12.2
gas	16.3	36.7	36.2	17

*For each system $ARD = 100/N_{data} \sum_{k=1}^{N_{data}} ((yield_k^{calc} - yield_k^{exp})/yield_k^{exp})$.

2.6. Conclusion

This study reviewed; the pyrolysis reactor type and optimum operating conditions, different process modeling, pyrolysis kinetic models, and the pyrolysis heat (i.e. heat of reaction). The results indicated that a shorter vapour residence time and a higher heating rate result in a higher py-oil yield with good quality. In addition, the investigation on the process modeling showed that the particle model should be coupled to the reactor model to simulate the pyrolysis reaction. Modeling of large scale chemical reactors requires knowledge of the reaction rates, either on a global or intrinsic level depending on the complexity of the reactions, as well as the mass and heat transfer rates. In this review, published reaction rate models and proposed mechanisms for the pyrolysis of woody biomass were compared. There are more than one hundred components involved in the pyrolysis of woody biomass and therefore the approach has been to develop “lumped” models where either feedstock and/or products are grouped. The model proposed by Chan et al. [67] predicted the py-oil product most accurately. In this model, woody biomass is converted to the products (i.e. py-oil, bio-char, and non-condensable gases) through competitive reactions. The review also indicated that both endothermic and exothermic reactions are reported in the literature for the pyrolysis of woody biomass.

Acknowledgment

This work has been supported by CFSI/ Department of Fisheries, Forestry and Agrifoods/ Government of Newfoundland and Labrador, BioFuelNet Canada, the Canadian Foundation for Innovation, the Natural Science and Engineering Research Council of

Canada and Memorial University of Newfoundland. In addition, the authors would like to thank the valuable contribution of Dr. Peter Fransham from ABRI-Tech Inc.

2.7. References

- [1] Naik SN, Goud V V., Rout PK, Dalai AK. Production of first and second generation biofuels: A comprehensive review. *Renew Sustain Energy Rev* 2010;14:578–97.
- [2] Mettler MS, Vlachos DG, Dauenhauer PJ. Top ten fundamental challenges of biomass pyrolysis for biofuels. *Energy Environ Sci* 2012;5:7797.
- [3] McKendry P. Energy production from biomass (part 2): Conversion technologies. *Bioresour Technol* 2002;83:47–54.
- [4] Goyal HB, Seal D, Saxena RC. Bio-fuels from thermochemical conversion of renewable resources: A review. *Renew Sustain Energy Rev* 2008;12:504–17.
- [5] Bahng MK, Mukarakate C, Robichaud DJ, Nimlos MR. Current technologies for analysis of biomass thermochemical processing: A review. *Anal Chim Acta* 2009;651:117–38.
- [6] Zhang L, Charles C, Champagne P. Overview of recent advances in thermo-chemical conversion of biomass. *Energy Convers Manag* 2010;51:969–82. doi:10.1016/j.enconman.2009.11.038.
- [7] Henriksson G, Lennholm H. *Pulp and Paper Chemistry and Technology Wood Chemistry and Wood Biotechnology*. vol. 1. 2009.
- [8] Brodin I. *C Hemical Properties and Thermal Behaviour of Kraft Lignins*. 2009.
- [9] Balat M. Production of bioethanol from lignocellulosic materials via the biochemical pathway: A review. *Energy Convers Manag* 2011;52:858–75.
- [10] Sjöström E. *Wood chemistry, fundamentals and applications*. vol. 252. 1993.
- [11] Vamvuka D. Bio-oil, solid and gaseous biofuels from biomass pyrolysis processes-An overview. *Int J Energy Res* 2011;35:835–62.
- [12] White JE, Catallo WJ, Legendre BL. Biomass pyrolysis kinetics: A comparative critical review with relevant agricultural residue case studies. *J Anal Appl Pyrolysis* 2011;91:1–33.
- [13] Meier D, Faix O. State of the art of applied fast pyrolysis of lignocellulosic materials - A review. *Bioresour Technol* 1999;68:71–7.

- [14] Jahirul M, Rasul M, Chowdhury A, Ashwath N. Biofuels Production through Biomass Pyrolysis —A Technological Review. *Energies* 2012;5:4952–5001.
- [15] Mohan D, Pittman Charles U., Steele PH. Pyrolysis of Wood/Biomass for Bio-oil: A Critical Review. *Energy & Fuels* 2006;20:848–89.
- [16] Zhang Q, Chang J, Wang T, Xu Y. Review of biomass pyrolysis oil properties and upgrading research. *Energy Convers Manag* 2007;48:87–92.
- [17] DIBLASI C. Modeling chemical and physical processes of wood and biomass pyrolysis. *Prog Energy Combust Sci* 2008;34:47–90.
- [18] Basu P. *Biomass Gasification, Pyrolysis and Torrefaction*. 2013.
- [19] Bridgwater A V. Review of fast pyrolysis of biomass and product upgrading. *Biomass and Bioenergy* 2012;38:68–94.
- [20] Heidari A, Stahl R, Younesi H, Rashidi A, Troeger N, Ghoreyshi AA. Effect of process conditions on product yield and composition of fast pyrolysis of *Eucalyptus grandis* in fluidized bed reactor. *J Ind Eng Chem* 2014;20:2594–602.
- [21] Ringer M, Ringer M, Putsche V, Putsche V, Scahill J, Scahill J. Large-Scale Pyrolysis Oil Production: A Technology Assessment and Economic Analysis. *Renew Energy* 2006:1–93.
- [22] Tang L, Huang H. Plasma pyrolysis of biomass for production of syngas and carbon adsorbent. *Energy and Fuels* 2005;19:1174–8.
- [23] Zhao Z, Huang H, Wu C, Li H, Chen Y. Biomass Pyrolysis in an Argon/Hydrogen Plasma Reactor. *Eng Life Sci* 2001;1:197–9.
- [24] Jenista J, Takana H, Hrabovsky M, Nishiyama H. Numerical Investigation of Supersonic Hybrid Argon–Water-Stabilized Arc for Biomass Gasification. *IEEE Trans Plasma Sci* 2008;36.
- [25] Ellens CJ, Brown RC. Optimization of a free-fall reactor for the production of fast pyrolysis bio-oil. *Bioresour Technol* 2012;103:374–80.
- [26] Onay Ö, Beis SH, Koçkar ÖM. Fast pyrolysis of rape seed in a well-swept fixed-bed reactor. *J Anal Appl Pyrolysis* 2001;58–59:995–1007.
- [27] Chen G, Liu C, Ma W, Zhang X, Li Y, Yan B, et al. Co-pyrolysis of corn cob and waste cooking oil in a fixed bed. *Bioresour Technol* 2014;166:500–7.
- [28] Li J. The optimal of pyrolysis process in the rotating cone reactor and pyrolysis product analysis. *Int. Conf. Challenges Environ. Sci. Comput. Eng. CESCE 2010*, vol. 1, 2010, p. 530–3.
- [29] Dijk PE, Janse AMC, Kuipers JAM, van Swaaij WPM. Hydrodynamics of liquid

- flow in a rotating cone. *Int J Numer Methods Heat Fluid Flow* 2015;11:386–412.
- [30] Luque R, Menéndez JA, Arenillas A, Cot J. Microwave-assisted pyrolysis of biomass feedstocks: the way forward? *Energy Environ Sci* 2012;5:5481.
- [31] Lei H, Ren S, Julson J. The effects of reaction temperature and time and particle size of corn stover on microwave pyrolysis. *Energy and Fuels* 2009;23:3254–61.
- [32] Zhang Z, Macquarrie DJ, De bruyn M, Budarin VL, Hunt AJ, Gronnow MJ, et al. Low-temperature microwave-assisted pyrolysis of waste office paper and the application of bio-oil as an Al adhesive. *Green Chem* 2014;17:260–70.
- [33] Ingram L, Mohan D, Bricka M, Steele P, Strobel D, Crocker D, et al. Pyrolysis of wood and bark in an auger reactor: Physical properties and chemical analysis of the produced bio-oils. *Energy and Fuels* 2008;22:614–25.
- [34] Brown JN, Brown RC. Process optimization of an auger pyrolyzer with heat carrier using response surface methodology. *Bioresour Technol* 2012;103:405–14.
- [35] Liaw SS, Zhou S, Wu H, Garcia-Perez M. Effect of pretreatment temperature on the yield and properties of bio-oils obtained from the auger pyrolysis of Douglas fir wood. *Fuel*, vol. 103, 2013, p. 672–82. doi:10.1016/j.fuel.2012.08.016.
- [36] Punsuwan N, Tangsathitkulchai C. Product characterization and kinetics of biomass pyrolysis in a three-zone free-fall reactor. *Int J Chem Eng* 2014.
- [37] Xue Q, Heindel TJ, Fox RO. A CFD model for biomass fast pyrolysis in fluidized-bed reactors. *Chem Eng Sci* 2011;66:2440–52.
- [38] Ozawa T. A New Method of Analyzing Thermogravimetric Data. *Bull Chem Soc Jpn* 1965;38:1881–6.
- [39] Ngo TA, Kim J, Kim SS. Fast pyrolysis of palm kernel cake using a fluidized bed reactor: Design of experiment and characteristics of bio-oil. *J Ind Eng Chem* 2013;19:137–43.
- [40] Abnisa F, Wan Daud WMA, Sahu JN. Optimization and characterization studies on bio-oil production from palm shell by pyrolysis using response surface methodology. *Biomass and Bioenergy* 2011;35:3604–16.
- [41] Xue Q, Dalluge D, Heindel TJ, Fox RO, Brown RC. Experimental validation and CFD modeling study of biomass fast pyrolysis in fluidized-bed reactors. *Fuel* 2012;97:757–69.
- [42] Papadikis K, Gu S, Bridgwater A V. CFD modelling of the fast pyrolysis of biomass in fluidised bed reactors. Part B. Heat, momentum and mass transport in bubbling fluidised beds. *Chem Eng Sci* 2009;64:1036–45.

- [43] Papadikis K, Gu S, Bridgwater A V, Gerhauser H. Application of CFD to model fast pyrolysis of biomass. *Fuel Process Technol* 2009;90:504–12.
- [44] Blondeau J, Jeanmart H. Biomass pyrolysis in pulverized-fuel boilers: Derivation of apparent kinetic parameters for inclusion in CFD codes. *Proc Combust Inst* 2011;33:1787–94. doi:10.1016/j.proci.2010.06.150.
- [45] Xue Q, Fox RO. Reprint of: Multi-fluid CFD modeling of biomass gasification in polydisperse fluidized-bed gasifiers. *Powder Technol* 2014;265:23–34.
- [46] Haseli Y, Van Oijen JA, De Goey LPH. Modeling biomass particle pyrolysis with temperature-dependent heat of reactions. *J Anal Appl Pyrolysis* 2011;90:140–54.
- [47] Sadhukhan AK, Gupta P, Saha RK. Modelling of pyrolysis of large wood particles. *Bioresour Technol* 2009;100:3134–9. doi:10.1016/j.biortech.2009.01.007.
- [48] Yeh A-I, Jaw Y-M. Predicting residence time distributions in a single screw extruder from operating conditions. *J Food Eng* 1999;39:81–9. doi:10.1016/S0260-8774(98)00150-2.
- [49] Trendewicz A, Braun R, Dutta A, Ziegler J. One dimensional steady-state circulating fluidized-bed reactor model for biomass fast pyrolysis. *Fuel* 2014;133:253–62. doi:10.1016/j.fuel.2014.05.009.
- [50] Xiong Q, Kong SC. Modeling effects of interphase transport coefficients on biomass pyrolysis in fluidized beds. *Powder Technol* 2014;262:96–105.
- [51] Xiong Q, Kong SC, Passalacqua A. Development of a generalized numerical framework for simulating biomass fast pyrolysis in fluidized-bed reactors. *Chem Eng Sci* 2013;99:305–13.
- [52] Anca-Couce A, Zobel N. Numerical analysis of a biomass pyrolysis particle model: Solution method optimized for the coupling to reactor models. *Fuel* 2012;97:80–8.
- [53] Miller RS, Bellan J. Numerical Simulation of Vortex Pyrolysis Reactors for Condensable Tar Production from Biomass. *Energy & Fuels* 1998;12:25–40.
- [54] Bandyopadhyay S, Chowdhury R, Biswas GK. Transient Behavior of a Coconut Shell Pyrolyzer: A Mathematical Analysis. *Ind Eng Chem Res* 1996;35:3347–55.
- [55] Klose W, Wiest W. Experiments and mathematical modeling of maize pyrolysis in a rotary kiln. *Fuel* 1999;78:65–72. doi:10.1016/S0016-2361(98)00124-0.
- [56] Biagini E, Fantei A, Tognotti L. Effect of the heating rate on the devolatilization of biomass residues. *Thermochim Acta* 2008;472:55–63.
- [57] Ren S, Lei H, Wang L, Bu Q, Chen S, Wu J. Thermal behaviour and kinetic study

for woody biomass torrefaction and torrefied biomass pyrolysis by TGA. *Biosyst Eng* 2013;116:420–6. doi:10.1016/j.biosystemseng.2013.10.003.

- [58] Zhao D, Chen K, Yang F, Feng G, Sun Y, Dai Y. Thermal degradation kinetics and heat properties of cellulosic cigarette paper: influence of potassium carboxylate as combustion improver. *Cellulose* 2013;20:3205–17.
- [59] Völker S, Rieckmann T. Thermokinetic investigation of cellulose pyrolysis - Impact of initial and final mass on kinetic results. *J Anal Appl Pyrolysis* 2002;62:165–77.
- [60] Aqsha A, Mahinpey N, Mani T, Salak F, Murugan P. Study of sawdust pyrolysis and its devolatilisation kinetics. *Can J Chem Eng* 2011;89:1451–7.
- [61] Slopiecka K, Bartocci P, Fantozzi F. Thermogravimetric analysis and kinetic study of poplar wood pyrolysis. *Appl Energy* 2012;97:491–7.
- [62] Kissinger HE. Variation of peak temperature with heating rate in differential thermal analysis. *J Res Natl Bur Stand (1934)* 1956;57:217.
- [63] Thurner F, Mann U. Kinetic investigation of wood pyrolysis. *Ind Eng Chem Process Des Dev* 1981;20:482–8.
- [64] Hashimoto K, Hasegawa I, Hayashi J, Mae K. Correlations of kinetic parameters in biomass pyrolysis with solid residue yield and lignin content. *Fuel* 2011;90:104–12.
- [65] Cardoso CR, Miranda MR, Santos KG, Ataíde CH. Determination of kinetic parameters and analytical pyrolysis of tobacco waste and sorghum bagasse. *J Anal Appl Pyrolysis* 2011;92:392–400.
- [66] Starink MJ. A new method for the derivation of activation energies from experiments performed at constant heating rate. *Thermochim Acta* 1996;288:97–104.
- [67] Chan W-CR, Kelbon M, Krieger BB. Modelling and experimental verification of physical and chemical processes during pyrolysis of a large biomass particle. *Fuel* 1985;64:1505–13.
- [68] Di Blasi C, Branca C. Kinetics of Primary Product Formation from Wood Pyrolysis. *Ind Eng Chem Res* 2001;40:5547–56.
- [69] Wagenaar BM, Prins W, van Swaaij WPM. Flash pyrolysis kinetics of pine wood. *Fuel Process Technol* 1993;36:291–8.
- [70] Scott DS, Piskorz J, Bergougnou MA, Overend RP, Graham R. The role of temperature in the fast pyrolysis of cellulose and wood. *Ind Eng Chem Res* 1988;27:8–15.

- [71] Scott DS, Piskorz J, Radlein D. Liquid products from the continuous flash pyrolysis of biomass. *Ind Eng Chem Process Des Dev* 1985;24:581–8.
- [72] Zanzi R, Sjöström K, Björnbom E. Rapid high-temperature pyrolysis of biomass in a free-fall reactor. *Fuel* 1996;75:545–50.
- [73] Lédé J, Li HZ, Villermaux J, Martin H. Fusion-like behaviour of wood pyrolysis. *J Anal Appl Pyrolysis* 1987;10:291–308.
- [74] Horne P a., Williams PT. Influence of temperature on the products from the flash pyrolysis of biomass. *Fuel* 1996;75:1051–9.
- [75] Kaushal P, Abedi J. Application of Monte-Carlo simulation to estimate the kinetic parameters for pyrolysis—Part I. *Can J Chem Eng* 2012;90:163–70.
- [76] Boutin O, Ferrer M, Lédé J. Radiant flash pyrolysis of cellulose—Evidence for the formation of short life time intermediate liquid species. *J Anal Appl Pyrolysis* 1998;47:13–31.
- [77] Dauenhauer PJ, Colby JL, Balonek CM, Suszynski WJ, Schmidt LD. Reactive boiling of cellulose for integrated catalysis through an intermediate liquid. *Green Chem* 2009;11:1555.
- [78] Piskorz J, Majerski P, Radlein D, Scott DS, Bridgwater a. . Fast pyrolysis of sweet sorghum and sweet sorghum bagasse. *J Anal Appl Pyrolysis* 1998;46:15–29.
- [79] Boutin O, Ferrer M, Lã J. Flash pyrolysis of cellulose pellets submitted to a concentrated radiation : experiments and modelling 2002;57:15–25.
- [80] Shafizadeh F, Bradbury AGW. Thermal degradation of cellulose in air and nitrogen at low temperatures. *J Appl Polym Sci* 1979;23:1431–42.
- [81] Vand V. A theory of the irreversible electrical resistance changes of metallic films evaporated in vacuum. *Proc Phys Soc* 2002;55:222–46.
- [82] Sonobe T, Worasuwanarak N. Kinetic analyses of biomass pyrolysis using the distributed activation energy model. *Fuel* 2008;87:414–21.
- [83] Lewis AD, Fletcher TH. Prediction of sawdust pyrolysis yields from a flat-flame burner using the CPD model. *Energy and Fuels* 2013;27:942–53.
- [84] Fletcher TH, Pond HR, Webster J, Wooters J, Baxter LL. Prediction of tar and light gas during pyrolysis of black liquor and biomass. *Energy and Fuels* 2012;26:3381–7.
- [85] Várhegyi G, Szabó P, Antal MJ. Kinetics of the thermal decomposition of cellulose under the experimental conditions of thermal analysis. Theoretical extrapolations to high heating rates. *Biomass and Bioenergy* 1994;7:69–74.

- [86] Radmanesh R, Courbariaux Y, Chaouki J, Guy C. A unified lumped approach in kinetic modeling of biomass pyrolysis. *Fuel* 2006;85:1211–20.
- [87] Barneto a. G, Carmona JA, Alfonso JEM, Serrano RS. Simulation of the thermogravimetry analysis of three non-wood pulps. *Bioresour Technol* 2010;101:3220–9.
- [88] González JF, Encinar JM, Canito JL, Sabio E, Chacón M. Pyrolysis of cherry stones: Energy uses of the different fractions and kinetic study. *J Anal Appl Pyrolysis* 2003;67:165–90.
- [89] Grønli MG. A theoretical and experimental study of the thermal degradation of biomass 1996:282.
- [90] Ounas A, Aboulkas A, El K, Bacaoui A, Yaacoubi A. Bioresource Technology Pyrolysis of olive residue and sugar cane bagasse: Non-isothermal thermogravimetric kinetic analysis 2011;102:11234–8.
- [91] Li D, Chen L, Zhang X, Ye N, Xing F. Pyrolytic characteristics and kinetic studies of three kinds of red algae 2011;5:1–8.
- [92] Gao W, Chen K, Xiang Z, Yang F, Zeng J, Li J, et al. Kinetic study on pyrolysis of tobacco residues from the cigarette industry. *Ind Crops Prod* 2013;44:152–7.
- [93] Huang YF, Kuan WH, Chiueh PT, Lo SL. A sequential method to analyze the kinetics of biomass pyrolysis. *Bioresour Technol* 2011;102:9241–6.
- [94] Janković B. The comparative kinetic analysis of Acetocell and Lignoboost® lignin pyrolysis: The estimation of the distributed reactivity models. *Bioresour Technol* 2011;102:9763–71.
- [95] Ma F, Zeng Y, Wang J, Yang Y, Yang X, Zhang X. Thermogravimetric study and kinetic analysis of fungal pretreated corn stover using the distributed activation energy model. *Bioresour Technol* 2013;128:417–22.
- [96] Reina J, Velo E, Puigjaner L. Thermogravimetric study of the pyrolysis of waste wood. *Thermochim Acta* 1998;320:161–7.
- [97] Liu S, Chu L, Chen M, Zhang W, Xin W. Modeling and analysis of the pyrolysis of bio-oil aqueous fraction in a fixed-bed reactor. *Fuel* 2014;133:1–6.
- [98] Yao L, Li C. Metamorphic grain pyrolysis and its kinetic parameters by different methods. *Asia-Pacific Power Energy Eng Conf APPEEC* 2009:1–4.
- [99] Amutio M, Lopez G, Aguado R, Artetxe M, Bilbao J, Olazar M. Effect of Vacuum on Lignocellulosic Biomass Flash Pyrolysis in a Conical Spouted Bed Reactor. *Energy & Fuels* 2011;25:3950–60.

- [100] Várhegyi G, Chen H, Godoy S. Thermal decomposition of wheat, oat, barley, and brassica carinata straws. a kinetic study. *Energy and Fuels* 2009;23:646–52.
- [101] Rath J, Staudinger G. Cracking reactions of tar from pyrolysis of spruce wood. *Fuel* 2001;80:1379–89.
- [102] Miller RS, Bellan J. A Generalized Biomass Pyrolysis Model Based on Superimposed Cellulose, Hemicellulose and Lignin Kinetics. *Combust Sci Technol* 1997;126:97–137.
- [103] Morf P, Hasler P, Nussbaumer T. Mechanisms and kinetics of homogeneous secondary reactions of tar from continuous pyrolysis of wood chips. *Fuel* 2002;81:843–53.
- [104] Lee CK, Chaiken RF, Singer JM. Charring pyrolysis of wood in fires by laser simulation. *Symp Combust* 1977;16:1459–70. doi:http://dx.
- [105] Bilbao R, Mastral JF, Ceamanos J, Aldea ME. Modelling of the pyrolysis of wet wood. *J Anal Appl Pyrolysis* 1996;36:81–97.
- [106] Milosavljevic I, Oja V, Suuberg EM. Thermal Effects in Cellulose Pyrolysis: Relationship to Char Formation Processes. *Ind Eng Chem Res* 1996;35:653–62.
- [107] Park WC. A STUDY OF PYROLYSIS OF CHARRING MATERIALS AND ITS APPLICATION TO FIRE SAFETY AND BIOMASS UTILIZATION by. Assessment 2008.
- [108] Koufopoulos CA, Papayannakos N, Maschio G, Lucchesi A. Modelling of the pyrolysis of biomass particles. Studies on kinetics, thermal and heat transfer effects. *Can J Chem Eng* 1991;69:907–15.
- [109] Bennini S, Castillo S, Traverse JP. Effects of an intense thermal flux on a lignocellulosic material. *J Anal Appl Pyrolysis* 1991;21:305–14.
- [110] Curtis LJ, Miller DJ. Transport model with radiative heat transfer for rapid cellulose pyrolysis. *Ind Eng Chem Res* 1988;27:1775–83.
- [111] MILLER CA, RAMOHALLI KNR. A Theoretical Heterogeneous Model of Wood Pyrolysis. *Combust Sci Technol* 1986;46:249–65.
- [112] Kanury AM, Holve DJ. Transient Conduction With Pyrolysis (Approximate Solutions for Charring of Wood Slabs). *J Heat Transfer* 1982;104:338–43.
- [113] Roberts AF. The heat of reaction during the pyrolysis of wood. *Combust Flame* 1971;17:79–86.
- [114] Kung H-C, Kalelkar AS. On the heat of reaction in wood pyrolysis. *Combust Flame* 1973;20:91–103.

- [115] Rath J, Wolfinger MG, Steiner G, Krammer G, Barontini F, Cozzani V. Heat of wood pyrolysis. *Fuel* 2003;82:81–91.
- [116] Agarwal G, Lattimer B. Physicochemical, kinetic and energetic investigation of coal-biomass mixture pyrolysis. *Fuel Process Technol* 2014;124:174–87.
- [117] Papari S, Hawboldt K, Helleur R. Pyrolysis: A Theoretical and Experimental Study on the Conversion of Softwood Sawmill Residues to Biooil. *Ind Eng Chem Res* 2015;54:605–11.
- [118] Calonaci M, Grana R, Barker Hemings E, Bozzano G, Dente M, Ranzi E. Comprehensive kinetic modeling study of bio-oil formation from fast pyrolysis of biomass. *Energy and Fuels* 2010;24:5727–34.

3.CHAPTER THREE

A Theoretical and Experimental Study on the Conversion of Softwood Sawmill residues to Pyrolysis Oil in a Lab-scale Reactor

This chapter has been **published**; Papari S, Hawboldt K, Helleur R. Pyrolysis: a theoretical and experimental study on the conversion of softwood sawmill residues to py-oil. Industrial & Engineering Chemistry Research. 2015 Jan 12;54(2):605-11.

Abstract

The literature review indicated that the final pyrolysis product distributions are a function of parameters, such as reactor type and operating conditions, type of feedstock, and properties. As such, the significant operating variables must be optimized prior to investigate the impact of biomass type and properties on py-oil yield and quality. In this chapter, an analysis of pyrolysis of sawmill residues is performed in a lab scale pyrolysis unit to minimize the heat and mass transfer effects. Three factors, including pyrolysis temperature, feedstock particle size and nitrogen flow rate in the reactor are optimized using response surface methodology. A two-factor based models, a three-factor quadratic model and a quadratic model without factor interactions coefficients and two kinetic models (one based on primary reactions only, the second including secondary reactions) are compared. The factor-based models (with and without interactions) were developed using design of experiment software and Genetic Algorithm, respectively. The results showed that the quadratic model with interactions between factors predicts the experimental data more accurately rather than other models. However, the quadratic models are experiment specific and can only be used as a design tool. The primary kinetic model predicts the experimental data trend below 550 °C well; however, as temperature rises (>550 °C), including secondary reactions gives better predictions.

Keyword: Softwood shavings, Pyrolysis, Py-oil, Kinetic modeling, Genetic algorithm, DOE, Water content

3.1. Introduction

The concerns associated with the use of fossil fuel have increased attention to other renewable and sustainable source of energy. Bio-based fuels, which are attractive alternative to fossil fuels, are obtained from different feedstock, such as forest residues, agricultural waste, sawmill residues, demolition wood, microalgae, etc. Enzymatic and thermochemical conversion are the most common methods for converting lignocellulosic biomass to biofuel [1]. Combustion, pyrolysis, torrefaction, and gasification are typical thermochemical conversion. Based on operating temperature and heating rate, pyrolysis is categorized in to slow (low heating rate in favor of bio-char production) and fast (high heating rate in favor of py-oil production). Fast pyrolysis produced the highest py-oil yield (50-75%) and offers the advantage of being a relatively fast process compared to enzymatic conversion and does not require the level of pretreatment of the woody biomass (e.g. steam explosion, hydrolysis etc.) [1-3].

Mathematical modeling and simulation of reactors for the pyrolysis of woody biomass have been developed by a number of researchers [4-7]. The results of these models can be valuable for scale-up. There are a few mathematical models for converting biomass to biofuel during pyrolysis. Abnisa et al. [4] optimized py-oil produced from palm shell waste using response surface methodology (RSM) in a fixed bed reactor. The optimum py-oil yield occurred at temperature of 500 °C, carrier gas (N₂) flow rate of 2 L/min, particle size of 2 mm, and reaction time of 60 min. Ellens and Brown [5] modeled a free-fall reactor for the production of py-oil from red oak feedstock. The effect of some significant variables including heater set-point temperature, biomass particle size, sweep

gas flow rate and biomass feed rate were investigated using the central composite design method. The optimum py-oil yield was obtained at a set-point temperature of 575 °C, feedstock rate of 2 kg/h, and particle size less than 300 µm. Ngo et al. [6] optimized and characterized the py-oil production from palm kernel cake feedstock in a fluidized bed reactor using design of experiment (DOE). A model for liquid production was developed based on feed rate, temperature, and particle residence time. Brown and Brown [7] optimized the operational parameters of an auger pyrolyzer with heat carrier using response surface methodology. Heat carrier, inlet temperature, mass flow rate, rotational speed of screws in the reactor, and volumetric flow rate of sweep gas were studied. The py-oil was maximized using a higher heat carrier temperature (600 °C), high auger speeds (63 rpm) and high heat carrier mass flow rates (18 kg/h). Paulsen et al. [8] investigated the influence of pyrolysis temperature and feedstock dimension on the yield of individual products from cellulose pyrolysis without transport effects. They concluded that differences in product yields between powdered feedstock and thin films are the result of mass transfer effects rather than temperature gradients within powdered samples.

Unlike previous work where the impacts of individual parameters were investigated, in this study the effects of all significant factors and interactions between factors were studied to determine the effect on yields. This information is critical for scale up and process modeling. In this study, two different types of models (factor based approach and kinetic based) were compared based on lab-scale reactor experiments. The objectives for developing factor based models were as follows: i) optimization of operating conditions, ii) investigation of the influence of interaction between factors. The kinetic study will

provide information to help select an appropriate model for inclusion for process model development of the larger scale pyrolysis reactor.

3.2. Experimental Design

DOE (Design-Expert 9.0.0) is a tool used in the management and optimization of a number of experiments. Response surface methodology (RSM), with a central composite design (CCD) was used to investigate the impact of factors on the product yield and to develop a model. Three significant variables including temperature (400°C to 600 °C), three average particle sizes between (0.1 to 2.0 mm) and sweep gas flow rate (200 mL/min to 800 mL/min) were investigated [9-12]. In this study, five center point replicate experiments were performed, for a total of 19 experiments. Each run was performed in duplicate.

3.2.1. Statistical Analysis

Experimental results were evaluated using analysis of variance (ANOVA) and standard least squares regression modeling. Quadratic models were developed to predict yields (py-oil and char) using the following power-second order polynomials as per CCD methodology:

$$Y_k = \beta_0 + \sum_{i=1}^4 \beta_i X_i + \sum_{i=1}^4 \sum_{j=1}^4 \beta_{ij} X_i X_j + \sum_{j=1}^4 \beta_{ii} X_i^2 \quad k= 1,2,3 \quad (3-1)$$

where, Y_1 and Y_2 represent py-oil and bio-char yields, respectively. The coefficients β_0 , β_i , β_{ij} , and β_{ii} are obtained from fitting the model and X_i , and X_j , are the factors being studied (e.g. temperature, N_2 flow rate and average particle size).

The factors are normalized to vary between -1 and +1, according to the equation 3-2 [13]:

$$X_i = \frac{x_i - x_i^0}{\Delta x_i} \quad (3-2)$$

where, x_i^0 is the midpoint, x_i is the real value, Δx_i is the half range, and X_i is the coded value which varies from -1 to +1.

The model coefficients (β_0 , β_i , β_{ij} and β_{ii}) were obtained using the following equations:

$$\beta_0 = a_1 \sum_{u=1}^n Y_u + a_2 \sum_{i=1}^k \sum_{u=1}^n Y_u X_{iu}^2 \quad (3-3)$$

$$\beta_i = a_3 \sum_{u=1}^n X_{iu} Y_u \quad (3-4)$$

$$\beta_{ij} = a_4 \sum_{u=1}^n X_{iu} X_{ju} Y_u \quad (3-5)$$

$$\beta_{ii} = a_5 \sum_{u=1}^n X_{iu}^2 Y_u + a_6 \sum_{i=1}^k \sum_{u=1}^n Y_u X_{iu}^2 - a_7 \sum_{u=1}^n Y_u \quad (3-6)$$

where a_1 , a_2 , a_3 , a_4 , a_5 , a_6 , and a_7 are determined from the literature [14]. After calculating the regression coefficients, the impact on the final yield was estimated. From this data the factor based model was developed.

3.3. Kinetic Model

A common approach to represent the components of pyrolysis is to lump them into generalized groups. The three parallel reactions scheme, which groups products as gas, oil, and char, has been widely used (Fig. 3-1) [9,15,16].

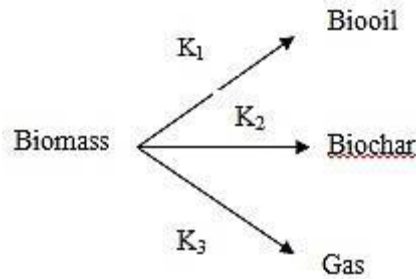


Figure 3-1: Primary reactions for converting biomass to py-oil, bio-char and gas

A number of researchers included a secondary oil cracking model as outlined in Figure 3-2 [17-20].

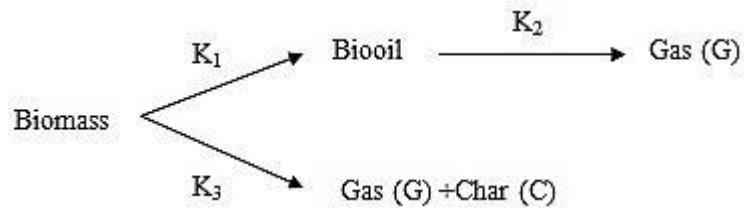


Figure 3-2: Primary with secondary oil cracking kinetic mechanism

In this model the biomass is decomposed during primary reactions to produce py-oil, bio-char and non-condensable gas. Subsequently, the oil is converted to light gas through secondary reactions (cracking). All the reactions are proposed as first order, this assumption was considered by many researchers [9,15,16]. In this study both primary and primary with secondary (oil cracking) reactions are compared. The primary reactions are those which convert biomass to py-oil, bio-char, and gas, and the secondary reaction is that which converts the oil to gas.

3.4. Experimental

3.4.1. Feedstock

Fresh balsam fir (softwood sawmill) shavings were obtained from Sexton Lumber sawmill (Bloomfield, Newfoundland and Labrador). The initial moisture content of feedstock was higher than 30 %. The feedstock was dried for two days at ambient temperature to decrease the moisture to ~12%; the moisture was lowered to 2.0 % by drying overnight in the oven at 70 °C. The softwood shavings were processed through a cutter mill with a range of particle sieves to produce the required particle sizes for each experiment (0.1 mm – 2.0 mm). Table 3-1 shows the composition of common softwood species in Newfoundland and Labrador.

Table 3-1: Proximate analysis of dried softwood feedstock

Composition [wt%]	Softwood
Low volatile matter	3.82
Medium volatile matter	78.14
Fixed carbon	17.21
Ash	0.83

3.4.2. Semi-batch reactor

The pyrolysis experiments were carried out in a semi-batch tube reactor (Thermolyne® 21100 tube furnace, USA) (Fig. 3-3). The furnace temperature was calibrated using a thermocouple at the centre and ends of the sample tube. The temperature gradient between the centre and ends was 2 °C – 3 °C. The sawmill shavings were milled and sieved to obtain three sample average particle size (ranges) of 0.3 mm (0.1 mm - 0.5 mm), 0.75 (0.5 mm – 1 mm), and 1.5 mm (1 mm-2 mm). The samples were placed in a 1.5 cm

(id) by 15 cm glass sample boat. The boat was flushed with nitrogen and then inserted into a 3 cm (id) by a 70 cm glass column equipped with a stopcock connected to a nitrogen supply for sweeping volatile products. To avoid air infiltration into the reactor a pre-drilled rubber stopper was used for the end of the column where the sample hook protruded. At the exit, the column was joined to a “T” shaped connector, with a 20 mL flask to collect produced py-oil with the other connected to an air condenser. The exit gases were further cooled in a liquid nitrogen-filled glass condenser trap to drop out liquids from the gas stream. The heating rate of the tube furnace in order to reach the set pyrolysis temperature was 30 °C/min.

One gram of feedstock was placed in the sample boat once the reactor temperature reached the set point. The nitrogen flow rate was varied from 200 mL/min to 800 mL/min and measured at 25°C and 1 atm. After pyrolysis, the sample boat was extracted and weighed to determine bio-char production. Some of the py-oil coated the inner parts of the exit surfaces, and therefore total py-oil yields were calculated by weighing the flasks, air condenser, elbow, nitrogen trap, and “T” connector. This py-oil weight calculation is therefore the sum of the collected and trapped oil and is a more accurate measurement. The oil and char yield were determined by using Eq. 3-7 and 3-8:

$$\text{Py-oil yield \%} = \frac{\text{mass of oil}}{\text{mass of feedstock biomass}} \times 100, \quad (3-7)$$

$$\text{Bio-char yield \%} = \frac{\text{mass of char}}{\text{mass of feedstock biomass}} \times 100, \quad (3-8)$$

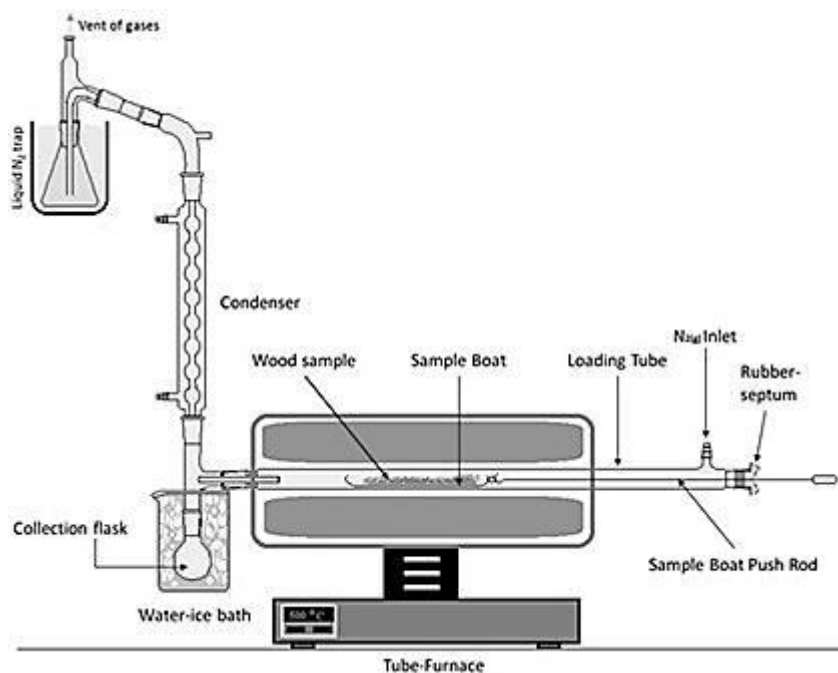


Figure 3-3: Schematic of lab-scale pyrolysis system

3.5. Results and Discussion

3.5.1. ANOVA analysis

The quadratic mathematical models were based on the backwards elimination method using the analysis of the response of the important combinations, fitting the experimental data, and evaluating the errors of the model. These models do not represent a reaction rate model, but rather can be used as tool in the scale up of pyrolysis systems in process optimization. The drawback to developing a reaction rate model is that it is difficult to produce a model which represents the entire range of pyrolysis operating conditions as the reaction mechanisms shift (primary to secondary and phases) over narrow temperature and other operating ranges. As previously stated, the significant factors were temperature

(x_1), average particle size (x_2) and the sweep gas flow rate (x_3), the responses were bio oil (Y_1) and char (Y_2) yields. Based on ANOVA (see Table 3-2 and 3-3) for the quadratic polynomial py-oil yield model, the F-value is adequately large and the p-value is small (less than 0.05) which indicates the models are in good agreement with the experimental data [14]. In addition, the Adj (adjusted) R-squared and Pred (predicted) R-squared should be in reasonable agreement with each other. Adjusted regression coefficient (Adj R-squared) accounts for the addition of extraneous parameters to a model and adjusts the regression coefficient accordingly [21]. Prediction regression coefficient (Pred R-squared) confirms the predictive ability of a proposed model [22].

The Adj R-squared and Pred R-squared values for the py-oil model are 0.97 and 0.94, respectively; the bio-char model are 0.97 and 0.94. The Adeq Precision, measures the signal-to-noise ratio and should be greater than four, the values from this analysis for py-oil and bio-char are 34.87 and 32.12, respectively. Adequate precision coefficient (Adeq Precision) was used to demonstrate the significance and adequacy of a model [23].

Table 3-2: ANOVA for response Surface reduced quadratic model (py-oil)

Source	SS	DF	MS	F-value	P-value	Mark
Quadratic Model	479.38	6	79.90	108.26	<0.0001	Significant
A-Temperature	0.023	1	0.023	0.031	0.8634	
B-Particle size	147.89	1	147.89	200.39	< 0.0001	
C-N ₂ Flowrate	40.00	1	40.00	54.20	< 0.0001	
AB	3.84	1	3.84	5.20	0.0417	

A^2	94.10	1	94.10	127.50	< 0.0001	
C^2	19.17	1	19.17	25.97	0.0003	
Residual	8.86	12	0.74			
Lack of fit	7.56	8	0.94	2.91	0.1589	Not significant
Pure error	1.30	4	0.33			
Cor Total	488.24	18				

Table 3-3: ANOVA for response surface reduced quadratic model (bio-char)

Source	SS	DF	MS	F-value	P-value	Mark
Quadratic Model	507.54	6	84.59	128.75	< 0.0001	Significant
<i>A</i> -Temperature	417.22	1	417.22	635.01	< 0.0001	
<i>B</i> -Particle size	0.43	1	0.43	0.66	0.4336	
<i>C</i> -N ₂ FR	0.026	1	0.026	0.040	0.8448	
<i>AB</i>	3.57	1	3.57	5.43	0.0381	
<i>BC</i>	6.71	1	6.71	10.22	0.0077	
A^2	71.90	1	71.90	109.43	< 0.0001	
Residual	7.88	12	0.66			
Lack of fit	7.18	8	0.90	5.13	0.0657	Not significant
Pure error	0.70	4	0.18			
Total	515.42	18				

The quadratic terms (i.e., A^2 and C^2), the interaction between average particle size-temperature (AB), average particle size (B), and N_2 flow rate (C) are significant model terms. The best mathematical fit is obtained by using the above statistical concepts and eliminating coefficients which have no significant effect on the response. For example, in this case study, the interaction between parameters, including average particle sizes-sweep gas flow rate (BC) and temperature- sweep gas flow rate (AC), are not significant. In the bio-char model, both AB and BC are significant and they appear in the model, while AC is eliminated. The following reduced term quadratic models are used to predict the py-oil and bio-char yield.

Table 3-4: Quadratic model: py-oil and bio-char yields based on coded factors

Py-oil	$65.12 + 0.049A - 6.36B + 2C + 1.15A \times B - 5.47A^2 - 2.47C^2$
Bio-char	$17.63 - 6.64A + 0.34B - 0.053C - 1.11A \times B + 1.52B \times C + 3.91A^2$
Code	$A = \text{temperature} , B = \text{Average particle size}, C = N_2 \text{ flow rate}$

These quadratic models are not process models, but rather can be used as a tool to optimize operating conditions in the larger scale systems, and, more importantly, to identify the scale and direction of the interactions between key operating parameters. Identifying these interactions would be extremely difficult in large scale systems due to transport effects and scale.

As Figure 3-4 illustrates the py-oil yield increases from 56% to 62% by increasing the temperature from 400 to 500 °C for an average particle size of 1.5 mm and a N₂ flow rate of 500 ml/min. This increase may be due to the fact that softwood components (lignin, cellulose, and hemicellulose) depolymerize at the higher pyrolysis temperature and result in a higher production of py-oil. As temperature increases, the bio-char yield decreases, and the amount of py-oil and non-condensable gas increases. At lower temperatures (i.e. 400 °C –450 °C) the degradation of components in the feedstock in shorter condensable molecules decreases, resulting in less py-oil. The py-oil yield increases from 62% to 70% when the average particle size decreases from 1.5 to 0.3 mm at 500 °C and 500 ml/min N₂ flow rate. Shen et al. [10] observed the same trend and concluded that the heating rate experienced by the particle, the rates will be slower and less uniform as the particle size increases. However, Shen et al. [10] also observed this effect was not significant as the particle size was increased to 5.6 mm (i.e. oil yield did not decrease further).

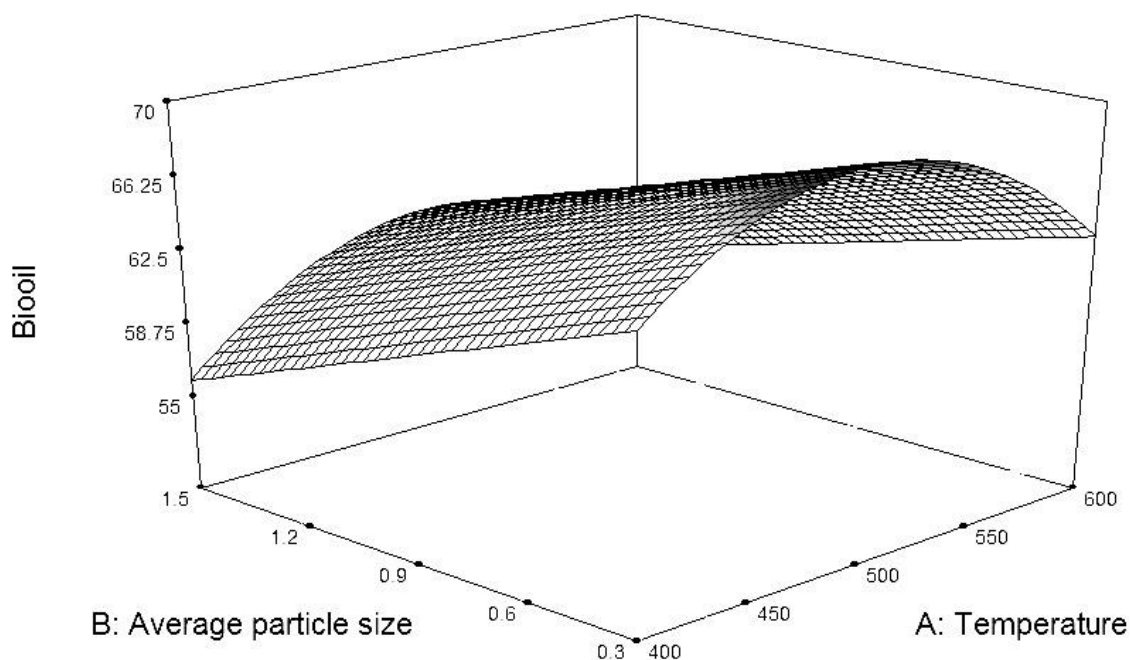


Figure 3-4: Effect of pyrolysis temperature ($^{\circ}\text{C}$) and particle size (mm) on Py-oil yield of wood shaving feedstock; N_2 flow rate = 500 mL/min

The effects of sweep gas flow rate and temperature are shown in the Fig. 3-5. The py-oil yield increases with N_2 flow rate. For example, the py-oil yield goes up from 57.5% to 62% when N_2 flow rate increased from 200 to 500 ml/min at 500 $^{\circ}\text{C}$ and 1.5 mm particles. This result has been demonstrated in other studies [11, 24]. Increasing the gas flow rate decreases the residence time of volatile gases and subsequently, the secondary reactions are reduced. Primary reactions are proposed as first order where py-oil and gas are favoured over bio-char. The subsequent secondary reactions result in py-oil components converting to biogas as a result of cracking reactions [25, 26]. A common way to minimize these secondary reactions is to decrease the volatile residence time. However, there are some limitations to this approach with this apparatus. An increase in

the sweep gas flow rate results in volatile gases quickly passing through both the condenser and nitrogen trap. The reduced residence time in the cooling system does not allow efficient separation of condensable and non-condensable gases and subsequently, the py-oil yield decreases.

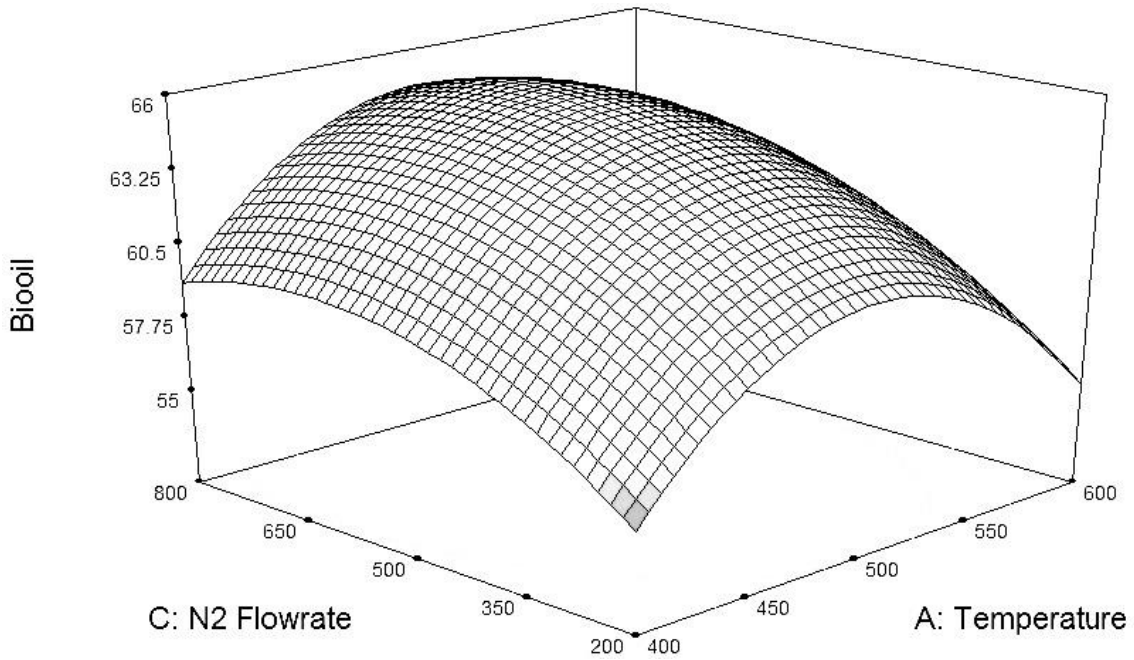


Figure 3-5: Effect of pyrolysis temperature ($^{\circ}\text{C}$) and N_2 flow rate (mL/min) on py-oil yield; average particle size = 0.75mm

Figures 3-6 to 3-8 illustrate the influence of temperature, average particle size, and N_2 flow rate on py-oil, bio-char, gas and water yield. The trend of bio-char and gas production is reversed (Fig. 3-3 to 3-6). The bio-char decreases with increasing temperature; however, the non-condensable gas increases as reactor temperature increases. The trend for py-oil is ascending for temperatures in the range of $400\text{-}550\text{ }^{\circ}\text{C}$, while descending for temperature higher than 550°C . Figures 6-8 summarizes the amount of

water chemically produced (water content (WC) of py-oil samples measured in duplicate using Karl-Fischer titration). The WC decreases when N₂ flow rate increases. This is likely as result of increasing N₂ flow rate decreases the vapour residence time and subsequently secondary reactions (cracking) decrease. In addition, feedstocks with smaller particle size produces lower amounts of water due to decreased heat/mass transfer resistances. These results are in agreement with work by Uzun et al [11].

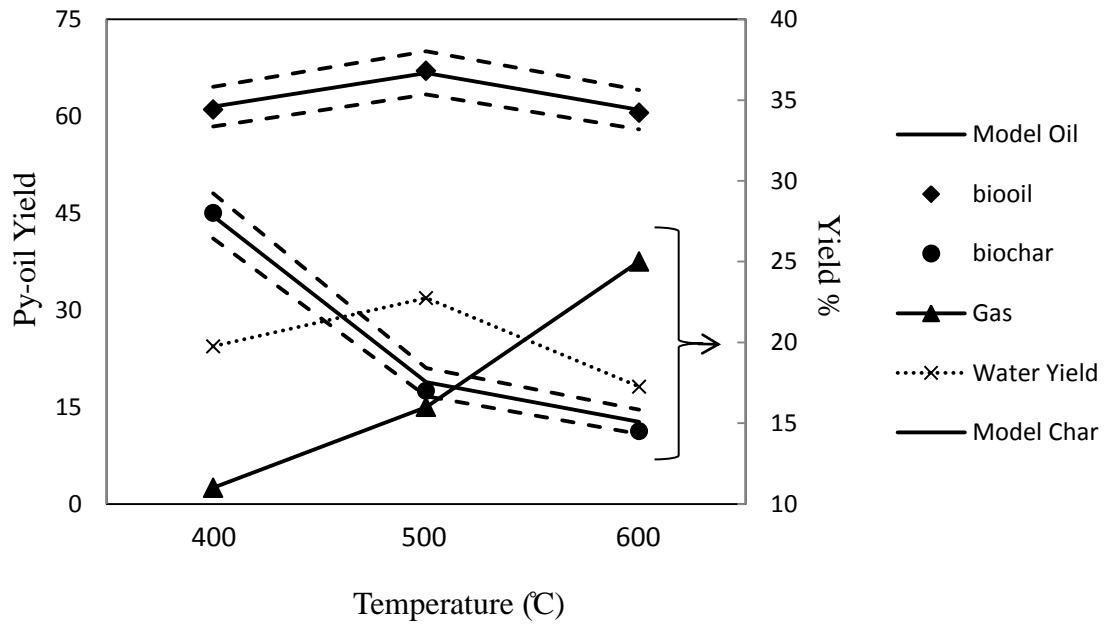


Figure 3-6: Py-oil, bio-char, gas* and water yield vs. temperature at 0.75mm particle size, 500 ml/min sweep gas flow rate (dotted lines represent 95% confidence interval).* the gas yield was measured by difference

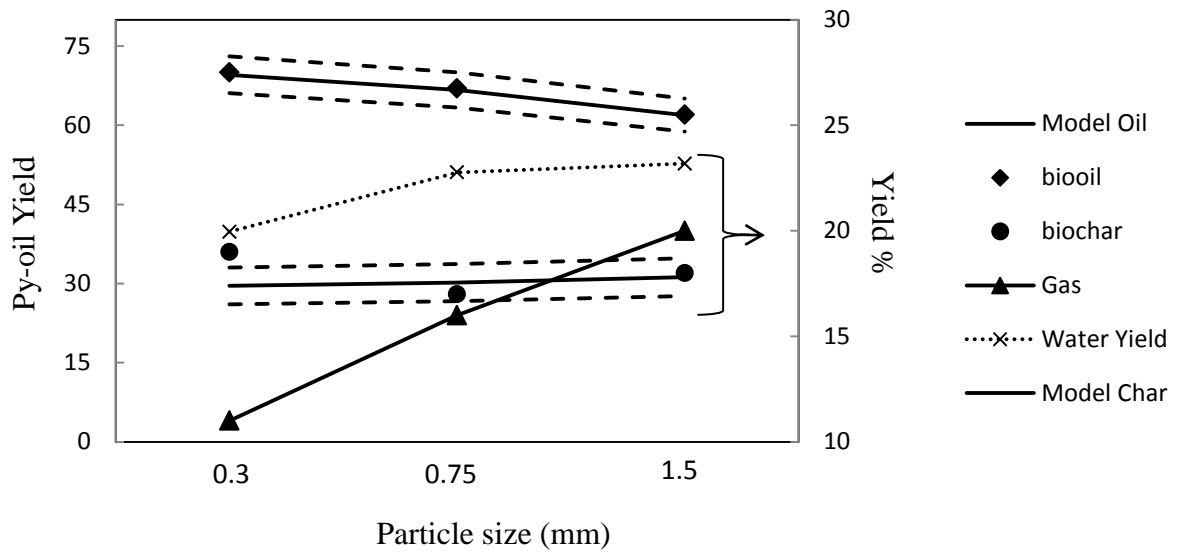


Figure 3-7: Py-oil, bio-char, gas* and water yield vs. temperature at 500°C temperature, 500 ml/min sweep gas flow rate (dotted lines represent 95% confidence interval). * gas yield was measured by difference

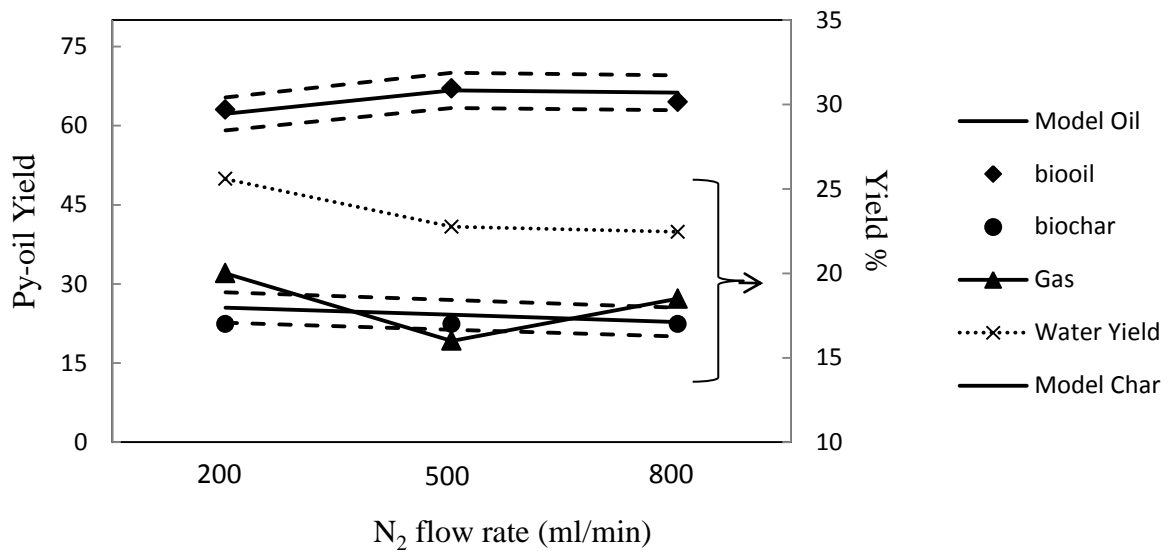


Figure 3-8: Py-oil, bio-char, gas* and water yield vs. temperature at 0.75mm particle size, 500°C temperature, (dotted lines represent 95% confidence interval). * gas yield was measured by difference

The kinetic and factor based models (Tables 3-4 and 3-5) are compared with the lab data (Fig. 3-9). The kinetic and quadratic parameters are summarized in Table 3-5.

As figure 9 shows, the quadratic model with interactions (Table 3-4) better predicts the py-oil yield compared to the quadratic model without interactions. This highlights the complex nature of the reactions occurring and the importance of the interactions between the various parameters. For temperatures below 550 °C, the primary reaction kinetic model predicts experimental data trend well; however, for those higher than 550 °C, the secondary reaction should be included. Although the quadratic models with considering interactions predict the experimental data very well, there is a limitation in using these types of factor based models in larger scale. For large scale process modeling, mass and heat transfer effects must be considered. Coupling these kinetic models with the heat, mass and momentum equations into a process model could be used as a simulation tool for larger scale reactor systems.

Table 3-5: Fitted parameters for the quadratic and kinetic models

Quadratic Model without interactions yield= $a + bT + cT^2$	Parameter a	Parameter b	Parameter c
	0.539	0.368	0.0004
Primary [9] $r = k_1 \times \exp\left(-\frac{E_1}{RT}\right)(M_{feed} - M_{feed}^\infty)$	$k_1(s^{-1})$, E_1 (kJ/mol)	$k_2(s^{-1})$, E_2 (kJ/mol)	
	9.38×10^9	149	-
Primary with secondary [12] $r = k_1 \times \exp\left(-\frac{E_1}{RT}\right)(M_{feed} - M_{feed}^\infty) - k_2 \times \exp\left(-\frac{E_2}{RT}\right)M_{oil}$	0.703×10^{13}	183.3	4.28×10^6
			107.5

M_{feed} is weight of biomass and M_{feed}^∞ is the weight of biomass when pyrolysis is completed.

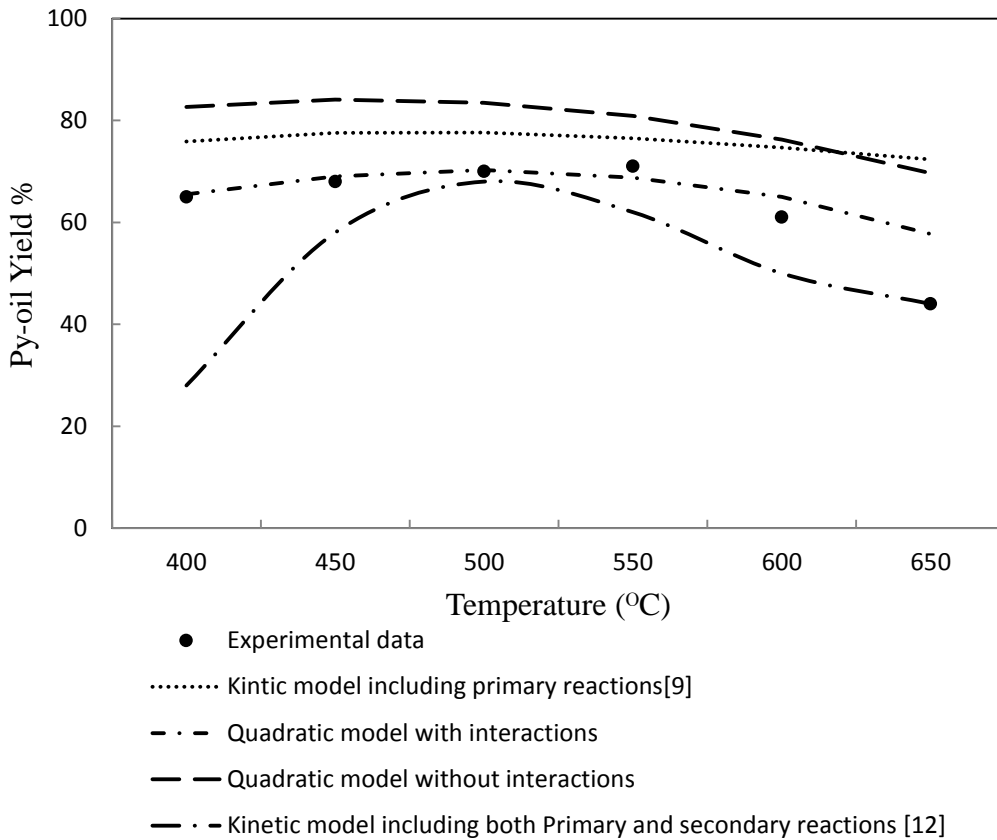


Figure 3-9: Comparison between experimental data and different models (Average particle size: 0.3 mm and sweep gas flow rate: 500 ml/min)

3.6. Conclusions

In this paper, a series of lab-scale pyrolysis experiments on softwood sawmill residues were performed to determine the impact of various operating parameters. Heat and mass transfer resistances are minimized in this type of reactor and therefore the impact of temperature, particle size and sweep gas flow rate on reaction rates could be studied independently of transport phenomena. The results showed that the quadratic model proposed in this study predicted the data well. The optimum values are as follows: a pyrolysis temperature in the range of 500 °C - 550 °C, a N₂ flow rate of 500 mL/min, and

an average particle size 0.3 mm. Furthermore, the higher sweep gas flow rate and smaller particle size resulted in lower amount of water produced during pyrolysis. In addition to optimization, two different factors based and kinetic models were compared. The results indicated that the quadratic model with interactions predicts the experimental data well; however, for process models to be used in larger scale systems, kinetic models are required. Two kinetic models were used; one was based on a primary reaction mechanism and the second on both primary and secondary reaction mechanism. The primary kinetic models are adequate for reactors operating at temperatures lower than 550 °C, while simultaneous primary and secondary reaction models should be used for temperatures higher than 550 °C.

Acknowledgment

This work has been supported by CFSI/ Department of Fisheries, Forestry and Agrifoods/ Government of Newfoundland and Labrador, BioFuelNet Canada, the Canadian Foundation for Innovation, the Natural Science and Engineering Research Council of Canada and Memorial University of Newfoundland. In addition, the authors would like to thank the valuable contribution of Dr. Peter Fransham from ABRI-Tech Inc.

3.7.References

- [1] Naik, S. N., Goud, V. V., Rout, P. K., & Dalai, A. K. Production of first and second generation biofuels (2010): a comprehensive review. *Renewable and Sustainable Energy Reviews*, 14, 578-597.
- [2] Matthew S. Mettler, Dionisios G. Vlachos and Paul J. Dauenhauer, Top ten fundamental challenges of biomass pyrolysis for biofuels (2012), *Energy Environ. Sci.*, 5, 7797-7809.
- [3] Bridgwater. A.V., IEA Bioenergy Annual Report (2007): Biomass Pyrolysis. 4-16
- [4] Abnisa, F., Wan Daud, W. M. A., & Sahu, J. N. Optimization and characterization studies on bio-oil production from palm shell by pyrolysis using response surface methodology (2011). *Biomass and Bioenergy*, 35, 3604-3616.
- [5] Ellens, C. J., & Brown, R. C. Optimization of a free-fall reactor for the production of fast pyrolysis bio-oil (2012). *Bioresource technology*, 103, 374-380.
- [6] Ngo, T. A., Kim, J., & Kim, S. S. Fast pyrolysis of palm kernel cake using a fluidized bed reactor: Design of experiment and characteristics of bio-oil (2013). *Journal of Industrial and Engineering Chemistry*, 19, 137-143.
- [7] Brown, J. N., & Brown, R. C. Process optimization of an auger pyrolyzer with heat carrier using response surface methodology (2012). *Bioresource technology*, 103, 405-414.
- [8] Paulsen, A. D., Mettler, M. S., & Dauenhauer, P. J. The role of sample dimension and temperature in cellulose pyrolysis (2013). *Energy & Fuels*, 27, 2126-2134.
- [9] Wagenaar, B. M., Prins, W., & Swaaij, V. W. Flash pyrolysis kinetics of pine wood (1993). *Fuel processing technology*, 36, 291-298.
- [10] Shen, J., Wang, X. S., Garcia-Perez, M., Mourant, D., Rhodes, M. J., & Li, C. Z. Effects of particle size on the fast pyrolysis of oil mallee woody biomass (2009). *Fuel*, 88, 1810-1817.
- [11] Uzun, B. B., Pütün, A. E., & Pütün, E. Rapid pyrolysis of olive residue. 1. Effect of heat and mass transfer limitations on product yields and bio-oil compositions (2007). *Energy & fuels*, 21, 1768-1776.
- [12] Liden, A. G., Berruti, F., & Scott, D. S. A kinetic model for the production of liquids from the flash pyrolysis of biomass (1988). *Chemical Engineering Communications*, 65, 207-221.

- [13] Balat, M., Balat, M., Kirtay, E., & Balat, H. Main routes for the thermo-conversion of biomass into fuels and chemicals (2009). Part 1: Pyrolysis systems. *Energy Conversion and Management*, 50, 3147-3157.
- [14] Draper N.R., Smith H. (1998), Applied Regression Analysis, Third ed., John Wiley & Sons Inc, Hoboken.
- [15] Chan, W. C. R., Kelbon, M., & Krieger, B. B. Modelling and experimental verification of physical and chemical processes during pyrolysis of a large biomass particle (1985). *Fuel*, 64, 1505-1513.
- [16] Di Blasi, C., & Branca, C. Kinetics of primary product formation from wood pyrolysis (2001). *Industrial & engineering chemistry research*, 40, 5547-5556.
- [17] Scott, D. S., Piskorz, J., & Radlein, D. Liquid products from the continuous flash pyrolysis of biomass (1985). *Industrial & Engineering Chemistry Process Design and Development*, 24, 581-588.
- [18] Scott, D. S., Piskorz, J., Bergougnou, M. A., Graham, R., & Overend, R. P. The role of temperature in the fast pyrolysis of cellulose and wood (1988). *Industrial & engineering chemistry research*, 27, 8-15.
- [19] Horne, P. A., & Williams, P. T. Influence of temperature on the products from the flash pyrolysis of biomass (1996). *Fuel*, 75, 1051-1059.
- [20] Zanzi, R., Sjöström, K., & Björnbom, E. Rapid high-temperature pyrolysis of biomass in a free-fall reactor (1996). *Fuel*, 75, 545-550.
- [21] Zhu, X. W., Liu, S. S., Qin, L. T., Chen, F., & Liu, H. L. Modeling non-monotonic dose-response relationships: Model evaluation and hormetic quantities exploration (2013). *Ecotoxicology and environmental safety*, 89, 130-136.
- [22] Meng, R., & Yu, X. Investigation of ultrasound assisted regeneration of Ni-bentonite with response surface methodology (RSM) (2011). *Applied Clay Science*, 54, 112-117.
- [23] Sahu, N. K., Sharma, M. C., Mourya, V., & Kohli, D. V. QSAR studies of some side chain modified 7-chloro-4-aminoquinolines as antimalarial agents (2010). *Arabian Journal of Chemistry*, 7, 701-707.
- [24] Antal, M. J., & Grønli, M. The art, science, and technology of charcoal production (2003). *Industrial & Engineering Chemistry Research*, 42, 1619-1640.
- [25] Fagbemi, L., Khezami, L., & Capart, R. Pyrolysis products from different biomasses: application to the thermal cracking of tar (2001). *Applied energy*, 69, 293-306.

[26] Shafizadeh, F. R. E. D., & Chin, P. P. Thermal deterioration of wood (1977). In *ACS Symposium Series American Chemical Society*. 57-81.

4. CHAPTER FOUR

A Study of Quality of Woody Biomass Feedstock on the Yield and Quality of Py-oil with a Lab-Scale Reactor

This chapter has been proofread and edited by Dr. Kelly Hawboldt and Dr. Robert Helleur.

Abstract

In the pyrolysis of biomass to bio products, in addition to the pyrolysis conditions the quality of the feedstock has an impact on the quality and yield of the bio products. Low quality feedstock can result in low yields and/or low quality py-oil and therefore pretreatment is sometimes required. However, there is a cost effectiveness balance between the degree of pretreatment and the yield/quality of the oil. In Chapter Three, the optimum temperature and N₂ flow rate for the lab scale reactor were 500 °C and 500 mL/min. In this Chapter the impact of the feedstock properties including moisture content, particle size, and age on the py-oil yield and quality (produced at optimum conditions) were investigated. Py-oil yield, Higher Heating Value (HHV), Total Acid Number (TAN), and amount of chemically produced water were studied. The impact of particle size on py-oil yield was investigated in previous chapter, in this chapter HHV and TAN was included. The results show initial moisture content has little effect on the water produced through dehydration of cellulose and hemicellulose. Increasing moisture did decrease the TAN and HHV, since water dilutes the organic acid and simultaneously decreases the carbon content of py-oil. Particle size reduction from 2-4 mm to 0.1-0.5 mm results in an increase in py-oil yield from 63 to 70% and a decrease in water content from 31 to 25% due to lower intraparticle heat/mass transfer resistances. There is no significant effect on HHV. A comparison between fresh and 4-5 year old feedstock indicates that the aged biomass produces slightly lower py-oil yield and higher produced water content, due to possible changes in the biomass chemical components during length of outside weathering. In addition, a qualitative assessment of the pyrolysis heat of reaction was performed. The results illustrate the overall endothermic nature of the pyrolysis of this type of biomass.

Keyword: Pyrolysis, Heat of reaction, Py-oil, Age of Feedstock, Moisture content, Particle size

4.1. Introduction

Biofuel is a potential alternative or blend with fossil fuel and is produced from biomass through different conversion methods including fermentation, combustion, gasification, mechanical extraction, anaerobic digestion, pyrolysis, liquefaction, and etc. [1,2].

Fast-intermediate pyrolysis has been used over a wide range of feedstock (i.e. sawmill, forest and farming residues, demolition wood, fish waste, municipal waste, algae, etc.) to produce py-oil (50-70 wt.% of products), bio-char (20-25 wt.% of products), and biogas (10-15 wt.% of products). Py-oil includes more than 400 organics including oxygenates (e.g. carboxylic acids, phenolics, esters, furans, ketones, aldehydes anhydrosugars, etc.) [3].

Py-oil feasibility as a fuel alternative or as blend with petroleum-based fuel, is a function of a number of properties (e.g. acid value, moisture content, heating value, and viscosity) and py-oil yield which are in turn a function of the feedstock and pyrolysis conditions. Py-oil can be further refined, such as by hydrodeoxygenation, catalyst cracking of pyrolysis vapour, emulsification, steam reforming, and chemical extraction from the py-oils in order to be used as fuel [4]. Pyrolysis studies confirm that a short vapour residence time and a temperature in the range of 500-550 °C, result in a py-oil with high yield and quality [5, 6]. In addition, the feedstock is a factor in the overall nature of the heat of reaction. The heat of reaction is important from a design and modelling perspective of the pyrolysis unit.

The pyrolysis heat of reaction has been reported to be overall endothermic or exothermic depending on the feedstock and pyrolysis conditions (Table 4-1). Bilbao et al. [7]

experimentally measured the reaction heat of pine wood (*Pinus Pinaster*) using a differential scanning calorimeter (DSC). The results showed that cellulose and hemicellulose decomposition correspond to an endothermic reaction ($\Delta H = 274$ kJ/kg) and lignin to an exothermic reaction ($\Delta H = -353$ kJ/kg), resulting in an overall exothermic reaction. Rath et al. [8] investigated the pyrolysis heat of beech and spruce wood by DSC as well. The results illustrated that heat of pyrolysis varies from endothermic to exothermic ($\Delta H = -221.8$ to 363.5 kJ/kg) depending on the initial sample weight and on the crucibles used in the measurements. Chan et al. [9] concluded that the reaction heat for wood pyrolysis is not well known and can range from -418 to $+418$ kJ/kg.

Table 4-1: Heat of pyrolysis

Heat of pyrolysis (kJ/kg)	Feedstock
538 (volatiles formation), -2000 (char formation)	cellulose [10]
150	biomass [11]
64	biomass[12]
274 (decomposition of carbohydrates), -353 (decomposition of lignin)	pine wood [7]
610 (at low heat flux), -1090 to -1725(at high heat flux)	maple [13]
-255 (low conversion), 20 (high conversion)	Biomass[14]
600	wood pellets [15]
1464 (tar), -301(char and gas)	Fibrous Cellulose [16]
300	Wood slabs [17]
1256	Wood [18]
450 (150 (tar), 150 (char), 150 (gas))	Sawdust [9]

203	Wood [19]
-420 - 0	Wood [20]

The impact of biomass quality on py-oil yield and produced water content has been investigated [21-25]. Aguilar et al. [21] investigated the influence of woody biomass (Chinese tallow tree) particle size on py-oil yield and composition in a tube furnace reactor at 550 °C and 25 g sample loading. The particle size varied from < 0.5 to 4.4 mm (< 0.5, 0.5 - 1.4, 1.4 - 2.4 and, 2.4 - 4.4 mm). The results showed that the range from 0.5–1.4 mm produced the “best” py-oil with respect to water content (~ 35%) and total oil yield (~ 46%). Particles finer than 0.5 mm produced lower py-oil (~ 44 %) yield and higher water content (~ 65 %). Shen et al. [22] found that py-oil yield increased by about 12–14 wt.% and water content decreased by about 12–13 wt.% when particle size was reduced from 5.6 mm to 0.18 mm for pyrolysis of mallee biomass in a fluidized bed reactor at 500 °C. Sensoz et al. [23] found that oil and char yields were independent of particle size for pyrolysis of rapeseed in a fixed-bed reactor at 500 °C and 40 °C/min heating rate. The particle size of rapeseed was varied from 0.224-1.8 mm. However, pyrolysis operating conditions, such as temperature, sample load, type of feedstock etc, combined with particle size could significantly impact the py-oil yield and water content.

The impact of initial moisture content of woody biomass on pyrolysis has been studied [e.g. 24,25]. Burhenne et al. [24] investigated moisture content (2.4- 55.4%), heating rate (4 -12.6 °C/min), and temperature (500 - 800 °C) on spruce wood chips pyrolysis product yield, structure, and reactivity of the bio-char in a batch reactor. The high water content

predictably led to a higher total oil yield and a lower bio-char yield with no significant impact on the microscopic structure of bio-char. The impact of the initial moisture content on the yields of total oily products from conventional pyrolysis of spruce wood, hazelnut shell, and wheat straw were investigated by Demirbas [25]. Their results illustrate that for biomass with higher moisture the maximum py-oil yield (dry feed basis) is obtained at lower pyrolysis temperatures (416-430 °C). In addition, qualitative observations showed that feedstock with low moisture produced a very viscous py-oil, particularly at higher pyrolysis temperatures.

As indicated above, moisture and particle size play a role in py-oil yield and quality. Although there has been research in feedstock quality impact on the oil yield, there are few comprehensive studies where the yield and quality (water content, HHV, and TAN) have been analyzed. Given the variability in sawmill residues, it is critical to determine feedstock quality on oil in order to determine if pretreatment is required and extent of this treatment. In this study, balsam fir from local sawmills was pyrolyzed in a lab scale reactor and quality and quantity of py-oil assessed. In addition a qualitative assessment of the pyrolysis heat of reaction was performed in order to use the information to develop better process models and scale up of pyrolysis systems.

4.2. Experimental Section

4.2.1. Feedstock Preparation

Fresh and aged (weathered in the open pile) balsam fir shavings were provided by Sexton Lumber sawmill in Bloomfield, Newfoundland and Labrador. The initial moisture content

of both feedstock was higher than 50%. After drying for 2 days at ambient temperature the moisture decreased to ~12%. For experiments requiring 0.5 % moisture a thin layer of sample was further dried overnight in an oven at 75 °C. The moisture content was measured using a moisture analyzer (METTLER TOLEDO HB43-5). The particle size was adjusted by processing through a cutter mill with a range of particle sieves to produce the required particle sizes for each experiment (0.1-0.5 (0.3), 0.5-1(0.75), 1-2(1.5), 2-4(3) mm).

4.2.2. Reactor Description

Pyrolysis experiments were carried out in a semi-batch tube furnace reactor (Thermolyne 21100 tube furnace, USA) (Fig. 4-1). The feedstock samples were placed in a 1.5 cm (i.d.) ×15 cm glass sample boat. The furnace reactor and sample (loading position) was flushed with nitrogen and then inserted into a 3 cm (i.d.) × 70 cm glass column equipped with a stopcock connected to a nitrogen supply for sweeping volatile products. To avoid air infiltration into the reactor, a predrilled rubber stopper was used for the end of the column where the sample hook protruded. At the exit, the column was joined to a “T” shaped connector, with a 20 mL flask to collect produced py-oil with the other connected to an air condenser. The exit gases were further cooled in a liquid nitrogen-filled glass condenser trap to drop out liquids from the gas stream. One gram of feedstock was placed in the sample boat and placed into the reaction loading position once the reactor temperature reached the set point. The nitrogen flow rate was varied between 200-800 mL/min, measured at 25 °C, and 1 atm. After pyrolysis, the sample boat was extracted and weighed to determine bio-char production. Py-oil can coat the inner parts of the exit surfaces, and therefore total py-oil yields are calculated by weighing the flasks, air condenser, elbow,

nitrogen trap, and “T” connector. The py-oil and bio-char yield were determined by using Eq. 4-1 to 4-3.

$$\text{Py - oil Yield\%} = \frac{\text{g pyrolysis oil collected}}{\text{g biomass}} \times 100 \quad (4-1)$$

$$\text{Bio - char Yield\%} = \frac{\text{g bio - char collected}}{\text{g biomass}} \times 100 \quad (4-2)$$

Py-oil and bio-char yield corrected for moisture are calculated as follow:

$$\text{Py - oil Yield} = \frac{\text{g oil collected} \times (1 - \text{initial moisture content})}{\text{g biomass} \times (1 - \text{initial moisture content})} \times 100 \quad (4-3)$$

$$\text{Bio - char Yield} = \frac{\text{g char collected}}{\text{g biomass} \times (1 - \text{initial moisture content})} \times 100 \quad (4-4)$$

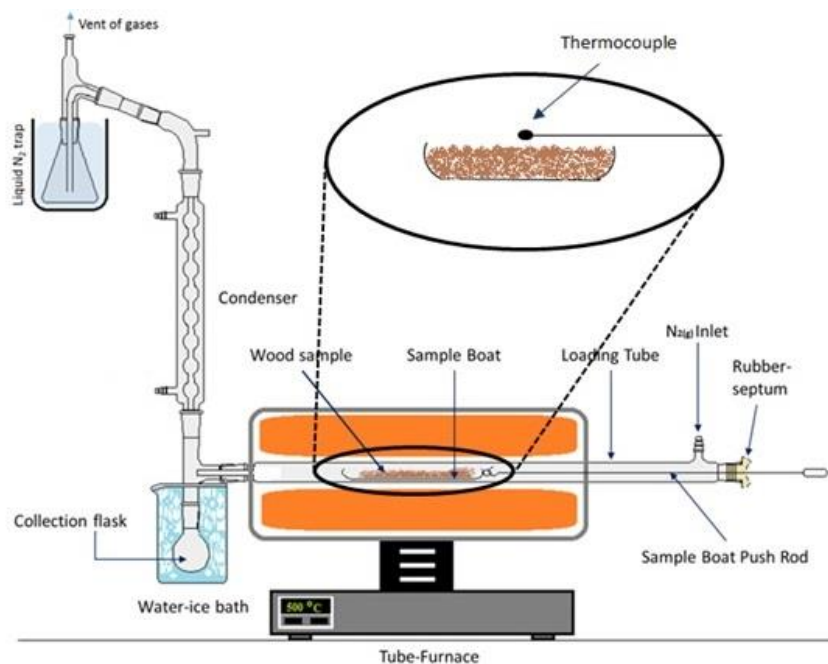


Figure 4-1: Schematic of lab-scale pyrolysis system

4.2.3. Py-oil Properties

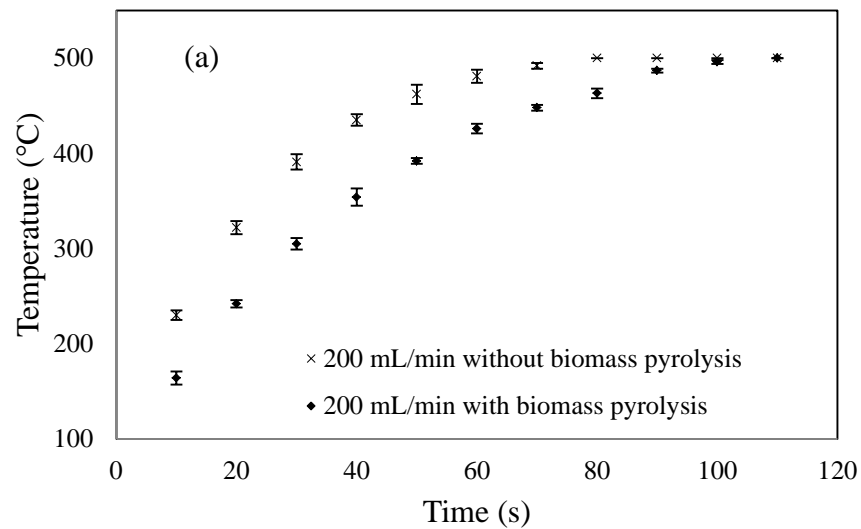
The water content of pyrolysis oil samples was measured using Karl-Fischer titration method (ASTM, E203), the Total Acid Number (TAN) was measured using potentiometric titration (ASTM, D664), and Higher Heating Value (HHV) was obtained by bomb calorimetric method (ASTM, D240).

4.3. Results and Discussion

4.3.1. Pyrolysis Heat

Fig. 4-2 summarizes the temperature of the thermocouple in the pyrolysis boat as a function of time. Two experiments were performed, one containing biomass and the second in an empty sample boat (without biomass). There is an impact on the temperature of the reactor

when the biomass is present compared to the empty reactor. When biomass is pyrolyzed in the sample boat the heat of reaction or heat of pyrolysis could contribute to temperature change, whereas in the empty boat this source is not present. As figure 2 indicates, the temperature increases more slowly when biomass is pyrolyzed compared to the empty boat for the same N₂ flow. The lower heating rate is likely due to the overall endothermic nature of the pyrolysis of this type of biomass. This is validated by the pyrolysis in this reactor being essentially complete by 80 seconds, where the two system temperature merge.



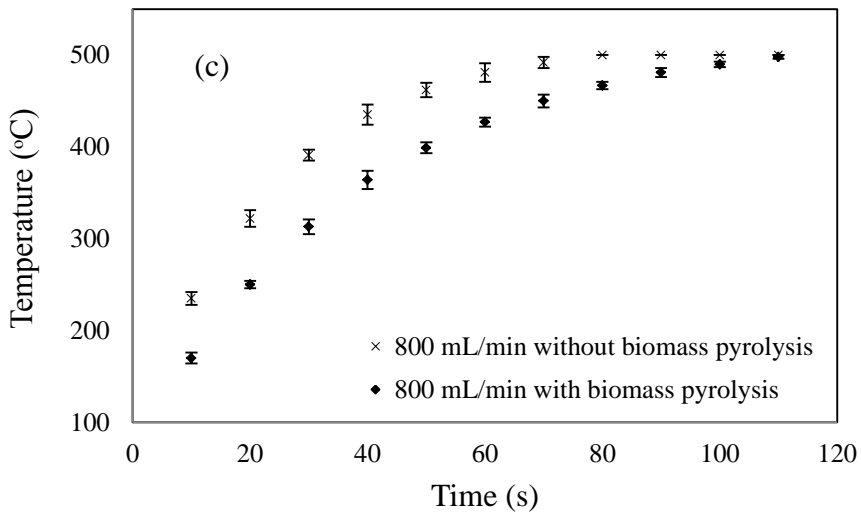
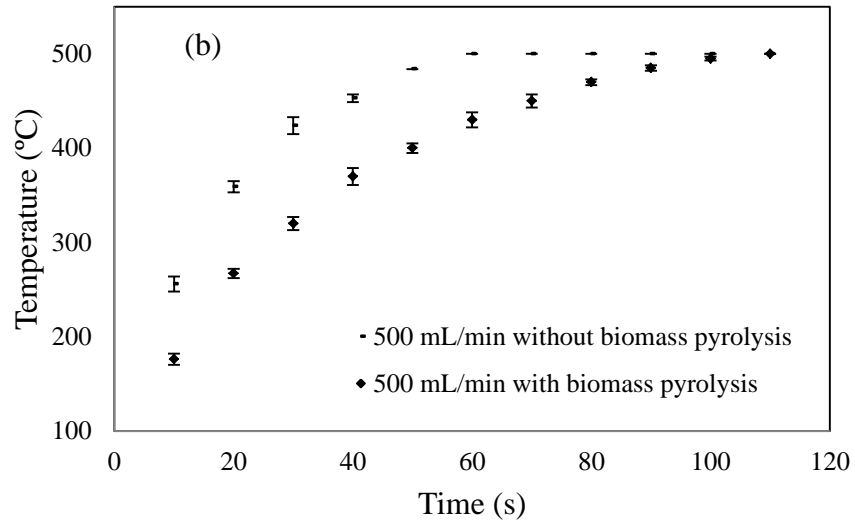
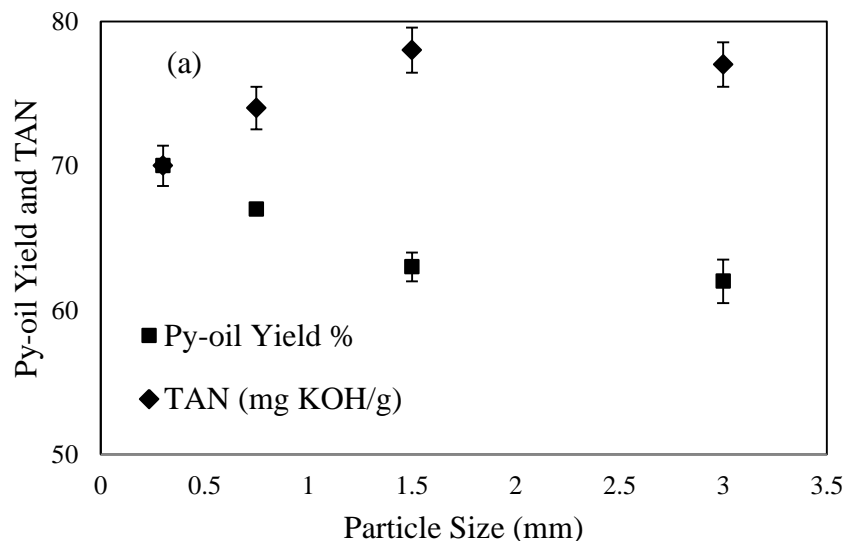


Figure 4-2: Temperature detected by thermocouple vs. time of the thermocouple situated near the biomass at 200 (a), 500 (b), and 800 (c) mL/min nitrogen flow rates (number of replicates = 2)

4.3.2. Effect of Particle Size on Biomass Pyrolysis

In Fig. 4-3, the impact of biomass particle size on product yields, water content, heating value, and TAN are summarized. Particles < 0.5 mm produce the highest py-oil yield and

lowest water content and TAN. However, the particle size does not have a significant effect on the heating value. Furthermore, particles in the range of 1-2 mm and 2-4 mm have approximately the same oil yield, water content, and TAN. As with other solid-gas systems (e.g. catalysts) there is a balance between particle size and py-oil yield. Smaller biomass particles minimize heat and mass transfer resistances and the subsequent shorter intraparticle solid-vapour contact time minimizes tar cracking reactions and consequently the py-oil yield increases. The results confirm this phenomenon for particles less than 2 mm. Although particle size reduction improves the py-oil yield and water content, further biomass grinding increases the capital cost of py-oil production without any enhancement in HHV.



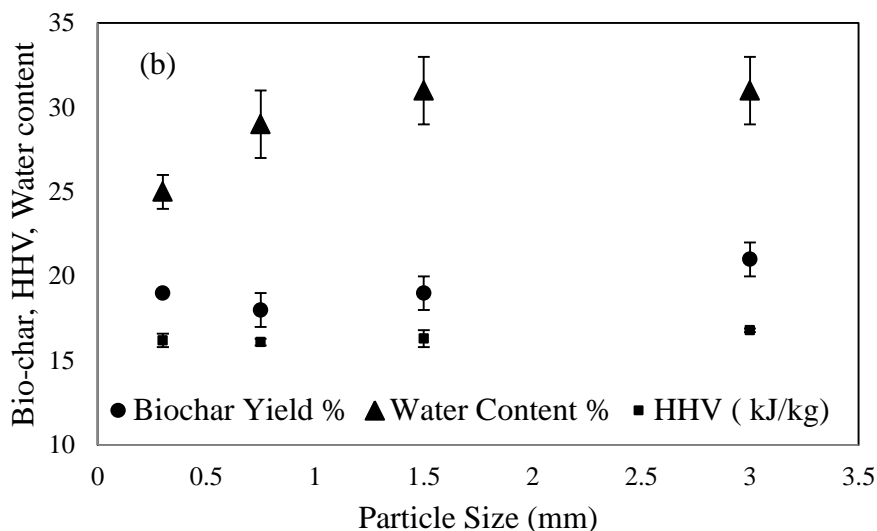


Figure 4-3: Impact of biomass particle size on the py-oil and bio-char yield, HHV, TAN, and water content at 500 °C and 500 mL/min (number of replicates = 2)

4.2.3. Impact of Feedstock Moisture Content on Py-oil

Fig. 4-4 shows the higher feedstock moisture content gives the higher water content in a py-oil with resulting lower TAN (water dilutes the organic acids), and HHV (water decreases the py-oil carbon content and simultaneously increases oxygen content). The results also show the feedstock moisture increase from 0.5 to 15 % does not have a significant effect on py-oil yield once the yield is corrected for initial moisture (see Eq. 3 and Fig. 4-5). The yield drops at moisture greater than 15 %. The chemically produced water (significant dehydration of cellulose and hemicellulose) is approximately the same regardless of initial feedstock moisture (Fig. 4-5). High water content in py-oil, usually more than 30%, causes phase separation, a top phase or aqueous phase and bottom phase or oily phase. The aqueous phase contains a wide variety of oxygenates including acetic acid,

methanol, and carbohydrates degradation products. The oily phase includes phenolic groups and other components with high molecular weight [25]. The phase separation could be advantageous for the extraction of valuable chemical components; however, it is detrimental for use as a fuel.

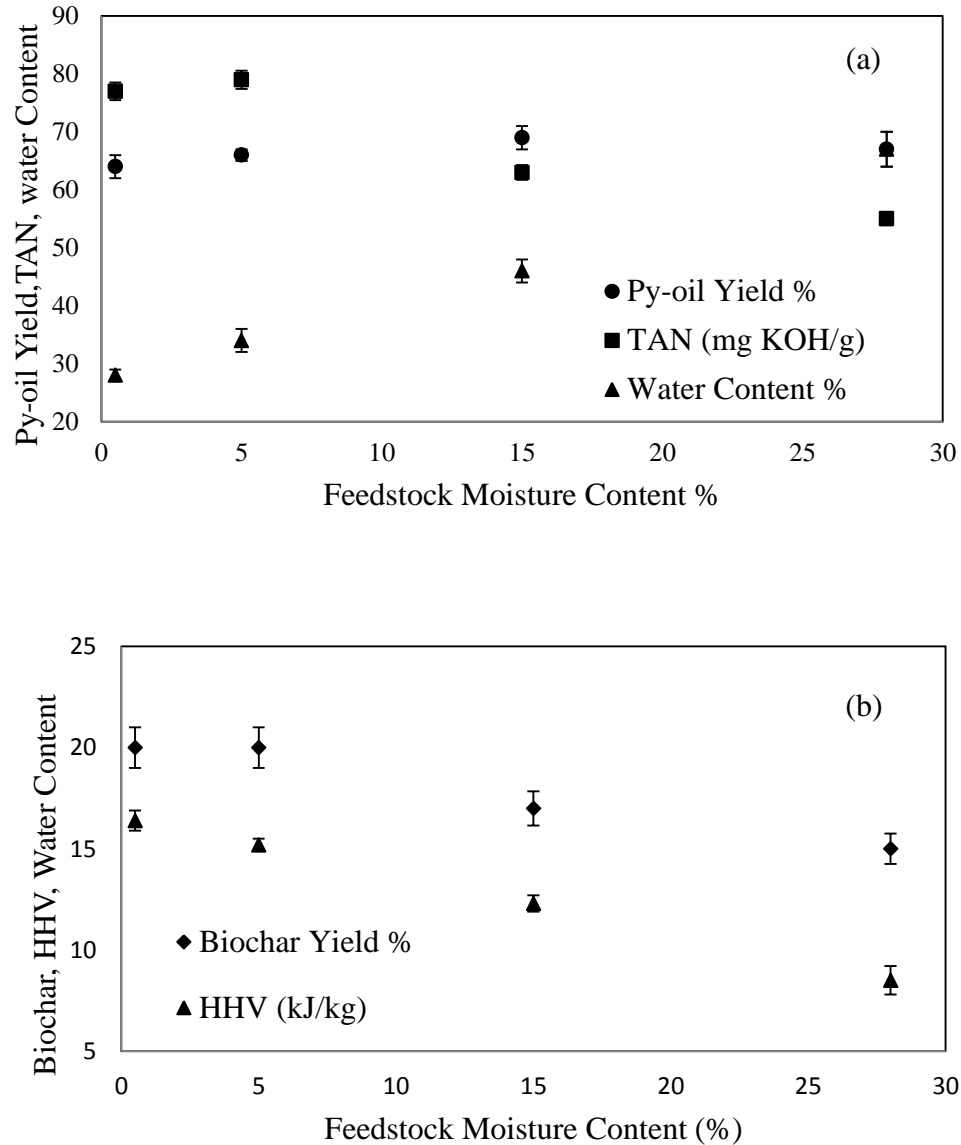


Figure 4-4: Impact of initial moisture content on the py-oil and bio-char yield (a), HHV, TAN, and water content (b) at 500 °C and 500 mL/min (number of replicates = 2)

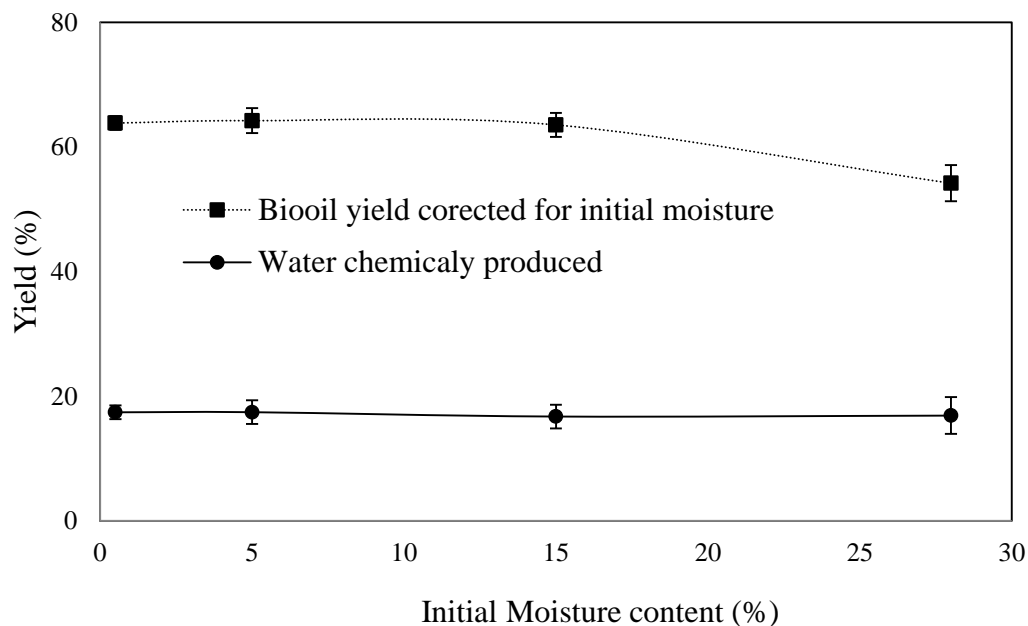


Figure 4-5: Impact of feedstock initial moisture content on the py-oil yield corrected for moisture, and water chemicaly produced at 500 °C and 500 mL/min

4.2.4. Effect of Age of Feedstock on Biomass Pyrolysis

As woody biomass ages in the open environment, microbial and chemical degradation occurs over time [26]. This aging therefore can significantly impacts the composition and yield of pyrolysis products. There is a slight decrease in py-oil yield, an increase in water content and bio-char is observed for biomass with 4-5 years of aging compared to fresh biomass (Fig. 4-6). Although, a slight increase in water content of 4-5 years feedstock is observed, the HHV does not decrease, due to possible changes in the liquid organics forming during pyrolysis of aged biomass. 2-3 years aging does not have significant impact on py-oil quality and quantity. The investigation on feedstock age is rare in the

literature and further studies are required, particularly on the impact of feedstock age on wood components, to better understand the biomass components changes during aging.

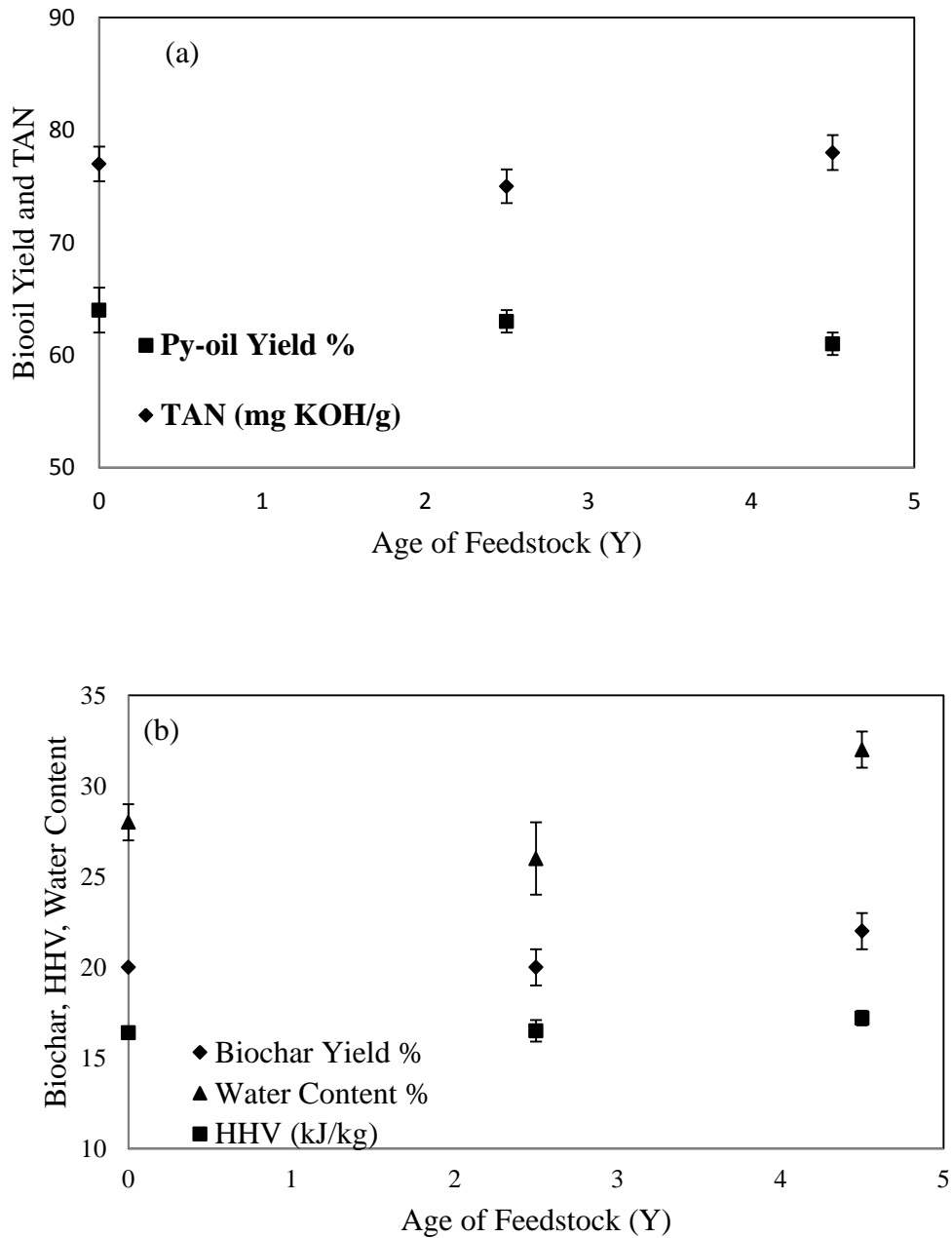


Figure 4-6: Impact of feedstock age on the py-oil and bio-char yield, HHV, TAN, and water content at 500 °C and 500 mL/min (number of replicates = 2)

4.5.Conclusion

A qualitative assessment on pyrolysis heat of reaction showed an overall endothermic reaction for the woody biomass used in this study. In addition, the impact of biomass particle size, initial moisture content, and age of feedstock were investigated on py-oil quantity and quality. The results illustrated that particles finer than 0.5 mm produced the highest py-oil yield, lowest water content and total acid number. A reduction in vapour-solid contact time due to the minimization of heat/mass transfer resistances when particle size decrease could be the logical reason for higher py-oil yield and lower water content. HHV was independent of biomass particle size. The py-oil yield corrected for initial moisture, showed no significant change on py-oil yield from 0.5 to 15 %. However, it dropped after 15 % moisture content. A continuous reduction in py-oil HHV and TAN was observed due to an increase in py-oil water content. Furthermore, no significant impact on water produced during carbohydrate dehydration reactions was observed when increasing initial moisture content. The effect of biomass aging due to length of outside storage showed a slight reduction in py-oil yield and slight increase in water content with 4-5 year old feedstock compared to fresh feedstock.

Acknowledgment

This work has been supported by CFSI/ Department of Fisheries, Forestry and Agrifoods/ Government of Newfoundland and Labrador, BioFuelNet Canada, the Canadian Foundation for Innovation, the Natural Science and Engineering Research Council of Canada and Memorial University of Newfoundland. In addition, the authors would like to thank the valuable contribution of Dr. Peter Fransham from ABRI-Tech Inc.

4.6. References

- [1] Papari S, Hawboldt K. A review on the pyrolysis of woody biomass to bio-oil: Focus on kinetic models. *Renewable and Sustainable Energy Reviews*. 2015 Dec 31;52:1580-95.
- [2] Kumar A, Kumar N, Baredar P, Shukla A. A review on biomass energy resources, potential, conversion and policy in India. *Renewable and Sustainable Energy Reviews*. 2015 May 31;45:530-9.
- [3] Wang L, Lei H, Bu Q, Ren S, Wei Y, Zhu L, Zhang X, Liu Y, Yadavalli G, Lee J, Chen S. Aromatic hydrocarbons production from ex situ catalysis of pyrolysis vapor over Zinc modified ZSM-5 in a packed-bed catalysis coupled with microwave pyrolysis reactor. *Fuel*. 2014 Aug 1;129:78-85.
- [4] Zhang Q, Chang J, Wang T, Xu Y. Review of biomass pyrolysis oil properties and upgrading research. *Energy conversion and management*. 2007 Jan 31;48(1):87-92.
- [5] Morgan TJ, Turn SQ, George A. Fast Pyrolysis Behavior of Banagrass as a Function of Temperature and Volatiles Residence Time in a Fluidized Bed Reactor. *PloS one*. 2015 Aug 26;10(8):e0136511.
- [6] Papari S, Hawboldt K, Helleur R. Pyrolysis: A Theoretical and Experimental Study on the Conversion of Softwood Sawmill Residues to Biooil. *Industrial & Engineering Chemistry Research*. 2015 Jan 12;54(2):605-11.
- [7] Bilbao R, Mastral JF, Ceamanos J, Aldea ME. Modelling of the pyrolysis of wet wood. *Journal of analytical and applied pyrolysis*. 1996 Apr 30;36(1):81-97.
- [8] Rath J, Wolfinger MG, Steiner G, Krammer G, Barontini F, Cozzani V. Heat of wood pyrolysis. *Fuel*. 2003 Jan 31;82(1):81-91.
- [9] Chan W-CR, Kelbon M, Krieger BB. Modelling and experimental verification of physical and chemical processes during pyrolysis of a large biomass particle. *Fuel* 1985;64:1505–13.

- [8] Milosavljevic I, Oja V, Suuberg EM. Thermal effects in cellulose pyrolysis:relationship to char formation processes. *Ind Eng Chem Res* 1996;35:653–62.
- [9] Grønli, MG. A theoretical and experimental study of the thermal degradation of biomass. PhD thesis; 1996.
- [10] Park WC. A study of pyrolysis of charring materials and its application to fire safety and biomass utilization by assessment; 2008.
- [11] Koufopoulos CA, Papayannakos N, Maschio G, Lucchesi A. Modelling of the pyrolysis of biomass particles. Studies on kinetics, thermal and heat transfer effects. *Can J Chem Eng* 1991;69:907–15.
- [12] Bennini S, Castillo S, Traverse JP. Effects of an intense thermal flux on a lignocellulosic material,. *J Anal Appl Pyrolysis* 1991;21:305–14.
- [13] Curtis LJ, Miller DJ. Transfer model with radiation heat transfer for rapid cellulose pyrolysis. *Ind Eng Chem Res* 1988;27:1775–83.
- [14] Miller CA, Ramohalli KNR, Theoretical A. Heterogeneous model of wood pyrolysis. *Combust Sci Technol* 1986;46:249–65.
- [15] Kanury AM, Holve DJ. Transient conduction with pyrolysis—approximate solutions for charring of wood slabs. *J Heat Transfer* 1982;104:338–43.
- [16] Chan W-CR, Kelbon M, Krieger BB. Modelling and experimental verification of physical and chemical processes during pyrolysis of a large biomass particle. *Fuel* 1985;64:1505–13.
- [17] Roberts AF. The heat of reaction during the pyrolysis of wood. *Combust Flame* 1971;17:79–86.
- [18] Kung H-C, Kalekar AS. On the heat of reaction in wood pyrolysis. *Combust Flame* 1973;20:91–103.
- [19] Roberts AF. The heat of reaction during the pyrolysis of wood. *Combust Flame* 1971;17:79–86.
- [20] Kung H-C, Kalekar AS. On the heat of reaction in wood pyrolysis. *Combust Flame* 1973;20:91–103.
- [21] Aguilar G, Muley PD, Henkel C, Boldor D. Effects of biomass particle size on yield and composition of pyrolysis bio-oil derived from Chinese tallow tree (*Triadica Sebifera* L.) and energy cane (*Saccharum complex*) in an inductively heated reactor.
- [22] Shen J, Wang XS, Garcia-Perez M, Mourant D, Rhodes MJ, Li CZ. Effects of particle size on the fast pyrolysis of oil mallee woody biomass. *Fuel*. 2009 Oct 31;88(10):1810-7.

- [23] Şensöz S, Angın D, Yorgun S. Influence of particle size on the pyrolysis of rapeseed: fuel properties of bio-oil. *Biomass and Bioenergy*. 2000 Oct 31;19(4):271-9.)
- [24] Burhenne L, Damiani M, Aicher T. Effect of feedstock water content and pyrolysis temperature on the structure and reactivity of spruce wood char produced in fixed bed pyrolysis. *Fuel*. 2013 May 31;107:836-47.
- [25] Demirbas A. Effect of initial moisture content on the yields of oily products from pyrolysis of biomass. *Journal of Analytical and Applied Pyrolysis*. 2004 Jun 30;71(2):803-15.

5. CHAPTER FIVE

Development and Validation of a Process Model to Describe Pyrolysis of Forestry Residues in an Auger Reactor

This chapter is under review by the Journal of Fuel Processing Technology. Development and validation of a process model to describe pyrolysis of forestry residues in an auger reactor. FUPROC_2016_262. Sadegh Papari*, Kelly Hawbold

Abstract

The study of kinetic models in Chapter Two indicated a number of models which can be used in process modeling. In addition, in Chapter Four a qualitative assessment on the feedstock used in this research indicated the pyrolysis reaction of this type of biomass is an endothermic reaction. In this chapter by using information obtained from Chapters Two and Four, a process model for an auger style biomass pyrolysis reactor is developed to use as a tool in process optimization and scale up. The plug flow model for both solid and gas phases are assumed. A comparison between the kinetic models widely used in the literature with the experimental data was performed to determine the “best” kinetic model for our system. The transport equations for each phase are combined with the kinetic model to predict py-oil, bio-char, and non condensable gas yields. The applied model was validated with experimental data from a 2-4 kg/h pilot scale auger reactor. This reactor uses steel shot as a heat carrier and without carrier gas. The results show good agreement between experimental data and model prediction. The model was used to predict yield of py-oil as a function of temperature, feed flow rate and reactor pressure. These simulations indicate the model is a useful tool in design and scale up of auger type pyrolysis reactors using a heat carrier.

Keyword: Pyrolysis, Process model, Auger reactor, Sawmill residues, Plug flow model

5.1. Introduction

Pyrolysis is a thermochemical conversion of organic and non-organic material (wood, algae, fish waste, scrap tire, heavy crude oil, and etc.) in the absence of oxygen. Based on temperature and heating rate, pyrolysis is classified into 1. slow (low temperature (~ 300 °C), low heating rate, and high solid residence time), 2. fast (moderate temperature (500-600 °C), fast heating rate (100 °C/s), and short vapor residence time (less than two seconds)), and 3. flash (high temperature (>600 °C), fast heating rate (>200 °C/s), and short vapor residence time). Fast pyrolysis produces up to 75% liquid yield which has a wide variety of applications [1,2]. Figure 5-1 shows the basic thermochemical decomposition of wood biomass to py-oil, bio-char and non-condensable gas.

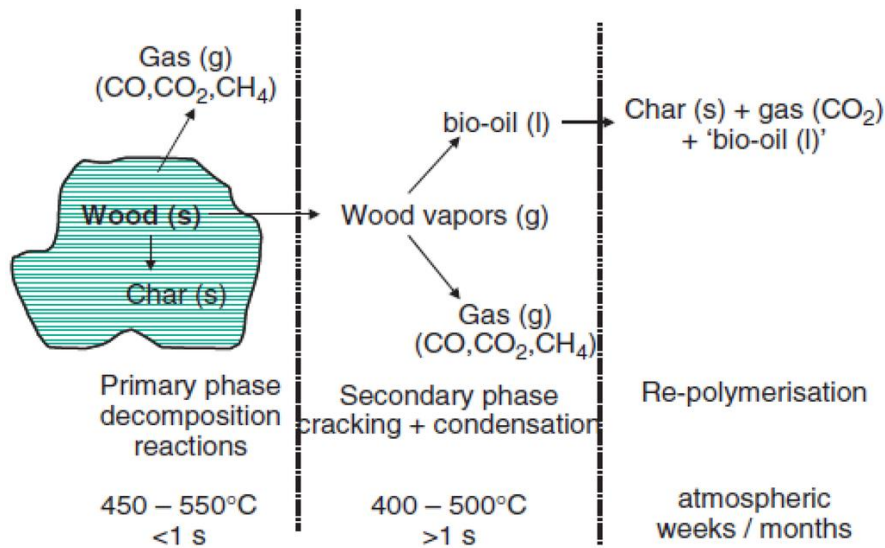


Figure 5-1: Reaction pathways for the pyrolysis of biomass [3] (without permission)

Process modeling is used as a tool in process optimization, scale up, and reactor design to reduce the cost of operation. The mass, energy and momentum transport equations are coupled with a kinetic model to predict process. Several studies [4-7] have proposed process models for pyrolysis reactors. Trendewicz et al. [4] used finite difference to solve the transport equation for a 0.023 kg/h circulating fluidized bed reactor and the kinetic model by Ranzi et al. [8]. This model assumes only primary reactions and did not include particle mass transfer. The results predicted the data extracted from literature well. Papadikis et al. [5] used CFD software to solve the transport equations and the kinetic model by Chan et al. [9] for primary reactions, and Liden et al. [10] and Di Blasi [11] for secondary reactions, for a 0.15 kg/hr entrained flow reactor. In this process model, intra-particle mass transfer was included. The results showed temperature gradients within the particle will impact the rate of reaction. As such, optimizing the particle size distribution to minimize these effects while balancing issues related to very fine particles (e.g. handling and cost of grinding) is important. Klose et al [6] used Runge-Kutta Fourth-Order to solve transport equations and kinetic model developed by Klose and Wiest [12] for a bench-scale rotary kiln reactor. This model assumes both primary and secondary reactions and did not include intra-particle mass transfer. The model results predicted the experimental data well. They concluded that the py-oil yield was not significantly impacted by solid residence time at the time scales and temperatures studied; however, temperature was a significant factor. Bandyopadhyay et al. [7] used a Runge-Kutta Fourth-Order method to solve transport equation in a vertical fixed-bed reactor and kinetic model developed by Bardbury et al. [13]. In this model secondary

reactions and intra-particle heat/mass transfer are neglected. The model represented the transient behavior of the biomass pyrolyzer well.

The models developed for auger type pyrolysis reactors are rare in the literature, particularly with those using a heat carrier such as sand or steel shot. Aramideh et al. [14] modeled a laboratory scale auger reactor, which was 0.16 m in length, using CFD and the kinetic model developed by Miller et al. [15]. Optimum temperature, nitrogen flow rate and biomass feed rate for py-oil production were determined.

In this study, a plug flow reactor model was assumed for both solid and gas streams to simulate a continuous auger reactor with steel shot as heat carrier with no carrier gas. The model was validated and then used to investigate the effect of different operating conditions (i.e. temperature, feed flow rate, and system pressure) on the py-oil, bio-char and gas yields.

5.2. Experimental Section

The process flow (PFD) of the auger reactor is outlined in Figure 5-2. The feeder is made up of two perpendicular augers (100 and 101) and a hopper. The biomass is fed in the hopper and the augers transfer the biomass at a desired rate into the reactor. The auger exit to the reactor (201) mixes the biomass with steel shot at a preset temperature and the woody biomass, is rapidly converted into py-oil vapours, gas and bio-char. A pressure gauge (P) measures the pressure of the gases inside the reactor. The hot pyrolysis vapour exit the reactor and enter a cyclone (303) to remove fine char entrained in the gas stream. The solid particles drop to the bottom of the cyclone, while the pyrolysis vapour and

gases leave the cyclone at the top connected to a shell and tube condenser (401) where the vapours are cooled to between 40-55 °C. The uncondensed gases are further cooled by a secondary condenser (402), with an exit temperature approximate the ambient temperature. An electrostatic precipitator (403) is located after condensers to collect the remaining oil which is not condensed in the primary and secondary condensers. The final py-oil product is a blend of the py-oil collected from the two condensers and the ESP. 90 % of the py-oil is collected in the first condenser, 8% in the second condenser and 2% in the electrostatic precipitator. The ID Fan (404) maintains the pressure in the reactor and assists the flow of gas from the reactor through to the fan discharge to the atmosphere.

The bio char and steel shot exit the reactor and are elevated by auger (202). The steel shot acts as a ball mill and reduces the bio-char to a fine powder. At the top of the inclined auger (202) the char and shot are discharged into a separator where the fine char is stripped from the shot using recycle gas from a small fan (304). A cyclone (302) separates the char from the recycle gas and the char drops out into container (305). The char fan speed is adjustable to ensure maximum collection of the fine char.

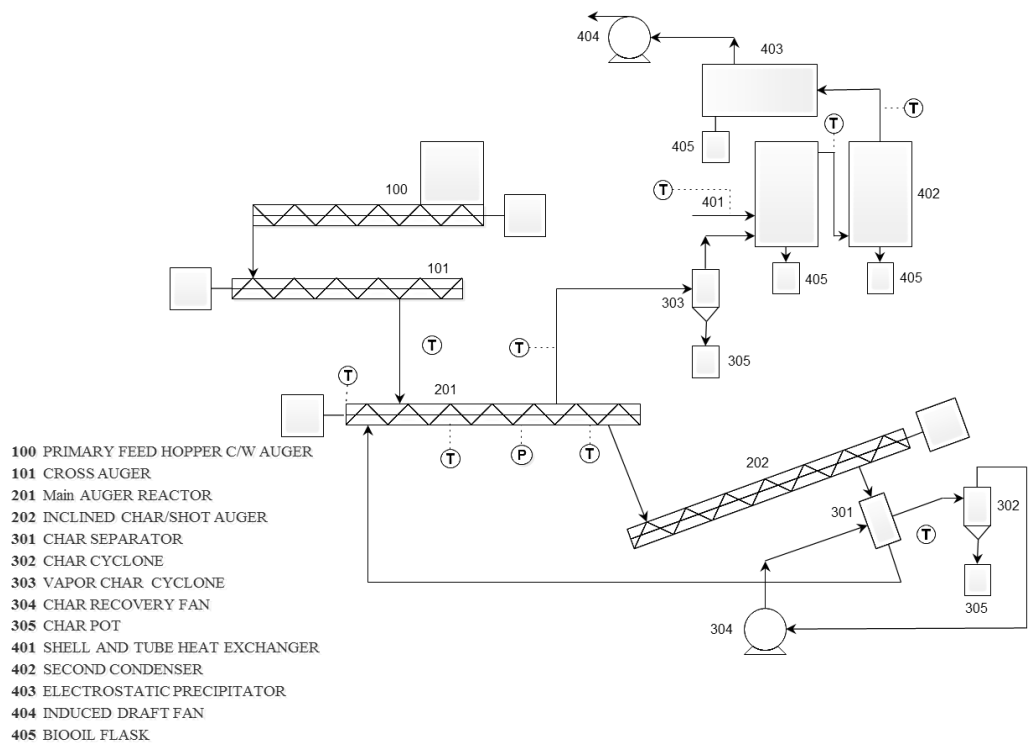


Figure 5-2: Process flow diagram for the auger reactor

Figure 5-3 is a schematic of the apparatus with the front of the oven removed. The oven is heated by two electric heating elements. An Opto 22 data acquisition system coupled to a laptop computer provides process control and data acquisition.

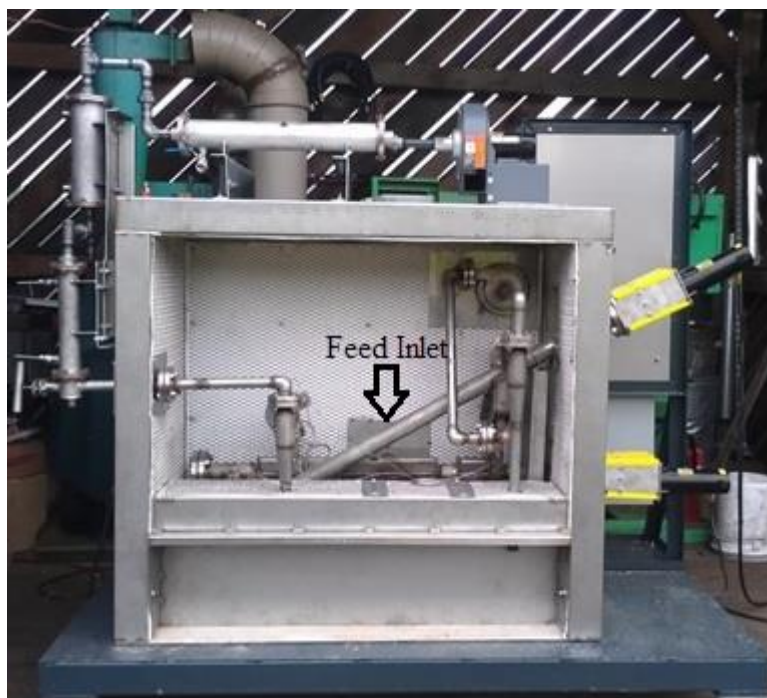


Figure 5-3: A photo of the inside of auger pyrolysis system built by ABRI-Tech Inc

5.2.1. Feedstock

Fresh balsam fir shavings were obtained from Sexton Lumber sawmill (Bloomfield, Newfoundland and Labrador) for this study. The shavings were milled and sieved at ~ 2 mm resulting in a particle size distribution of 28% of 2-3 mm, 47% of 1-2 mm, 19% 0.5-1 mm, and 6% 0.1-0.5 mm. The feedstock was dried at 75 °C overnight to lower the moisture content below 2%. Table 5-1 summarizes the proximate analysis conducted by TGA. Cellulose, hemicellulose, and lignin content of the balsam fir wood are presented in Table 5-2 (extracted from [16]).

Table 5-1: Proximate analysis of balsam fir wood

Analyte (%)	Balsam Fir wood
-------------	-----------------

low volatile matter	2.21
medium volatile matter	80.77
fixed carbon	16.79
Ash	0.23

Table 5-2: Composition of balsam fir in Newfoundland and Labrador [16]

Component	%
Extractives	3.6
Cellulose	42.2
Hemicellulose	20.7
Lignin	28.4
Other components	5.1

5.2.2. Model Description

Modeling of biomass particles moving along an auger conveyor can be challenging; however, Nachenius et al. [17] showed that coarse and fine material biomass in an auger or screw system can be assumed to behave in a plug flow. Tsai et al. [18] also concluded that the degree of mixing between the former element and the latter element in a screw feeder is low and the granular flow is near plug flow. Equation 5-1 was used to calculate the mean residence time and average particle velocity. It should be noted that the dimensions of the auger conveyor in [17] is approximately similar to the system used in this work (screw conveyor length from inlet to outlet is 1.64 m, shell diameter is 0.052 m, and pitch is 0.046 m).

$$\tau_{model} = \frac{L}{(P \times u_{screw})} \times (k_0 + k_1 \frac{Q}{u_{screw}}) \quad (5-1)$$

where τ_{model} is the estimated mean residence time of a particle, Q is volumetric flow rate within the screw and u_{screw} is screw conveyor frequency. k_0 and k_1 are the model coefficients [17].

A schematic carton of the reactor is shown in Figure 5-4. The reactor is divided into two parts in terms of the solid and gas flows. In the first part of the reactor, starting from the feed entrance to 1/3 of the reactor's length, the solids and the gas flow co-currently. In the second part (Figure 5-4), the gas is counter-current to the solid flow.

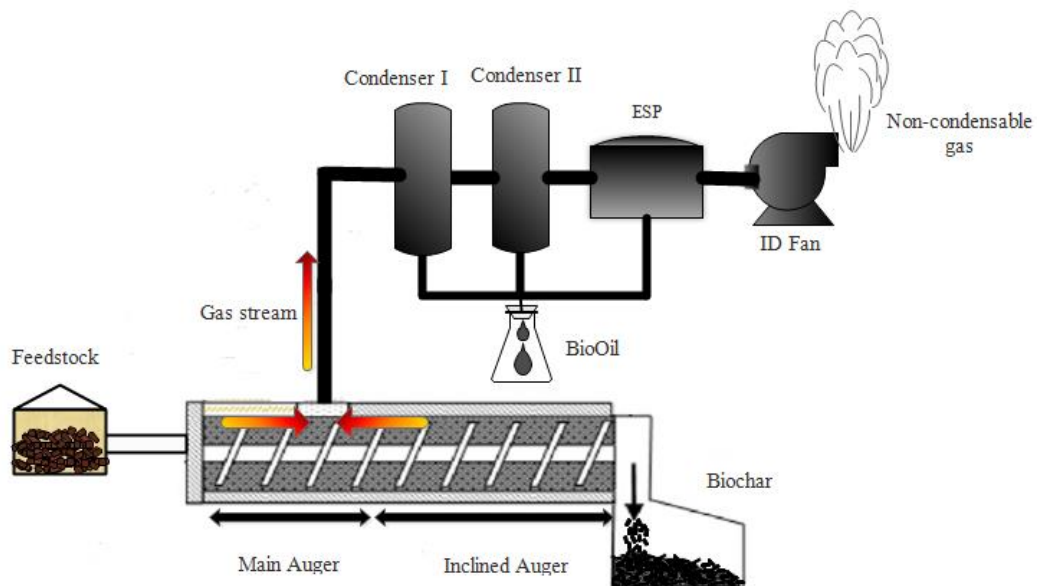


Figure 5-4: Schematic of process flow of auger reactor and product collection system

The additional assumptions used to develop our model are as follows; plug flow in solid and gas phase, gases are assumed to be ideal, steady state, intra-particle temperature gradients are negligible, particles are assumed to be spherical, vapour and biomass are in a thermal equilibrium, and the temperature of the steel shot is constant.

The auger reactor, biomass and steel shot dimensions are outlined in Tables 5-3 and 5-4.

Table 5-3: Auger reactor dimensions

Parameter	
Pitch (m)	0.044
Auger Speed (rpm)	45
Feed rate (kg/h)	1-3.5
Reactor length (m)	1.80
Diameter (m)	0.054
Steel shot diameter (m)	0.001

Table 5-4: Properties of steel shot and biomass

Property	
Density of standard carbon steel (kg/m ³)[19]	7800
Heat capacity of steel shot (J/kg.k) [19]	500
Thermal conductivity of steel shot (W/m.K)[19]	15
Density of wood (biomass) (kg/m ³)[20]	318
Heat capacity of wood(J/kg.K)[21]	1500
Thermal conductivity of wood (W/m.K) [22]	0.25
Surface emissivity (-) [22]	0.85

With the previous assumptions, the mass balance for the biomass particles is as follows:

$$(1 - \varepsilon) \frac{1}{(1 + \theta)} S U_b \rho_b |_x - (1 - \varepsilon) \frac{1}{(1 + \theta)} S U_b \rho_b |_{x+dx} - \sum_{j=1}^3 (1 - \varepsilon) \frac{1}{(1 + \theta)} \rho_b A_j \exp\left(\frac{-E_j}{RT}\right) S dx = 0 \quad (5-2)$$

here the index j indicates the phase (e.g. char, condensable and non-condensable gases). ρ_b (kg/m³) is the biomass density, A_j (s⁻¹) is the Arrhenius constant, E_j (J/mol) is activation energy (Table 5-7), R (J/mol.K) is the universal gas constant, T (K) is temperature, ε (-) is porosity, U_b (m/s) is biomass velocity in the reactor, S (m²) is cross section area, and x (m) is axial direction.

The overall mass balance for the gas phase:

$$\varepsilon U_g \rho_g S |_x - \varepsilon U_g \rho_g S |_{x+dx} + \sum_{j=1}^2 (1 - \varepsilon) \frac{1}{(1 + \theta)} \rho_b A_j \exp\left(\frac{-E_j}{RT}\right) S dx = 0 \quad (5-3)$$

The index j indicates condensable or non-condensable gases, θ (-) is the volume ratio of shot to biomass, U_g (m/s) is gas velocity,

The mass balance for the individual gas species (condensable and non-condensable) in the co-current section:

$$\begin{aligned} \varepsilon U_{gco} \rho_{ng} S|_x - \varepsilon U_{gco} \rho_{ng} S|_{x+dx} + (1 - \varepsilon) \frac{1}{(1 + \theta)} \rho_b A_1 \exp\left(\frac{-E_1}{RT}\right) S dx \\ + \varepsilon \rho_{cg} A_4 \exp\left(\frac{-E_4}{RT}\right) S dx = 0 \end{aligned} \quad (5-4)$$

$$\begin{aligned} \varepsilon U_{gco} \rho_{cg} S|_x - \varepsilon U_{gco} \rho_{cg} S|_{x+dx} + (1 - \varepsilon) \frac{1}{(1 + \theta)} \rho_b A_3 \exp\left(\frac{-E_3}{RT}\right) S dx \\ - \varepsilon \rho_{cg} A_4 \exp\left(\frac{-E_4}{RT}\right) S dx = 0 \end{aligned} \quad (5-5)$$

Where ρ_{ng} (kg/m^3) and ρ_{cg} (kg/m^3) are densities for non-condensable and condensable gases respectively. U_{gco} (m/s) is gas velocity in co-current section.

The mass balance for the counter-current section of reactor also is written like the co-current section with respect to the gas and biomass velocity direction.

Energy Balance for the biomass:

$$\begin{aligned} (1 - \varepsilon) \frac{1}{(1 + \theta)} S U_b \rho_b C_{p,b} T_b|_x - (1 - \varepsilon) \frac{1}{(1 + \theta)} S U_b \rho_b C_{p,b} T_b|_{x+dx} \\ = dq_{\text{cond}} + dq_{\text{rad}} + dq_{\text{rxn}} \end{aligned} \quad (5-6)$$

Where $C_{p,b}$ (J/kg K) is biomass heat capacity, dq_{cond} is conductive heat transfer, dq_{rad} is radiative heat transfer, dq_{rxn} is pyrolysis heat.

The heat transfer by conduction between steel shot and biomass particles is outlined below:

$$dq_{\text{cond}} = \frac{2k_b k_s}{(k_b + k_s)} S_b R_{bs} \frac{(T_s - T_b)}{(d_{p,s} + d_{p,b})} S dx \quad (5-7)$$

Where k_b (W/m K) and k_s (W/m K) are conductivity for biomass and steel shot respectively. $d_{p,s}$ (m) and $d_{p,d}$ (m) are shot and biomass diameter respectively. S_b (m^2) is biomass external surface area per unit volume (m^2/m^3) in the reactor and R_{bs} (-) is ratio of contact area to biomass surface area. The contact area diameter is calculated, $d_c = 0.2d_{p,s}$, as assumed [23].

The radiative heat transfer between steel shot and biomass particles is described as:

$$dq_{\text{rad}} = \sigma \beta S_b (1 - R_{bs}) (T_s^4 - T_b^4) S dx \quad (5-8)$$

Where σ is the Stefan–Boltzman constant ($\text{W}/\text{m}^2 \text{K}^4$), and β is the emissivity factor (-), T_s (K) is the shot temperature.

The heat of reaction is calculated by the following equation:

$$dq_{\text{rxn}} = \left[\sum_{j=1}^3 r_j \Delta H_j \right] \frac{1 - \varepsilon}{(\theta + 1)} S dx \quad (5-9)$$

The surface area of biomass is presented in equations 5-10 and 5-11.

$$S_b = a_b \frac{1}{1 + \theta} \quad (5-10)$$

$$a_b = \frac{6(1 - \varepsilon)}{d_{pb}} \quad (5-11)$$

S_b (m^2/m^3) is biomass surface area per unit volume (reactor). a_b (m^2/m^3) is biomass surface area per unit volume (biomass).

The reaction rate constants used for equation 5-12 are listed in Tables 5-5 to 5-7.

$$\dot{r}_j = \rho_b A_j \exp\left(\frac{-E_j}{RT}\right) \quad j = 1,3 \quad (5-12)$$

Table 5-5 outlines the constants from work by Chan et al. [9] and Morf [24]. Table 5-6 outlines the parameters from the Miller model [15]. This mechanism is more detailed than Chen, and based on the three main constituents of the wood. The derivation of this reaction rate expression was based on a reactor model that included intra-particle effects. Other global kinetic models used in this study are listed in Table 5-7. It should be noted that after testing different secondary tar cracking reactions (e.g. Morf et al. [24], Anata et al. [25], Liden et al. [10], Boroson et al. [26], Cozani et al. [27], Fagbemi et al. [28]); coupling Morf model with a primary reaction provides a better prediction of the experimental data. The experimental conditions of the kinetic models used in this study are presented in Table 5-8

Table 5-5: Reaction rate constants for biomass pyrolysis, Chan et al. (primary) coupled with Morf (secondary) [9, 24]

	Reactions	A(s ⁻¹)	E (kJ/mol)	ΔH (kJ/kg)
Primary [9]	wood→gas	1.3 × 10 ⁸	140.3	150
Primary [9]	wood→char	2.0 × 10 ⁸	133.1	150
Primary [9]	wood →oil	1.1 × 10 ⁷	121.3	150
Secondary [24]	oil→gas	4.0× 10 ⁴	76.6	-

Table 5-6: Reaction kinetics for biomass pyrolysis, Miller et al [15]

#	Reactions	A(S ⁻¹)	E (kJ/mol)	Y*	ΔH (kJ/kg)
1	cellulose→active cellulose	2.8× 10 ¹⁹	242.4		0
2	active cellulose→tar	3.28× 10 ¹⁴	196.5	0.35	255
3	active cellulose→Ychar+(1-Y)gas	1.3× 10 ¹⁰	150.5		-20
4	hemicellulose→active hemicellulose	2.1× 10 ¹⁶	186.7		0
5	active hemicellulose→tar	2.6× 10 ¹⁶	202.7	0.6	255
6	active hemicellulose→Ychar +(1-Y)gas	2.6× 10 ¹¹	143.7		-20
7	lignin→active lignin	9.6× 10 ⁸	107.6		0
8	active lignin→tar	1.5× 10 ⁹	143.8		255
9	active lignin→Ychar+(1-Y)gas	7.7× 10 ⁶	111.4	0.75	-20
10	tar →gas	1.3× 10 ⁸	108		-42

*The char formation mass ratios.

Table 5-7: Kinetic constants for woody biomass pyrolysis

Kinetic Models	wood→gas	wood→oil	wood→char	oil→gas
	A(S ⁻¹), E(kJ/mol)	A(S ⁻¹), E(kJ/mol)	A(S ⁻¹), E(kJ/mol)	A(S ⁻¹), E(kJ/mol)
Wagennar et al.	1.4 $\times 10^{11} \exp(-\frac{177}{RT})$	9.28 $\times 10^9 \exp(-\frac{149}{RT})$	3.05 $\times 10^7 \exp(-\frac{125}{RT})$	4.0 $\times 10^4 \exp(-\frac{76.6}{RT})$
Font et al.	1.52 $\times 10^7 \exp(-\frac{139}{RT})$	5.85 $\times 10^6 \exp(-\frac{119}{RT})$	2.98 $\times 10^3 \exp(-\frac{73}{RT})$	4.0 $\times 10^4 \exp(-\frac{76.6}{RT})$
Di Blasi and Branca	4.4 $\times 10^9 \exp(-\frac{153}{RT})$	1.1 $\times 10^{10} \exp(-\frac{148}{RT})$	3.3 $\times 10^6 \exp(-\frac{112}{RT})$	4.0 $\times 10^4 \exp(-\frac{76.6}{RT})$

Table 5-8: Experimental conditions from literature for kinetic models used in this study

Model	Feedstock	Method of analysis	Sample load	Temperature range	Particle size
Wagennar et al.	Pine wood	TGA, Drop tube	-	553-873	100–125 μm
Chan et al.	wood	-	-	-	-
Di Blasi and Branca	Beech	Tube furnace	9 mg	573–708	< 80 μm
Font et al.	Almond shells	Pyroprobe 100	2 mg	733–878 K	300–500 μm
Miller et al.	Cellulose, hemicellulose, and lignin	-	-	500-1200 K	-

5.2.3. Solution Method

All heat and mass differential equations were discretized and solved using the forward Euler method in MATLAB 2014a. As outlined in Figure 5-4, the first step is to calculate initial estimate for vapour velocity. This value is required for equations 5-3 to 5-5:

$$Q_{out} = m_{in}(1 - yield_{char})\left(\frac{RT}{PM_{mix}}\right) \quad (5-13)$$

Where, Q_{out} (m³/s) is volumetric gas flow rate at the reactor exit, m_{in} (kg/s) is inlet feedstock mass flow rate, P (kPa) is pressure and M_{mix} (kg/kmol) is the average molecular weight in the gas stream. The average molecular weight of condensable gases including water vapour (25 wt%, experimentally measured) is calculated to be 50 kg/kmol by using data from Table 5-9 (extracted from a work conducted by Westerhof et al. [32] on pine wood pyrolysis at 460 °C in a fluidized bed reactor).

Table 5-9: Organic components of py-oil [32]

Groups of Components	Average Molecular weight (kg/kmol)	Mass fraction
formaldehyde, acetaldehyde	31.4	1.2
propionaldehyde, glycolic acid, glyoxal, acetone	65.4	0.9
methanol, 2-oxobutanoic acid, ethanol, MEK, 2-propanol, (5H)-furan-2-one	48.4	3.3
formic acid, hydroxyacetaldehyde, 5-hydroxymethylfurfural acetic acid, butanol, lactic	61.6	9.2
acid, 4-propylguaiaicol, propionic acid, acrylic acid, acetol	71.0	18.0
isobutyric acid, 2-hydroxy-2-cyclopentene-1-one,	105.8	2.9

2-hydroxy-1-methyl-1-cyclopentene-3-one, 1-hydroxy-2-butanone, furfural, methacrylic acid, <i>n</i> -butyric acid, coniferylaldehyde		
phenol, crotonic acid, valeric acid, 3-hydroxypropanoic acid, <i>o</i> -cresol, tiglic acid, 4-methylpentanoic acid, <i>p</i> -cresol, <i>m</i> -cresol, hexanoic acid, guaiacol, 4-hydroxybenzaldehyde, 4-methylguaiacol, vinylguaiacol	125.3	2.5
4-ethylguaiacol, 1,2-benzendiol, levulic acid, benzoic acid, eugenol, syringol, vanillin, isoeugenol (cis + trans)	150.9	2.4
levoglucosan, glucose, xylose, cellobiosan, hydroquinone, ...	160	17.3
some components in sugar constituent group	320	17.3
some components in low molecular mass lignin group	450	18
Some components in extractives group	460	3
some components in high molecular mass lignin group	1050	4

The average molecular weight of permanent gases, a mixture of CO₂ (33.14 mol. %), CO (35.79 mol. %), CH₄ (13.98 mol. %), and H₂ (17.5 mol. %), was approximated as 27 kg/kmol [33].

The average velocity requires an initial value for the yield of char, an initial “guess” based on experimental work is used. The calculated average velocity is used to solve the entire set of equations to determine the char and gas mass flow rates and velocities within each finite difference computational block. The calculated velocities are then compared to the previous set of predictions. The simulation is repeated until the velocities within each

computational block agree within 10^{-4} . The gas velocity is a function of the void fraction and the biomass conversion. According to ABRI-Tech Inc (developer of auger reactor used) the reactor void fraction is 50% for in the co-current auger reactor section (or first 0.33 m), 50% for the counter current section (0.20 m long) and 29% in the final 1.27 m.

Figure 5-5 outlines the solution algorithm.

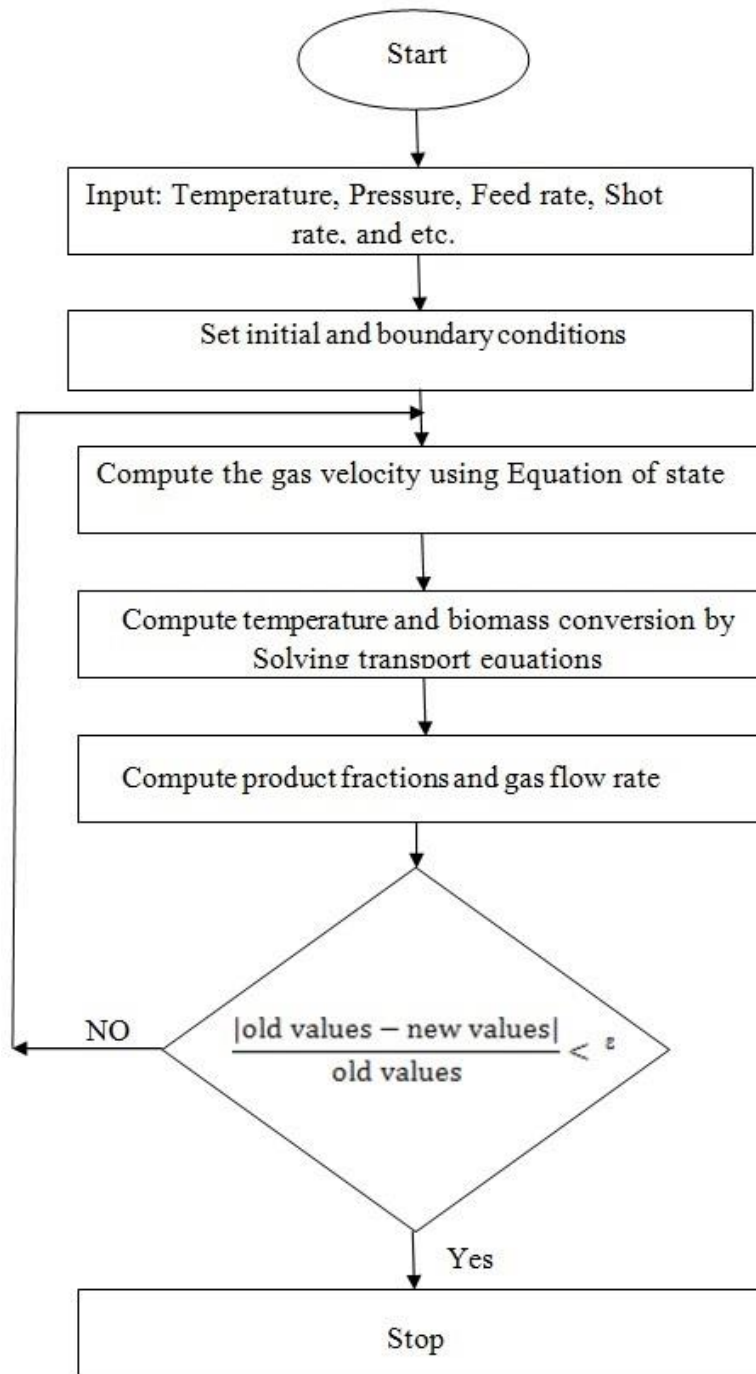


Figure 5-5: Auger reactor process model solution algorithm

5.3. Results and Discussion

5.3.1. Kinetic model selection

In order to select the optimum kinetic model for the reactor system in this study, different kinetic models were compared [9,15,29-31] with the experimental data at different temperatures (Figure 5-6 and 5-7). The results show that all kinetic models predict the trend of the impact of feed flow rate on py-oil yield; however, the Chan model [9] has the minimum Average Relative Deviation (ARD) from the experimental data (i.e. py-oil and bio-char); and therefore, was selected for further investigations. The other kinetic models did not fit well due to a number of variables including differences in feedstock type, heating rate, temperature range, and scale of reactor/system.

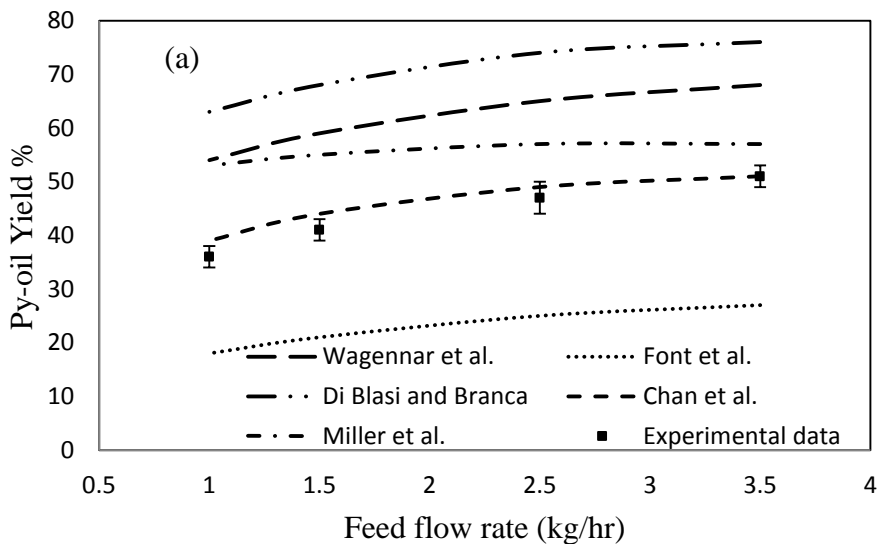


Figure 5-6: Comparison of kinetic models with experimental data at 450 °C

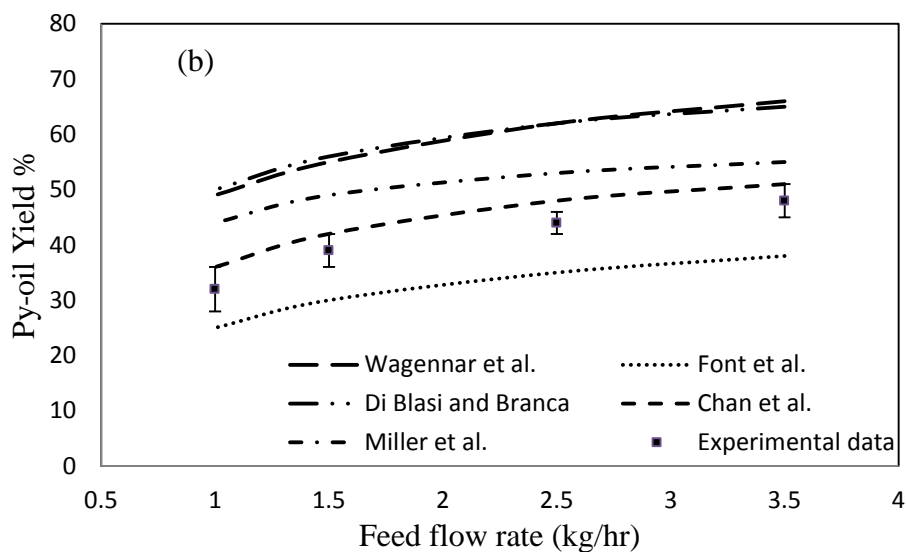


Figure 5-7: Comparison of kinetic models with experimental data at 500 °C

5.3.2. Model validation

Figure 5-8 is a parity plot of py-oil, and char yield at different temperatures (450-500 °C) and feed flow rates (1-3.5 kg/hr). Gas was not included in the figure as yield is calculated directly but by difference. The model predictions are in good agreement with the py-oil and char yield (~11% ARD). The validated model can now be used to study various operating conditions and model parameters.

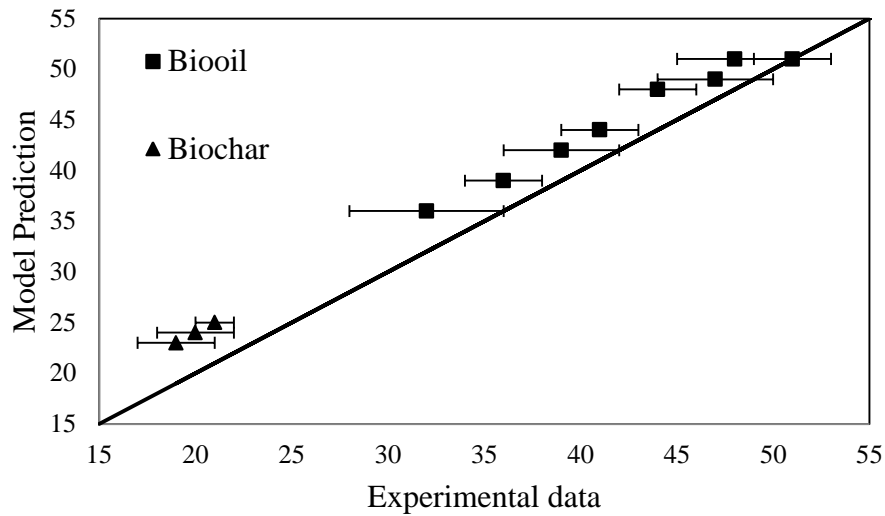


Figure 5-8: Validation of model with experimental data using yields of products (feed rates = 1-3.5 kg/h, temperatures = 450-500 °C)

5.3.3. Heat transfer

Figure 5-9 summarizes the impact of heat transfer. In these simulations, specific heat transfer mechanisms, conduction and radiation, were taken out of the process model to determine influence on the process. The results show that conduction and radiation have similar effect on particle heating at a reactor temperature of 450 °C. However, at 500 °C the role of radiation is more significant. As Figure 8 illustrates, the heat of reaction has a significant impact, particularly at 500 °C. It should be noted that the heat transfer equations can be neglected (i.e. assume the reactor system is isothermal) when using the Chan rate equations without any significant effect on product yields. When the Miller reaction rates are used, the impact of heat transfer on system temperature cannot be ignored (Table 5-10). The reason is that in the Miller model, intra-particle mass transfer

resistances were included in the analysis of chemical reaction rate, resulting in very high Arrhenius constants relative to the Chan model (Table 5-5 and 5-6). In this model, intra-particle mass/heat resistance are not included and therefore the overall rate of conversion is much faster. This is reflected in the residence times shown in Table 5-10.

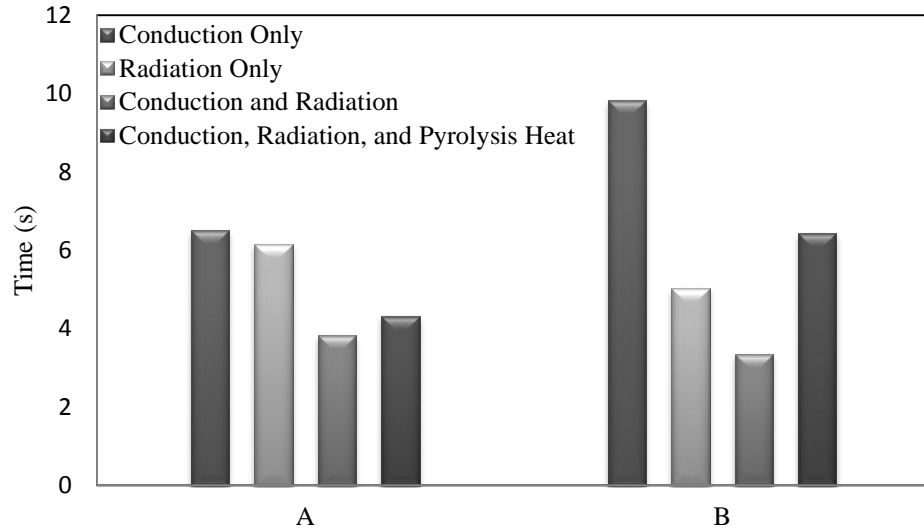


Figure 5-9: Residence time for biomass particles require to reach the pyrolysis temperature of 450 °C (A) and of 500 °C (B)

Table 5-10: Comparison between two kinetic models

Different Conditions	Miller model [15]		Chan model [9]	
	Py-oil yield	Conversion time (s)	Py-oil yield	Conversion time (s)
Heat equations included	57	1.3	51	60
Constant temperature	64	0.2	52	55

5.4. Parametric investigation

5.4.1. Feed flow rate

The feed flow rate controls the vapour residence time, a higher biomass mass flow rate will result in more vapour evolving from the reacting biomass. The mass of shot (and subsequent volume) is much greater than the biomass (~29:1 v/v) and therefore the increase in biomass, while increasing mass of gas produced, does not impact the space occupied by solids in the reactor. As such, the volume available for the vapour is constant while the vapour mass rate increases resulting in a decrease in vapour residence time. This is demonstrated in equation 5-13. As the mass flow rate of biomass increases the gas velocity increases (at constant pressure and temperature) and vapour residence time decreases.

There is a corresponding increase in py-oil yield (Figure 5-6 and 5-7) when the biomass mass feedrate increases. The longer residence time, provides more time for the secondary vapour cracking reactions. For instance, in the Morf model, the “oil” to “gas” reaction Arrhenius constant is half that of the primary wood to oil and char reactions while the activation energies are on the same order of magnitude. As such, these secondary reactions will be favoured at longer residence times. Based on the simulation results, the impact of decreasing vapour residence time from 28 seconds to 11 seconds leads to a py-oil yield increase from 36 % to 51 %. Ellens and Brown [34] also showed that at highest feed rate (2kg/h) in a free-fall reactor, the highest py-oil (71%) was obtained. They concluded that the higher feed rates led to a higher gas flow rates and consequently shorter times for gas–solid interaction; therefore, the py-oil yield increased.

5.4.2. Temperature

Figure 5-10 shows the effect of temperature on py-oil, bio-char and bio-gas yield. It is well known that py-oil yield is a function of temperature and vapour residence time [35-37]. As the vapour residence time is also a function of temperature, increasing temperature will increase the volumetric flow rate of the vapour (at constant pressure) and vapour residence time. Although a higher temperature results in a shorter vapour residence time, the higher temperature enhances secondary tar reactions, creating more noncondensables in the vapour. The vapour residence time reduces from 21 to 17 seconds as the temperature increases from 450 °C to 500 °C at 1.5 kg/h feed flow rate, however, the py-oil yield decreases from 44% to 42%. The results match with the work on fast pyrolysis as a function of temperature and vapours residence time conducted by Morgan et al [30].

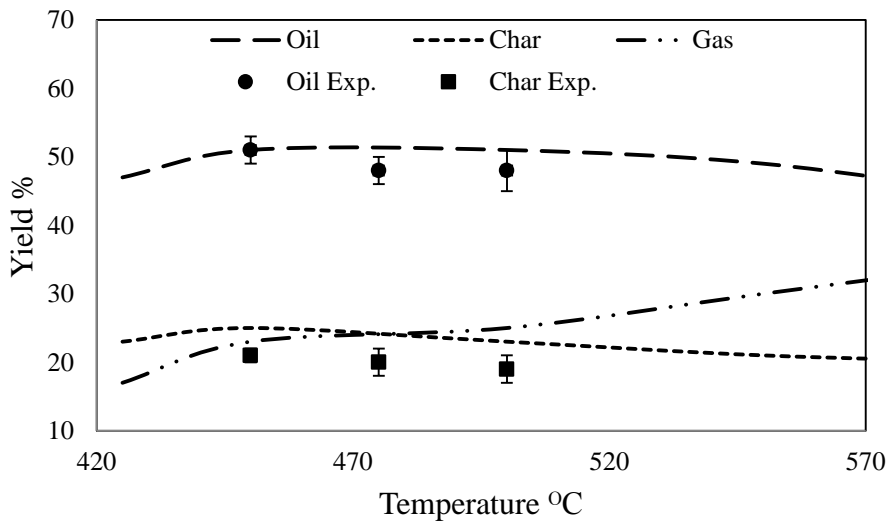


Figure 5-10: Py-oil and bio-char yield vs. temperature at 3.5 kg/h feed flow rate

5.4.3. Pressure

In addition to temperature and feed flow rate, the system pressure will also impact the vapour residence time and hence py-oil yield and quality for our system. The reactor operates under a slight vacuum, by adjusting the vacuum pressure, the pressure of the produced gas is changed. Figure 5-11 shows the predicted yields by the numerical simulation as the pressure of the system was increased from 5 kPa to 100 kPa. Atmospheric pressure (100 kPa) corresponds to 11 seconds vapour residence time while 5 kPa corresponds to one second at 450 °C and 3.5 kg/hr feed flow rate. Approximately 31% of the vapour is noncondensable for the 100 kPa case and 17% for the 5 kPa. It is worth mentioning that only one experimental data is added to Figure 5-11 to demonstrate fit, since we could not operate the reactor at lower pressures.

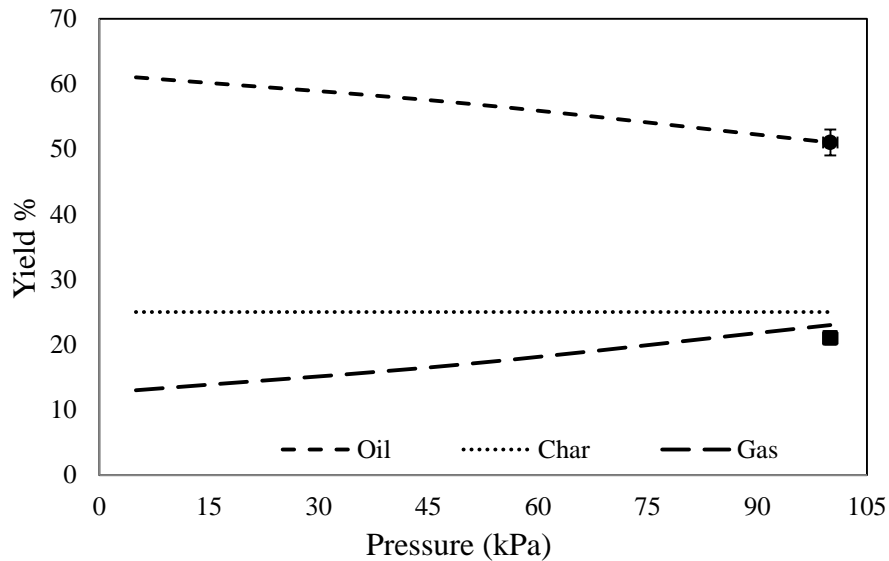


Figure 5-11: Py-oil (●) and bio-char (■) vs. reactor pressure at 450 °C temperature and 3.5 kg/h feed flow rate

5.5.Conclusion

A 2-4 kg/hr auger reactor with steel shot as heat carrier and no sweeping gas was modeled using a plug flow assumption for the both solid and gas streams. The comparison between different kinetic models with the experimental data indicate the model proposed by Chan (primary) coupled with Morf (secondary) better predicted the experimental data and was used in subsequent reactor analyses. The process model was validated with the experimental data at different temperatures and feedstock flow rates. The reactor operating conditions where varied within the model to determine impact on final py-oil yield. Increasing the feed flow rate from 1 to 3.5 kg/hr decreased the vapour residence time from 28 s to 11 s and consequently the py-oil yield increased from 39% to 51 %. That means a percentage of the total py-oil is “lost” as bio gas through cracking reactions. Py-oil yield increased from 51% to 61% by decreasing the produced gas pressure from 100 kPa to 5 kPa due to a reduction in the gas residence time. The results also showed that at temperatures higher than 450 °C the py-oil yield decreased as cracking reactions accelerated and the production of non-condensable gases increased. This modeling approach can now be used as a tool in scale up and optimization of the reactor. Further, the model can be sued for other types of feedstocks by modifying the kinetic model used.

Acknowledgment

This work has been supported by CFSI/ Department of Fisheries, Forestry and Agrifoods/ Government of Newfoundland and Labrador, BioFuelNet Canada, the Canadian Foundation for Innovation, the Natural Science and Engineering Research Council of Canada and Memorial University of Newfoundland. In addition, the authors would like to thank the valuable contribution of Dr. Peter Fransham from ABRI-Tech Inc.

5.6. References

- [1] Jahirul MI, Rasul MG, Chowdhury AA, Ashwath N. Biofuels production through biomass pyrolysis—a technological review. *Energies*. 2012 Nov 23;5(12):4952-5001.
- [2] Papari S, Hawboldt K. A review on the pyrolysis of woody biomass to py-oil: Focus on kinetic models. *Renewable and Sustainable Energy Reviews*. 2015 Dec 31;52:1580-95.
- [3] Venderbosch RH, Prins W. Fast pyrolysis technology development. *Biofuels, bioproducts and biorefining*. 2010 Mar 1;4(2):178-208.
- [4] Trendewicz A, Braun R, Dutta A, Ziegler J. One dimensional steady-state circulating fluidized-bed reactor model for biomass fast pyrolysis. *Fuel*. 2014 Oct 1;133:253-62.
- [5] Papadikis K, Gu S, Bridgwater AV, Gerhauser H. Application of CFD to model fast pyrolysis of biomass. *Fuel Processing Technology*. 2009 Apr 30;90(4):504-12.
- [6] Klose W, Wiest W. Experiments and mathematical modeling of maize pyrolysis in a rotary kiln. *Fuel*. 1999 Jan 31;78(1):65-72.
- [7] Bandyopadhyay S, Chowdhury R, Biswas GK. Transient behavior of a coconut shell pyrolyzer: a mathematical analysis. *Industrial & engineering chemistry research*. 1996 Oct 8;35(10):3347-55.
- [8] Ranzi E, Cuoci A, Faravelli T, Frassoldati A, Migliavacca G, Pierucci S, et al. Chemical kinetics of biomass pyrolysis. *Energy Fuels* 2008;22(6):4292–300.
- [9] Chan WC, Kelbon M, Krieger BB. Modelling and experimental verification of physical and chemical processes during pyrolysis of a large biomass particle. *Fuel*. 1985 Nov 30;64(11):1505-13.
- [10] Liden AG, Berruti F, Scott DS. A kinetic model for the production of liquids from the flash pyrolysis of biomass. *Chemical Engineering Communications*. 1988 Mar 1;65(1):207-21.
- [11] Di Blasi C. Analysis of convection and secondary reaction effects within porous solid fuels undergoing pyrolysis. *Combustion Science and Technology*. 1993 Apr 1;90(5-6):315-40.
- [12] Klose W, Wiest W. In: 23rd Biennial Conference on Carbon, 18–23 July 1997:62–3.
- [13] Bradbury AG, Sakai Y, Shafizadeh F. A kinetic model for pyrolysis of cellulose. *Journal of Applied Polymer Science*. 1979 Jun 1;23(11):3271-80.
- [14] Aramideh S, Xiong Q, Kong SC, Brown RC. Numerical simulation of biomass fast pyrolysis in an auger reactor. *Fuel*. 2015 Sep 15;156:234-42.

- [15] Miller RS, Bellan J. A generalized biomass pyrolysis model based on superimposed cellulose, hemicellulose and lignin kinetics. *Combustion science and technology*. 1997 Jul 1;126(1-6):97-137.
- [16] Zhang SY, Koubaa A. *Softwoods of Eastern Canada: Their silvics, characteristics, manufacturing and end-uses*. FPInnovations; 2008.
- [17] Nachenius RW, Van De Wardt TA, Ronsse F, Prins W. Residence time distributions of coarse biomass particles in a screw conveyor reactor. *Fuel Processing Technology*. 2015 Feb 28;130:87-95.
- [18] Tsai WR, Lin CI. On the mixing of granular materials in a screw feeder. *Powder technology*. 1994 Aug 31;80(2):119-26.
- [19] Outokumpu Stainless AB. *Handbook of Stainless Steel*. Avesta: Outokumpu Stainless AB. 2013.
- [20] Shen, K. C; Shields, J. A. *Waferboard from black spruce, balsam fir, and white birch grown in Newfoundland*. 1980. Forintek Canada Corp., Ottawa, Ontario.
- [21] Al-Haddad M, Rendek E, Corriou JP, Mauviel G. Biomass fast pyrolysis: experimental analysis and modeling approach†. *Energy & Fuels*. 2010 Mar 4;24(9):4689-92.
- [22] Anca-Couce A, Zobel N. Numerical analysis of a biomass pyrolysis particle model: Solution method optimized for the coupling to reactor models. *Fuel*. 2012 Jul 31;97:80-8.
- [23] Liang P, Wang Z, Bi J. Simulation of coal pyrolysis by solid heat carrier in a moving-bed pyrolyzer. *Fuel*. 2008 Apr 30;87(4):435-42.
- [24] Morf P, Hasler P, Nussbaumer T. Mechanisms and kinetics of homogeneous secondary reactions of tar from continuous pyrolysis of wood chips. *Fuel*. 2002 May 31;81(7):843-53.
- [25] Antal MJ. Effects of reactor severity on the gas-phase pyrolysis of cellulose- and kraft lignin-derived volatile matter. *Ind Eng Prod Res Dev* 1983;22:366–75.
- [26] Boroson ML, Howard JB, Longwell JP, Peters AW. Products yields and kinetics from the vapor phase cracking of wood pyrolysis tars. *AIChE J* 1989;35:120–8.
- [27] Cozzani V, Nicolella C, Petarca L, Rovatti M, Tognotti L. A fundamental study on conventional pyrolysis of a refuse-derived fuel. *Ind Eng Chem Res* 1995;34:2006–20.
- [28] Fagbemi L, Khezami L, Capart R. Pyrolysis products from different biomasses: application to the thermal cracking of tar. *Appl Energy* 2001;69:293–306.

- [29] Wagenaar BM, Prins W, Van Swaaij WP. Flash pyrolysis kinetics of pine wood. *Fuel processing technology*. 1993 Dec 1;36(1-3):291-8.
- [30] Font R, Marcilla A, Verdu E, Devesa J. Kinetics of the pyrolysis of almond shells and almond shells impregnated with cobalt dichloride in a fluidized bed reactor and in a pyroprobe 100. *Industrial & engineering chemistry research*. 1990 Sep;29(9):1846-55.
- [31] Di Blasi C, Branca C. Kinetics of primary product formation from wood pyrolysis. *Industrial & engineering chemistry research*. 2001 Nov 14;40(23):5547-56.
- [32] Westerhof RJ, Kuipers NJ, Kersten SR, van Swaaij WP. Controlling the water content of biomass fast pyrolysis oil. *Industrial & Engineering Chemistry Research*. 2007 Dec 19;46(26):9238-47.
- [33] Burhenne L, Damiani M, Aicher T. Effect of feedstock water content and pyrolysis temperature on the structure and reactivity of spruce wood char produced in fixed bed pyrolysis. *Fuel*. 2013 May 31;107:836-47.
- [34] Ellens CJ, Brown RC. Optimization of a free-fall reactor for the production of fast pyrolysis bio-oil. *Bioresource technology*. 2012 Jan 31;103(1):374-80.
- [35] Kim KH, Eom IY, Lee SM, Choi D, Yeo H, Choi IG, Choi JW. Investigation of physicochemical properties of biooils produced from yellow poplar wood (*Liriodendron tulipifera*) at various temperatures and residence times. *Journal of Analytical and Applied Pyrolysis*. 2011 Sep 30; 92(1):2-9.
- [36] Morgan TJ, Turn SQ, George A. Fast Pyrolysis Behavior of Banagrass as a Function of Temperature and Volatiles Residence Time in a Fluidized Bed Reactor. *PloS one*. 2015 Aug 26;10(8):e0136511.
- [37] Papari S, Hawboldt K, Helleur R. Pyrolysis: A Theoretical and Experimental Study on the Conversion of Softwood Sawmill Residues to Biooil. *Industrial & Engineering Chemistry Research*. 2015 Jan 12;54(2):605-11.

6.CHAPTER SIX

Optimization of an Auger Reactor for the Production of Py-oil from Sawmill Residues

This Chapter has been **published**. Papari S, Hawboldt KA, Helleur R. Production and Characterization of Pyrolysis Oil from Sawmill Residues in an Auger Reactor. Industrial & Engineering Chemistry Research. 2017 Feb 6.

Abstract

In the previous chapter, the process simulations indicated the impact of temperature and vapour residence time on py-oil yield in the auger reactor. In current chapter, in addition to oil yield, the physicochemical characteristic of py-oil as a function of operating conditions is investigated. The significant process variables of a pilot (2-4 kg/h) auger reactor (i.e. temperature, feed flow rate, and the vacuum fan speed) are investigated to optimize pyrolysis oil (py-oil) yield and properties. The auger reactor uses steel shot as a heat carrier to rapidly heat up fine grained biomass to convert the biomass to liquid (py-oil), solid (bio-char) and non-condensable gas. This reactor does not use inert carrier gas, and operates under a light vacuum to transport the resulting gases from the reactor into the condensation system. For the pyrolysis of softwood shavings, the optimum conditions are 450-475 °C temperature, a 4 kg/h feed flow rate, and a 2415 rpm vacuum fan speed producing an oil yield of 53%. The water content of the oil was minimized under these conditions to 24-26% and produced a single phase liquid. Hardwood sawdust (HW), Softwood shavings (SW), and Softwood Bark (SB) were pyrolyzed at these conditions to compare py-oil yield and chemical and physical characteristics, such as chemical composition, water content, total acid number (TAN), pH, density, viscosity, solids content and HHV. The results show that SW and HW produce a single phase oil, while SB oil separated into top (SBT) and bottom layer (SBB) phase. The highest HHV of 22.7 kJ/kg was measured in the SBB, while the highest TAN of 99 mg KOH/g occurred in the HW. The most abundant chemical components in py-oil identified by GC-MS are 4-propenylguaiacol for HW, 4-methylguaiacol for SW, levoglucosan for SBT,

and 4-propenylguaiacol for SBB. The results of this study are compared to the other auger reactors.

Keyword: Pyrolysis, Auger Reactor, Optimization, Phase Separation, Water Content

6.1. Introduction

Although there are many alternatives to fossil fuels, bio-based fuels are attractive due to the ability to be integrated into existing fuel transport and use infrastructure as stand-alone or in blends with petroleum based fuels. Pyrolysis is a thermochemical process performed in the absence of oxygen, fast pyrolysis of solid biomass is of particular interest as it produces a significant yield of a liquid that can be used as a fuel. Pyrolysis systems that are commercial or near to commercialization include VTT, Ensyn, BTG, and ABRI-Tech [1]. Reactors used in the pyrolysis process include augers, fluidized beds, fixed-beds, rotating cone reactors, and free fall reactors [2-5]. Many of these systems have been extensively investigated and reported in the literature; however, optimization studies of auger systems are rare [6-8]. Ingra et al. [6] investigated the physical and chemical properties of py-oil produced at 450 °C by fast pyrolysis in a continuous auger reactor, with mass yields of 48.7–55.2% for pine wood, 49.6–56.3% for oak wood, 42.8 – 44.2% for pine bark, and 43.8–49.8% for oak bark. Brown and Brown [7] produced 73% oil yield (the initial biomass moisture content was 5.84 %) using red oak wood at a heat carrier temperature at 600 °C, an auger speed of 63 rpm, and a heat carrier flow rate of 18 kg/h. Thangalazhy-Gopakumar et al. [8] investigated the effect of temperature on py-oil quality and quantity using pine wood as a feedstock in an auger reactor. The results showed that 450 °C produced the highest yield, and as temperature

increased from 425 to 500 °C phenols and derivatives increased in concentration, while that of guaiacol and its derivatives decreased. The guaiacol compounds are important from an oil upgrading perspective as these compounds are further cracked to phenols at higher temperatures, and phenol derivatives are easier to hydrogenate compared to the equivalent guaiacol derivatives [8]. The concentration of acetic acid remained constant, however the TAN (total acid number) of the oil decreased and pH increased with increasing temperature.

Auger reactors, are used at lab and commercial scale (Fransham, Pers comm). There has been virtually no systematic investigation of this style of fast pyrolysis system with continuous circulating steel shot as heat carrier and without carrier gas. This paper presents the results of a parametric study of the auger pyrolysis of forestry residues combined with characterization of py-oil using this reactor system. The optimization results could be used to compare other systems using similar or different types of pyrolysis reactors.

6.2. Experimental

6.2.1. Feedstock

Fresh balsam fir shavings (SW) were obtained from Sexton Lumber sawmill in Bloomfield, Newfoundland and Labrador, ash wood sawdust (HW) and softwood bark (SB) were obtained from ABRI-Tech Inc, Quebec. SW and HW were ground and sieved at 2 mm; however, bark was not ground, as the particles were fine enough. The feedstock was dried at 75 °C overnight to lower the moisture content to less than 2% .Table 6-1

summarizes the proximate analysis of SW,HW, and bark obtained by thermogravimetric analysis (TGA).

Table 6-1: Proximate analysis of hardwood, softwood, and softwood bark

Composition [wt. %]	SW	HW	Bark [9]
Low volatile matter	2.2	1.6	0.1
Medium volatile matter	80.8	80.4	70.2
Fixed carbon	16.8	17.5	27.0
Ash	0.2	0.5	2.7

6.2.2. Auger Reactor

The process flow diagram (PFD) of the auger reactor is outlined in Figure 1. The feeder is made up of two perpendicular augers (100 and 101) and a hopper. The biomass is fed into the hopper and the augers transfer the biomass at a desired rate into the reactor. The auger exit to the reactor (201) mixes the biomass with steel shot at a present temperature, and the woody biomass is rapidly converted into py-oil vapours, gas and char. A pressure gauge (P) measures the pressure of the gases inside the reactor.

The hot pyrolysis vapours exit the reactor and enter a cyclone (303) to remove fine char entrained in the gas stream. The solid particles drop to the bottom of the cyclone, while the pyrolysis vapours and gases leave the cyclone at the top connected to a water cooled shell and tube condenser (401) where the vapours are cooled to between 40-55 °C. The uncondensed gases are further cooled by a secondary water cooled condenser (402), with an exit temperature approximate to ambient temperature. An electrostatic precipitator (403) is located after the condensers to collect the remaining oil, which is not condensed in the primary and secondary condensers. The final py-oil product is a blend of the py-oil collected from the two condensers and the ESP. About 90 % of the py-oil is

collected in the first condenser, 8% in the second condenser and 2% in the electrostatic precipitator. The Vacuum Fan (404) maintains the slight vacuum pressure in the reactor and assists the flow of gas from the reactor through to the fan discharge to the outside atmosphere.

The bio-char and steel shot exit the reactor and are elevated by an auger (202). The steel shot acts as a ball mill and reduces the bio-char to a fine powder. At the top of the inclined auger (202) the char and shot are discharged into a separator where the fine char is stripped from the shot using recycle gas from a small fan (304). A cyclone (302) separates the char from the recycle gas and the char drops out into a container (305). The char fan speed is adjustable to ensure maximum collection of the fine char. Figure 6-2 is a schematic of the apparatus with the front of the oven removed. The oven is heated by two electric heating elements. An Opto 22 data acquisition system coupled to a laptop computer provides process control and data acquisition.

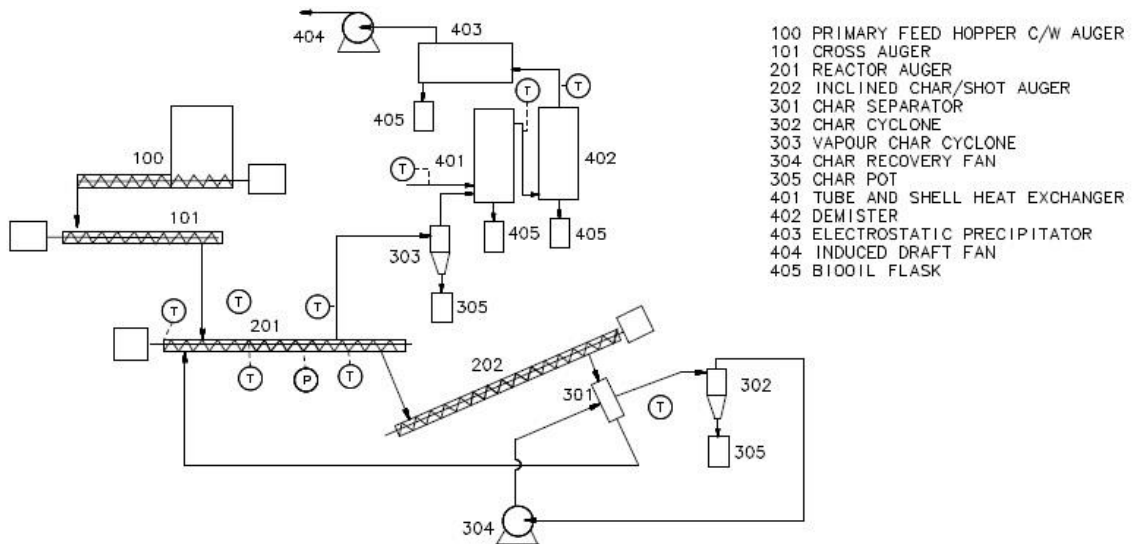


Figure 6-1: Process flow diagram for the auger reactor

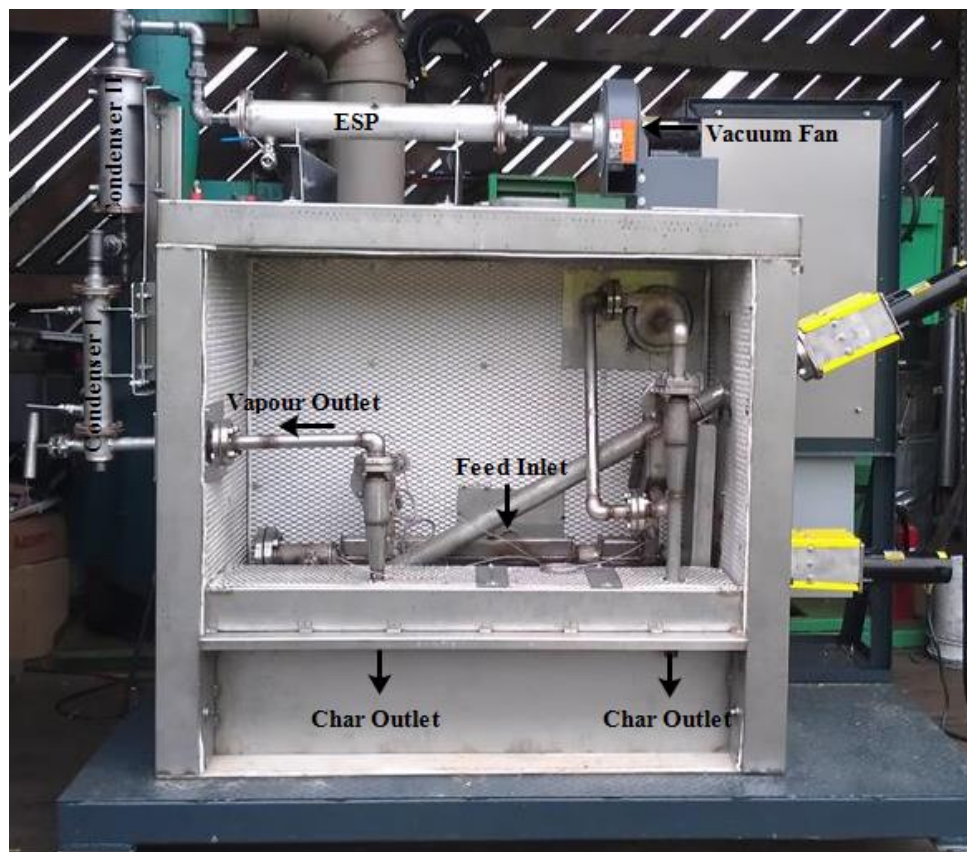


Figure 6-2: Photo (inside of the oven) of the auger pyrolysis system as built by ABRI-Tech Inc

6.2.3. Py-oil characterization testing protocols

The physicochemical py-oil properties were measured using the methods listed in Table 6-2.

Table 6-2: Methods for measuring physical and chemical properties of py-oil

Property	ASTM Method	Method of determination
Density	D4052	Digital Density Meter
Water Content	E203	Karl Fisher Titration
Viscosity	D4287	Rotational Viscometer
High Heating Value	D240	Bomb Calorimeter
Total Acid Number	D664	Potentiometric Titration
Solid Content	D7579	Sintered Glass Filter

6.3. Result and Discussion

6.3.1. Impact of reactor operating conditions on py-oil yield and quality

The impact of temperature, feed flow rate, and vacuum fan speed on py-oil yield, phase separation, and water content are investigated in a pilot 2-4 kg/h auger reactor with steel shot as heat carrier and without inert sweeping gas. The results of each operating parameter are summarized below. Pyrolysis runs on SW were performed in duplicate under each set of conditions for a total of 13 runs (Table 6-3)

6.3.1.1. Temperature

The py-oil mass yield for SW increases from 43% to 53% with temperature over the range of 400 °C to 450 °C (Table 6-3). However, at higher temperatures of 475 °C the yield slightly decreases. Cracking reactions are favoured at temperatures higher than 450 °C which increases gas and decreases oil yield. Low temperature (e.g. 400 °C) results in less py-oil production and simultaneously the bio-char formation is favoured due to nature of fast pyrolysis reactions [4]. The lowest water content in the resulting oils (24%)

is obtained at approximately 475 °C. The bio-char measurement is challenging as approximately 5% of char always remains in the system, recirculating (the 5% value was obtained by running the system with no feedstock for 12 h and collecting the char from the cyclones). If this approximation is included the bio-char yield is: 28% at 400 °C, 21% at 450 °C, 20% at 475 °C, and 19% at 500 °C.

Table 6-3: Impact of auger reactor parameters on py-oil yield and water content from SW

Run #	Temperature (°C)	Feed flow rate (kg/h)	Fan speed (rpm)	phase separation	Py-oil Yield	Top phase water content	Bottom phase water content	Average water content
1	400	4	2415	yes	43	54	18	51
2	450	1.5	2415	yes	41	51	24	41
3	450	2.5	2415	yes	47	46	22	38
4	450	3.5	2415	yes	51	-	-	-
5	450	4	2415	no	53	-	-	26
6	450	5	2415	no	50	-	-	25
7	450	7.5	2415	no	45	-	-	23
8	475	4	2415	no	50	-	-	24
9	500	1.5	2415	yes	39	53	22	46
10	500	2.5	2415	yes	44	49	28	40
11	500	4	2415	no	49	-	-	27
12	450	4	1725	no	51	-	-	27
13	450	4	3450	yes	44	46	23	41

6.3.1.2. Feed flow rate

As the feed flow rate is increased from 1 to 4 kg/hr the py-oil yield increases; and decreases after 4 kg/h as the design feed flow rate of the apparatus is exceeded, and the various operations (e.g. condensers etc.) cannot process the increased volumes. Higher feed flow rates produce more volatile vapour and therefore, at a constant temperature and pressure, the vapour volumetric flow rate increases. Higher gas flow rate results in shorter

vapour residence time, and a corresponding reduction in cracking reactions leading to higher py-oil yield. The increased vapour flow rates with feed rate were observed in the experiments. The reduction in cracking produces a py-oil with lower water content. The py-oil from lower feed flow rates showed two phases, an aqueous and “oil” distinct phases. Ellens and Brown [10] showed similar results in a free-fall reactor where the highest feed rate (2 kg/h) corresponded to the highest py-oil yield.

4.1.2. Vacuum fan speed

Vacuum fan speed impacts reactor pressure, that is a low vacuum corresponds to higher reactor pressure and consequently longer vapour residence time, since at constant reactor volume and temperature, reactor pressure correlates to gas residence time. Conversely, very high vacuum fan speed impacts the condensation system as vapours have a shorter residence time in system and therefore cannot capture all condensable gases. Table 3 summarizes the effect of the vacuum fan speed on py-oil yield. The difference in reactor pressure between 2415 rpm (corresponds to -200 Pa) and 1725 rpm (corresponds to -125 Pa) is minimal and therefore there is little impact on yield. However, at 3450 rpm (corresponds to -250 Pa), the py-oil yield drops. Although higher vacuum fan speeds correlated to shorter residence time, as mentioned above, the condensation system is not designed for these speeds.

6.3.1.3. Physical and Chemical py-oil properties

The physical and chemical properties including water content, TAN, pH, density, HHV, and viscosity are compared with the available results in the literature (Table 6-4). The oil and char yield from SW and HW are similar at the same conditions; however, bark py-oil

yields are lower overall and char yield is higher due to the lower volatile matter and the higher fixed carbon in feedstock bark compared to soft/hard wood (Table 6-1). SW and HW produce single phase oil at the optimum condition, while bark gives a two phase py-oil. The top phase of the bark oil contains 46 % water with a low HHV (8.3 kJ/kg), while the bottom layer has a low water content (20%) which contributes to greater HHV (22.7 kJ/kg). The higher water content of bark oil compared to wood oil decreases its average HHV. This result is in agreement with other studies of bark produces in a pilot-scale auger reactor [6]. Bark contains a higher lignin content compared to wood to produce less condensable vapours [11], and lower py-oil yield. Lower devolatilization of bark compared to wood results in a lower gas flow rate and subsequently a longer residence time and consequently vapours are converted to non-condensable gases and water through cracking reactions [6,12]. The lower py-oil yield from bark may be a presence of the ash resulting in greater cracking reactions [13] (Table 6-1). Oasmaa et al. [14] showed there is a decrease from over 65 wt.% py-oil yield to 55 wt.% as feedstock ash increases from less than 0.2 wt.% to 1 wt.% and then decreases less dramatically (from 55 wt.% to 45 wt.%) as the ash increases from 1-4 wt.%. The risk of phase separation of the oil begins with feedstock ash content of 1 wt.% and by approximately 2 wt.% there are two phases. The proposed reason for the decreased yield with ash increase is the catalytic effect of alkali metals which are present in much larger proportions in bark than in twigs, sawdust etc. [15].

Comparison of the py-oil properties and yield obtained from different auger reactors is challenging due to different feedstock and operating conditions. Table 6-4 illustrates woody biomass can produce 47-59 % py-oil yield in the lab/pilot-scale auger reactors. In

theory, decreasing the vapour residence time could further increase the oil yield. Water content is a key property in py-oil as impacts fuel properties and is a factor in corrosion etc. As Table 4 shows, the water content of py-oil obtained from different auger reactors ranges from 13% to 50%. A broad range of water produced by auger reactors can be the result of the differences in biomass initial moisture content, the volatile vapour residence time, and the nature of feedstock (e.g. cellulose, hemicellulose, lignin, and extractives content).

Table 6-4: Physicochemical properties of py-oil obtained from different auger reactors

	SW this work	HW this work	Bark (Sum of two phases) this work	Auger/pine wood [6]	Auger/oak wood [6]	Auger/Pine wood [16]	Auger/pine wood [17]	Auger/pine wood [8]	Auger/Japanese cedar [12]
Particle size	< 2 mm	< 2 mm	-	2 - 4 mm	2 - 4 mm	< 15 mm	1 mm	0.84 mm	< 0.71 mm
Moisture content	< 1 %	< 1 %	< 1 %	Dried	Dried	< 2%	< 1%	Dried	15.5
Temperature (°C)	450	450	460	450	450	450	500	450	450
Feed rate (kg/h)	4	4	4	1	1	N/A	0.3	< 1	0.3-0.4
Heat carrier	Steel shot	Steel shot	Steel shot	Not used	Not used	Hot sand	Hot sand	Hot sand	Not Used
Gas Carrier	Not Used	Not Used	Not Used	Not Used	Not Used	Nitrogen (5 L/min)	Nitrogen (2.5 L/min)	Nitrogen (N/A)	Nitrogen (2 L/min)
Oil Yield	53	55	39	49–55	50–56	47	59	50	54
Char Yield	21	22	30	17–20	17–20	27	16	26	35
Water	26	25	33	16	22	13	20	21	50

Content									
TAN (g KOH/g oil)	72	99	56	90	120	70	103	N/A	N/A
Solid Content	2.4	2.7	3.2	0.19	0.8	N/A	N/A	0.4	N/A
pH	2.9	3.1	4.1	3.1	3.1	2.9	N/A	2.2	2.1
Density (g/cm ³)	1.16	1.16	N/A	1.19	1.20	1.24	N/A	1.15	1.13
Viscosity Cp (20 °C)	36	38	N/A	N/A	N/A	N/A	N/A	33	N/A
HHV (kJ/kg)	16.7	17.6	15.8	21.9	18.7	22.4*	N/A	19.1	N/A

*Lower Heating Value (LHV)

Py-oil is a complex mixture of many components including acids, ketones, aldehydes, alcohols, aromatics, guaiacols, furans, phenols, hydrosugars and others [18]. Identifying all py-oil components is complex. The ten most abundant chemical compounds of py-oil samples (based in their relative peak area) identified by GC-MS are presented in Table 6-5. The results show that phenol derivatives (i.e. guaiacol, vanillin, vinylguaiacol, 4-methylguaiacol, allyl-guaiacol) are abundantly found in SW, HW, and bark oil. Phenolic compounds of py-oil are mostly exclusively produced from the thermal degradation of lignin [19]. Pyrolytic phenols are used as in “liquid smoke” food flavouring [20] and have antioxidant and antifungal properties [21,22]. They can also be used in making synthetic resins [23]. Levoglucosan is formed from cellulose depolymerisation reaction through transglycosylation [24] and is an important chemical used in food additive, antibiotic, pesticide, polymer, and surfactant [20]. Acetic acid, predominately responsible for the high acidity of py-oil [25] is chiefly produced through removal of acetyl groups in hemicelluloses [26]. Further degradation of levoglucosan can also produce acetic acid [27]. Biomass-derived aldehydes have a potential application as a renewable fuel in fuel cells. Furfural which has pharmaceutical application [18] is formed through further dehydration of cellulose and hemicellulose, and is a major pyrolysis product in bark py-oil. Coldfinger distillation is an efficient way to separate volatile components from py-oil.

Table 6-5: GC-MS results: most abundant components in py-oils obtained from soft/hard wood and bark

SW	*RPA %	HW	RPA %	SB Top	RPA %	SB Bottom	RPA %
4-Methylguaiacol	7.3	4-Propenylguaiacol	12.5	Levoglucosan	16	4-Propenylguaiacol	9.7
Guaiacol	4.9	4-Methylguaiacol	12.2	Acetol	6.1	4-Methylguaiacol	7.8
4-Propenylguaiacol	4.6	Guaiacol	9.8	4-Methyl-guaiacol	4.8	Guaiacol	6.6
Unknown	3.5	Levoglucosan	9.7	Guaiacol	4.4	Levoglucosan	6.6
Levoglucosan	2.7	Unknown	3.9	Acetic acid	3.6	Vinylguaiacol	6.1
Vanillin	2.6	Vanillin	3.8	Furfural	3.4	3-Methylcyclopentane-1,2-dione	3.6
4-Allyl-guaiacol	2.6	Vinylguaiacol	3.6	Unknown	3.2	Unknown	3.2

Unknown	2.5	5-Hydroxymethyl-2-furancarbaldehyde	3.5	Unknown	2.9	Acetol	2.9
3-Methylcyclopentane-1,2-dione	2.2	Unknown	3.2	4-Propenylguaiacol	2.9	Hydroxyacetaldehyde	2.8
5-Hydroxymethyl-2-furancarbaldehyde	2.1	Acetoguaiacone	1.8	3-Methylcyclopentane-1,2-dione	2.7	Furfural	2.7
Total of other GC peaks	65	Total of other GC peaks	36	Total of other GC peaks	50	Total of other GC peaks	48

*Relative Peak Area

6.4. Conclusion

In this study a series of pyrolysis experiments were performed to compare py-oil yields and properties under various operating conditions and using different types of forestry residues. The impact of feed flow rate (1 – 7.5 kg/h), temperature (400 - 500 °C), and vacuum fan speed (1725 to 3450 rpm) on the pyrolysis oil yield, water content, and phase separation were investigated. The optimum parameters were found to be 450-475 °C, 2415 rpm and 4 kg/h. Under these conditions, HW and SW produced a single phase oil with water content of approximately 25%, while bark oil showed phase separation with a 33% total water content. Volatile vapour residence time was varied by increasing feed flow rate from 1 to 4 kg/h; as such, the tar cracking reactions were minimized and subsequently the pyrolysis oil yield increased. While higher temperatures will favour higher yields over a range but this favours secondary reactions. Higher vacuum fan speed resulted in a shorter vapour residence time, and consequently higher pyrolysis oil yield; however, at maximum speed (3450 rpm) the pyrolysis oil yield dropped down. Short vapour residence time within the condensing system due to their high speed caused less capture of the condensable gases. As a result, 2415 rpm was optimum fan speed. HW had the highest pyrolysis oil yield, HHV, TAN, and viscosity, while bark had the lowest yield, HHV, and TAN. Bark produced a lower oil yield and a higher char yield due to a higher fixed carbon in raw bark compared to soft/hard wood. The GC-MS results indicated that 4-propenylguaiacol for HW, 4-methylguaiacol for SW, levoglucosan for SBT, and 4-propenylguaiacol for SBB are the most abundant components.

Acknowledgment

This work has been supported by CFSI/ Department of Fisheries, Forestry and Agrifoods/ Government of Newfoundland and Labrador, BioFuelNet Canada, the Canadian Foundation for Innovation, the Natural Science and Engineering Research Council of Canada and Memorial University of Newfoundland. In addition, the authors would like to thank the valuable contribution of Dr. Peter Fransham from ABRI-Tech Inc.

6.5. References

- [1] Wright L , Boundy B , Diegel S W, Davis S C. Biomass Energy Data Book, Edition 4.
- [2] Ngo, T-A., and J. Kim. "Fast Pyrolysis of Pine Wood Chip in a Free Fall Reactor: The Effect of Pyrolysis Temperature and Sweep Gas Flow Rate." *Energy Sources, Part A: Recovery, Utilization, and Environmental Effects* 36, no. 11 (2014): 1158-1165.
- [3] Jahirul, Mohammad I., Mohammad G. Rasul, Ashfaque Ahmed Chowdhury, and Nanjappa Ashwath. "Biofuels production through biomass pyrolysis—a technological review." *Energies* 5, no. 12 (2012): 4952-5001.
- [4] Papari S, Hawboldt K. A review on the pyrolysis of woody biomass to bio-oil: Focus on kinetic models. *Renewable and Sustainable Energy Reviews*. 2015 Dec 31;52:1580-95.
- [5] Papari S, Hawboldt K, Helleur R. Pyrolysis: a theoretical and experimental study on the conversion of softwood sawmill residues to biooil. *Industrial & Engineering Chemistry Research*. 2015 Jan 12;54(2):605-11.
- [6] Ingram, Leonard, Dinesh Mohan, Mark Bricka, Philip Steele, David Strobel, David Crocker, Brian Mitchell, Javeed Mohammad, Kelly Cantrell, and Charles U. Pittman Jr. "Pyrolysis of wood and bark in an auger reactor: physical properties and chemical analysis of the produced bio-oils." *Energy & Fuels* 22, no. 1 (2007): 614-625.
- [7] Brown, J. N., and R. C. Brown. "Process optimization of an auger pyrolyzer with heat carrier using response surface methodology." *Bioresource technology* 103, no. 1 (2012): 405-414.
- [8] Thangalazhy-Gopakumar, Suchithra, Sushil Adhikari, Harideepan Ravindran, Ram B. Gupta, Oladiran Fasina, Maobing Tu, and Sandun D. Fernando. "Physiochemical

properties of bio-oil produced at various temperatures from pine wood using an auger reactor." *Bioresource technology* 101, no. 21 (2010): 8389-8395.

[9] Ceballos DC, Hawboldt K, Helleur R. Effect of production conditions on self-heating propensity of torrefied sawmill residues. *Fuel*. 2015 Nov 15;160:227-37.

[10] Ellens CJ, Brown RC. Optimization of a free-fall reactor for the production of fast pyrolysis bio-oil. *Bioresource technology*. 2012 Jan 31;103(1):374-80.

[11] Mohan D, Pittman CU, Steele PH. Pyrolysis of wood/biomass for bio-oil: a critical review. *Energy & fuels*. 2006 May 17;20(3):848-89.

[12] Kato Y, Enomoto R, Akazawa M, Kojima Y. Characterization of Japanese cedar bio-oil produced using a bench-scale auger pyrolyzer. *SpringerPlus*. 2016 Apr 1;5(1):1.

[13] Lin F, Waters CL, Mallinson RG, Lobban LL, Bartley LE. Relationships between biomass composition and liquid products formed via pyrolysis. *Frontiers in Energy Research*. 2015 Oct 21;3:45.

[14] Oasmaa A, Sundqvist T, Kuoppala E, Garcia-Perez M, Solantausta Y, Lindfors C, Paasikallio V. Controlling the phase stability of biomass fast pyrolysis bio-oils. *Energy & Fuels*. 2015 Jun 17;29(7):4373-81.

[15] Wang L, Dibdiakova J. Characterization of ashes from different wood parts of Norway spruce tree. *Chemical Engineering Transactions*. 2014;37:37-42.

[16] Veses A, Aznar M, López JM, Callén MS, Murillo R, García T. Production of upgraded bio-oils by biomass catalytic pyrolysis in an auger reactor using low cost materials. *Fuel*. 2015 Feb 1;141:17-22.

[17] Yildiz G, Pronk M, Djokic M, van Geem KM, Ronsse F, Van Duren R, Prins W. Validation of a new set-up for continuous catalytic fast pyrolysis of biomass coupled with vapour phase upgrading. *Journal of Analytical and Applied Pyrolysis*. 2013 Sep 30;103:343-51.

[18] Alsbou EM. *Pyrolysis bio-oil as a renewable fuel and source of chemicals: its production, characterization and stability* (Doctoral dissertation, Memorial University of Newfoundland).

[19] Smith EA, Park S, Klein AT, Lee YJ. Bio-oil analysis using negative electrospray ionization: comparative study of high-resolution mass spectrometers and phenolic versus sugarcane components. *Energy & Fuels*. 2012 May 25;26(6):3796-802.

[20] Ortega JV, Renehan AM, Liberatore MW, Herring AM. Physical and chemical characteristics of aging pyrolysis oils produced from hardwood and softwood feedstocks. *Journal of Analytical and Applied Pyrolysis*. 2011 May 31;91(1):190-8.

- [21] Mohan D, Pittman CU, Steele PH. Pyrolysis of wood/biomass for bio-oil: a critical review. *Energy & fuels*. 2006 May 17;20(3):848-89.
- [22] Dobele G, Dizhbite T, Urbanovich I, Andersone A, Ponomarenko J, Telysheva G. Pyrolytic oil on the basis of wood and the antioxidant properties of its water-soluble and-insoluble fraction. *Journal of Analytical and Applied Pyrolysis*. 2009 May 31;85(1):81-6.
- [23] Nakai T, Kartal SN, Hata T, Imamura Y. Chemical characterization of pyrolysis liquids of wood-based composites and evaluation of their bio-efficiency. *Building and Environment*. 2007 Mar 31;42(3):1236-41.
- [24] Mullen CA, Boateng AA, Hicks KB, Goldberg NM, Moreau RA. Analysis and comparison of bio-oil produced by fast pyrolysis from three barley biomass/byproduct streams. *Energy & Fuels*. 2009 Nov 13;24(1):699-706.
- [25] Isahak WN, Hisham MW, Yarmo MA, Hin TY. A review on bio-oil production from biomass by using pyrolysis method. *Renewable and sustainable energy reviews*. 2012 Oct 31;16(8):5910-23.
- [26] Isahak WN, Hisham MW, Yarmo MA, Hin TY. A review on bio-oil production from biomass by using pyrolysis method. *Renewable and sustainable energy reviews*. 2012 Oct 31;16(8):5910-23.
- [27] Hu X, Wang Y, Mourant D, Gunawan R, Lievens C, Chaiwat W, Gholizadeh M, Wu L, Li X, Li CZ. Polymerization on heating up of bio-oil: A model compound study. *AIChE Journal*. 2013 Mar 1;59(3):888-900.

7. CHAPTER SEVEN

Summary and Recommendations for Future Work

Studies have that the yield and the quality of py-oil obtained from the pyrolysis of biomass can be a function of the biomass quality, the reactor operating conditions, the condensing system, and the catalyst utilization. This study focused on the impact of optimization of reactor operating conditions and feedstock properties on py-oil yield and properties. A lab-scale tube furnace reactor and a pilot 2-4 kg/h auger reactor were used to produce py-oil under different operating conditions. Several analytical techniques were employed to characterize the py-oil samples. In addition, a process model was developed for the auger reactor and used as a tool to investigate the impact of process variables on py-oil yield. This thesis was comprised of five sections: literature review (Chapter Two), optimization of the lab-scale reactor (Chapter Three), investigation on feedstock properties (Chapter Four), process modeling for auger reactor (Chapter Five), and evaluation of auger oil yield and properties (Chapter Six).

7.1. Literature Review

The objective of this initial phase of the thesis was to investigate the pyrolysis units, pyrolysis process modeling, kinetic models, and heat of pyrolysis in order to use this information further. The literature was reviewed to evaluate oil yield and properties (water content, TAN, HHV, Viscosity, pH, solid content, etc.) as a function of the type of pyrolysis units and their operating conditions. The results indicated that the pyrolysis reactors operating at high heating rate (> 100 °C/s), low vapour residence time (< 2 s), and temperature near 450-550 °C are in the favour of py-oil production. Low heating rate and high vapour residence time contribute to high bio-char and high permanent gas production, respectively. Modeling of commercial-scale pyrolysis reactor requires knowledge of the

reaction rates, either on a global or intrinsic level depending on the complexity of the reactions, as well as the mass and heat transfer rates. Different process models available in the literature were reviewed. The results showed that kinetic model with consideration of both primary and secondary reactions were mostly used to simulate the pyrolysis process in different reactors. The published reaction rate models and proposed mechanisms for the pyrolysis of woody biomass were compared with our experimental data obtained from the lab-scale reactor. The results showed that the competitive model (Chan et al. [1]) showed very good agreement for py-oil experimental data.

7.2. Lab-Scale Reactor

This phase of the study investigated the impact of pyrolysis process parameters and their interactions on py-oil and water content. As such, a series of lab-scale pyrolysis experiments on softwood shavings were carried out to determine the impact of temperature (impacts particle heating rate and secondary tar cracking), N₂ flow rate (impacts vapour residence time), and particle size (impacts intra particle heat/mass transfers) on py-oil yield and quality. The optimum conditions were found to be a 500-550 °C temperature, a 500 mL/min N₂ flow rate, and a 0.1-0.5 mm particle size. At such conditions, the vapour residence time was minimized and subsequently secondary tar cracking were minimized resulting in maximum oil (70 wt.%) yield . Furthermore, the higher carrier gas flow rates and smaller particle size resulted in a lower amount of water produced during pyrolysis. A comparison between the factor-based models with and without interactions indicated that the quadratic model with interactions better predicted the experimental data. However, for process models to be used in larger scale systems,

kinetic models are required. Two kinetic models were used; one was based on a primary reaction mechanism and the second based on both primary and secondary reaction mechanisms. The primary kinetic models are adequate for reactors operating at temperatures lower than 550 °C, while simultaneous primary and secondary reaction models should be used for temperatures higher than 550 °C.

7.3. Investigation on feedstock quality

The aim of this phase of study was to evaluate the py-oil yield and quality (water content, TAN, and HHV) as a function of feedstock particle size, feedstock moisture content, and feedstock age. The results illustrated that particles finer than 0.5 mm produced the highest py-oil yield (70 wt. %), lowest water content (25 wt.%) and lowest total acid number (70 mg KOH/g). A decrease in vapour-solid contact time as the result of particle size reduction resulted in a higher py-oil yield and a lower water content. HHV was independent of biomass particle size. The py-oil yield corrected for initial moisture (0.5 to 15%., showed no significant change on py-oil yield from However, yield dropped for feedstock with moisture content greater than 15%. A continuous reduction in py-oil HHV and TAN was observed due to an increase in py-oil water content. Furthermore, no significant impact on water produced during carbohydrate dehydration reactions was observed when increasing initial moisture content. The effect of biomass aging due to length of outside storage showed a slight reduction in py-oil yield and slight increase in water content with 4-5 year old feedstock compared to fresh feedstock. In addition, a qualitative assessment on pyrolysis heat of reaction showed an overall endothermic reaction for the woody biomass used in this study.

7.4. Process modeling for auger reactor

The objective of this phase of the study was to develop a process model for pyrolysis of woody biomass in auger reactor. This model can be used as a tool in process optimization and scale up. The model was developed based on plug flow manner for both solid and gas phases. The validation of model with the experimental data obtained from the 2-4 kg/h illustrated that the model can be used for the prediction of experimental data. The parametric investigation of the auger reactor showed a significant amount of volatile vapour was converted to permanent gases through secondary reactions at high volatile vapour residence time. For instance, the simulation results showed that an increase in the feed flow rate from 1 to 3.5 kg/h decreased the vapour residence time from 28 s to 11 s and consequently the py-oil yield increased from 39 wt.% to 51 wt.%. Py-oil yield increased from 51 wt.% to 61 wt.% by decreasing the produced gas pressure from 100 kPa to 5 kPa due to a reduction in the gas residence time from 11 s to < 2 s. The results also showed that at temperatures higher than 450 °C the py-oil yield decreased as cracking reactions accelerated and the production of non-condensable gases increased.

7.5. Evaluation of auger oil yield and properties

This phase of study focused on optimizing the auger reactor to produce the highest py-oil yield and quality; therefore, a series of pyrolysis experiments (i.e. temperature, feed flow rate, and vacuum fan speed) were performed in a 2-4 kg/h auger reactor to identify the impact of temperature, feed rate, and vacuum fan speed on py-oil yield, water content, and more importantly phase separation occurring in the collected py-oil. The results indicated that at the optimum conditions (450-475 °C, 4 kg/h, and 2415 rpm) the water

content of oil lowered to 24-26% with subsequent single-phase py-oil while producing the highest yield (50-53%). Bark as compared to soft/hard wood inherently showed oil phase separation and with lower yield (39%), lower TAN, the lowest HHV and highest water content (33%). Volatile vapour residence time was varied by increasing feed flow rate from 1 to 4 kg/h; as such, the tar cracking reactions were minimized and subsequently the py-oil yield increased. While higher temperatures will favour higher yields over a range but this favours secondary reactions. As such at temperature higher than 450 °C the oil yield decreases and the optimum yield was at 450 °C. Higher vacuum fan speed resulted in a shorter vapour residence time, and consequently higher py-oil yield; however, at maximum speed (3450 rpm) the py-oil yield dropped down. Short vapour residence time within the condensation system due to their high speed caused less capture of the condensable gases. Hardwood had the highest py-oil yield, HHV, TAN, and viscosity, while bark had the lowest yield, HHV, and TAN. Bark produced a lower oil yield and a higher char yield due to a higher fixed carbon in feedstock bark compared to soft/hard wood. The most abundant chemical components in py-oil identified by GC-MS were 4-methyl-guaiacol for softwood oil, 4-propenyl-guaiacol for hardwood oil, levoglucosan for softwood bark top phase, and 4-propenyl-guaiacol for bark oil bottom phase.

7.6.Recommendations for Future Work

The production of py-oil with high yield and good quality from sawmill residues was investigated in this study; however, further efforts are still required to minimize the secondary (eg., cracking) reactions, increase the particle heating rate, improve the condensing system, and decrease solid-vapour contact time in both lab-scale and auger reactor. The recommendations for future work based on the results of this thesis are summarized below:

- In Chapter Three, the optimum particle size, temperature, and feed flow rate were obtained according to series of lab-scale experiments in tube furnace reactor. The author suggests conducting a set of lab-scale experiments in two tube furnace reactors connected in series. At first, the biomass is fed to the first reactor which operates at a high temperature (e.g. 600 °C) for a few seconds, and then it is directed to the next reactor which operates at a lower temperature (e.g. 450 °C). The overall objective is to minimize the secondary reactions (in the second reactor) while the particle heating up is kept fast (in the first reactor). Generally, a high particle heating rate and a low vapour residence time are both in favour of py-oil production; however, in practice the high temperature attributing to the high particle heating rate accelerates the cracking reactions simultaneously. This might be helpful to increase py-oil yield and decrease water content.
- The literature study on the lab-scale pyrolysis reactors indicated that drop tube reactor gives a high py-oil yield with low water content due to a better heat/mass

transfer compared to fixed-bed reactor. As such, it is recommended to use drop furnace instead of tube furnace used in this study.

- Based on the current study and literature review, it was found that temperature, and vapour residence time significantly impact py-oil yield and water content. The author suggests to experimentally measure the gas residence time with high accuracy in the auger reactor. A CCD model based on temperature and residence time should be developed to demonstrate the impact of these significant parameters and their interactions on py-oil yield, compositions, and water content
- The impact of steel shot (heat carrier) to biomass ratio was investigated in Chapter Six. The steel shot fill level was kept constant and only feed flow rate was changed in this chapter. It is suggested for future work that the shot level should be varied as the different heat carrier loads result in various reactor void fractions and subsequently impact volatile gas velocities and/or gas residence time. Theoretically, greater amount of heat carrier leads to a higher gas velocity in the pyrolysis zone due to a smaller cross sectional area. It should be noted that at low shot:biomass ratios, the shot temperature should be checked, since if more biomass is injected into the shot then the shot has to have a hotter starting temperature to transfer the required energy otherwise the temperature will drop.
- While the reactor conditions are the main drivers in oil yield and quality, the condensers in the auger system can be modified in order to increase the volatile vapour residence time especially when vacuum fan speed is high. Therefore,

pyrolysis system handles higher gas flow rate and subsequently the vapour residence time decreases in pyrolysis zone which is in favour of py-oil production.

- The process model developed in this study was validated with experimental data obtained from the 2-4 kg/h auger reactor. This model can also be validated with experimental data from 1 ton/day auger reactor (ABRI-Tech Inc). The model was developed based on the assumption of plug flow for both gas and solid phases. The back mixing (axial dispersion) term also can be included in the model to better mimic the auger reactor behavior. Although the intra-particle mass/heat transfer resistances were ignored in the current model, they can be coupled with the reactor model in future work.
- Computational Fluid Dynamic (CFD) is usually used as a tool to solve the sophisticated transport equations. The author suggests applying CFD in order to predict temperature, velocity and conversion along the auger reactor.
- An elemental analysis should be utilized to experimentally measure the yield of non-condensable gases. The carbon content of biomass, bio-char, and py-oil can be measured by CHN/O analyzer and GC can be used to determine the non-condensable gases. The GC results can also help us to detect the possible missing volatile gasses in condensing system.
- Bark produces py-oil with two phases, a top phase which is watery and a bottom phase which is oily, while wood usually give only a single phase oil. Co-pyrolysis of wood and bark with different ratios would be an efficient way to produce a single phase oil from bark. The impact of different bark/wood mixing ratios on phase

separation could be an interesting topic in future work. Additionally, the effect of softwood age was investigated in Chapter Four. Bark has a different compositions compared to wood; therefor, the impact of aging on bark is a suggestion for future work.

- In addition to co-pyrolysis of different type of sawmill residues, co-pyrolysis of these residues with other waste materials (e.g. fish waste) could change/modify py-oil quality. This change might be in favour of better HHV for the fuel application py-oil.

References:

- [1] Chan W-CR, Kelbon M, Krieger BB. Modelling and experimental verification of physical and chemical processes during pyrolysis of a large biomass particle. *Fuel* 1985;64:1505–13. doi:10.1016/0016-2361(85)90364-3.

Appendix

Py-oil Procedures Manual

This Py-oil Procedure Manual has been accomplished through mutual collaboration of Mr. Shofiur Rahman, Mr. Peter Allan Chesley Benson, Mr. Leroy J Anderson, and myself (sadegh Papari).

Higher Heating Value (HHV)

Location: C3041; contact Nick Ryan

The data summary sheet which immediately follows the procedure can be used to record the data for this experiment.

Materials:

- Parr 1341 Plain Jacket Bomb Calorimeter
 - Parr 6775 Digital Thermometer
 - Parr 1108 Oxygen Bomb
 - Parr 2901EB Ignition Unit
 - Parr Nichrome Fuse Wire
 - Parr Gelatin Capsules
1. Cut approximately 10 cm of iron fuse wire from the card provided by Parr. Bring the piece of wire to an analytical balance. Measure and record its mass.
 2. Disassemble the oxygen bomb by unscrewing the threaded retaining ring on top of the bomb. Remove the electrode assembly from the top of the bomb and hang it in its specially designed holder. Remove the metal combustion capsule mounted in the ring electrode.
 3. Obtain a pellet of thermochemical standard benzoic acid (provided by Parr) and wipe it gently with a paper towel to remove any loose benzoic acid. Take the capsule and the pellet to an analytical balance. Place the empty capsule on the balance pan and tare (zero) the balance. Place the benzoic acid tablet in the capsule and record the mass.

4. Return to the bench and place the capsule containing the pellet back in the ring electrode. Raise the metal sleeve on the ring electrode to reveal a small hole. Place a few millimeters of the fuse wire through the hole and push the sleeve back down to clamp it in place. In the same fashion, clamp the other end of the fuse wire to the straight electrode.
5. Bend the fuse wire downward so that it presses against the top of the benzoic acid pellet, ensuring that no portion of the wire is touching the combustion capsule. Make sure that the pellet is in the center of the capsule and is not touching the walls.
6. Pipette 1.00 mL of distilled water into the stainless steel bomb. Carefully, so as to not disturb the pellet, lift the electrode assembly out of its holder and gently place it in the top of the bomb. Thread the retaining ring on the top so that the electrode assembly is held down tightly. The ring is tight enough when you reach a SOLID stop.
7. Carefully bring the assembled bomb to a compressed oxygen cylinder equipped with a filling regulator. Attach the oxygen filling fitting to the valve on top of the bomb by simply slipping the fitting over the valve. Ensure that the black knob on top of the filling regulator is closed and open the tank's main valve. SLOWLY open the black regulator knob and introduce 25-30 atm of oxygen into the bomb. IF A PRESSURE OF 35 atm IS EXCEEDED, THE GAS SHOULD BE VENTED AND THE BOMB FILLED AGAIN. Release the pressure in the line by pressing the black toggle switch down and remove the fitting from the top of the bomb.
8. Remove the shiny metal pail from the calorimeter's jacket and place it on a top loading balance. Zero the balance and carefully fill the pail with 2000.0 g of distilled

water that is slightly above room temperature. Do not splash any water out of the pail as precisely the same volume of water must be used for each run.

9. Place the pail back in the calorimeter jacket, ensuring that the pins in the bottom of the jacket fit into the indentations in the bottom of the bucket.

10. Insert the lifting handle into the two holes in the bomb's threaded retaining ring. Carefully lift the bomb and partially submerge it in the water in the pail. Holding the bomb with one hand, attach the ignition leads to the terminals on the top of the bomb and then completely lower it into the water, ensuring that it is centered on the raised circular area in the bottom of the pail.

11. Raise the calorimeter's lid assembly out of its holder and place it on top of the calorimeter. Rotate the large pulley on top of the lid to ensure that the stirrer turns freely. Attach the belt around the large pulley and the smaller shaft protruding out of the stirring motor. Turn the knob on top of the motor clockwise to begin stirring, and then turn on the thermometer using the switch located on the back of the unit. The thermometer has a built-in timer. After the stirrer has been running for 5 minutes you are ready to begin the run.

12. Switch the thermometer off and back on. Record the initial temperature to the nearest 0.001°C. Continue to record the temperature for 5 minutes, at one-minute intervals. Then, at the start of the 6th minute press and hold the grey button on the ignition unit for a few seconds. The red light should flash when the grey button is pressed.

If it does not then the circuit was broken before the run began and the run must be started over.

CAUTION: Do not have your head or hands over the calorimeter when firing the bomb, and continue to stand clear for 30 seconds after firing.

The temperature will begin to rise within 20 seconds of firing. The rise will be rapid at first, before slowing as the temperature approaches a stable maximum. Record the temperature at 45, 60, 75, 90 and 105 seconds after firing the bomb as precisely as possible.

****** If the temperature does not rise within 45 seconds of firing, the run must be discarded.

After the rapid rise period (8 minutes after firing), resume recording the temperature at one-minute intervals until the change between the successive readings has been constant for five minutes.

When data recording is finished, stop the stirrer motor. Remove the belt from the pulleys, lift the lid from the calorimeter and hang it back in its holder. Partially lift the bomb out of the bucket using the metal holder and remove the ignition leads. Dry the outside of the bomb with paper towels.

Slightly open the kurlled nut on the top of the bomb to release the gas pressure. When the hissing stops, unscrew the threaded retaining ring and lift the electrode assembly out of the bomb, hanging it in its special holder. Examine the combustion capsule and bomb

interior for evidence of incomplete combustion. If any is found, the run must be discarded.

Remove the two unburned pieces of fuse wire from the electrodes. Weigh them together on the same analytical balance used previously, and record the mass.

Pour the water out of the pail and thoroughly dry it, inside and out. Wash the bomb with soap and water. Rinse and dry it well. Be sure all other parts of the calorimeter are also dry.

Perform two additional runs. The first run uses an empty gelatin capsule (blank) and follows the same procedure. The second run uses a gelatin capsule filled with a py-oil sample. The procedure is the same as for the calibration run, except that a disposable Pasteur pipette is used to deposit approximately 0.1000 g of liquid oil or tar into the gelatin capsule before it is closed. The mass of the capsule and the sample is determined in the same way described for the calibration run in step 3.

Note: For the runs that use the gelatin capsules, the nichrome fuse wire must be threaded through the capsule before it is closed in order for combustion to occur.

Data Summary Sheet

Measurement or Calculation	Symbol	Value	Unit
Mass of Benzoic Acid Pellet or Gelatin Capsule	m_{BA}		g
Mass of Iron Fuse Wire	--		g
Mass of Uncombusted Wire	--		g
Mass of combusted wire	m_{wire}		g
Time of Firing	a		min
Time when temp reaches 60% of total rise	b		min

Time after combustion at which the rate of temperature change is constant	c	min
Temperature at time a	T_a	°C
Temperature at time b	T_b	°C
Temperature at time c	T_c	°C
Rate of temperature change before firing	r_1	°C/min
Rate of temperature change after time c	r_2	°C/min
Net corrected temperature rise	ΔT	°C

The molar enthalpy of combustion of benzoic acid at 25 °C and 1 atm is -3228.0 kJ/mol and the specific enthalpy of combustion of nichrome wire is -5.858 kJ/g.

Sample Calculations

Calibration Run

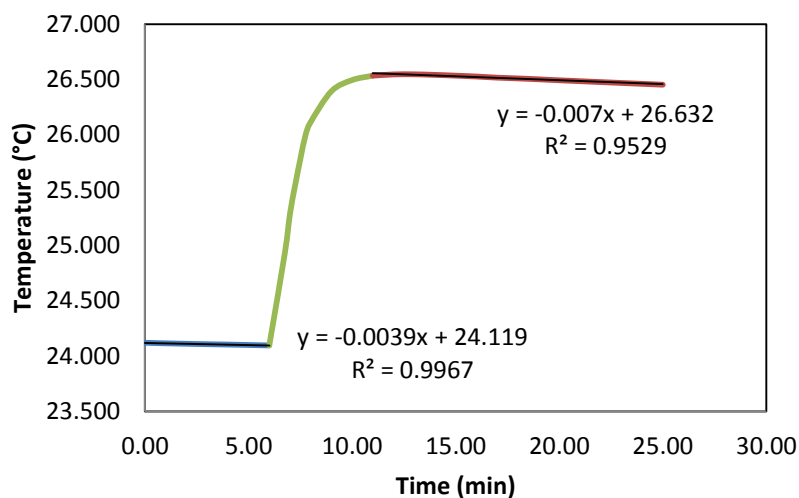
Time (min)	Temperature (°C)	Time (min)	Temperature (°C)	Time (min)	Temperature (°C)
0.00	24.120	9.00	26.393	22.00	26.476
1.00	24.115	10.00	26.494	23.00	26.468
2.00	24.111	11.00	26.534	24.00	26.460
3.00	24.107	12.00	26.545	25.00	26.452
4.00	24.104	13.00	26.546		
5.00	24.100	14.00	26.541		
6.00	24.096	15.00	26.534		
6.75	24.929	16.00	26.526		
7.00	25.286	17.00	26.516		
7.25	25.544	18.00	26.509		
7.50	25.780	19.00	26.501		

7.75	25.997	20.00	26.492
8.00	26.115	21.00	26.484

Measurement or Calculation	Symbol	Value	Unit
Mass of Benzoic Acid Pellet or Gelatin Capsule	m_{BA}	0.95829	g
Mass of combusted wire	m_{wire}	0.00778	g
Time of Firing	a	6	min
Time when temp reaches 60% of total rise	b	7.27	min
Time after combustion at which the rate of temperature change is constant	c	11	min
Temperature at time a	T_a	24.096	°C
Temperature at time b	T_b	25.559	°C
Temperature at time c	T_c	26.534	°C
Rate of temperature change before firing	r_1	-0.0039	°C/min
Rate of temperature change after time c	r_2	-0.007	°C/min
Net corrected temperature rise	ΔT	2.469	°C

Plot a graph of temperature versus elapsed time (in minutes). Perform regressions on the data collected before firing and after time c when the rate of the temperature change was constant. In Excel, to perform this regression on the graph (using the trendline function) you must add the data before firing and after time c in separate data series. The slopes of these two lines are r_1 and r_2 respectively. Draw the regression lines by hand or have Excel add the lines.

Temperature vs. Time
Calorimeter Calibration



Now determine the calorimeter's heat capacity, C_{cal} . To do this, first calculate the temperature at 60% of the total rise, T_b :

$$T_b = [0.60(T_c - T_a)] + T_a$$

$$T_b = [0.60(26.537 - 24.096)] + 24.096$$

$$T_b = 25.559 \text{ } ^\circ\text{C}$$

Calculate the time, b , corresponding to this temperature by linearly interpolating between the appropriate pair of successive readings at 45, 60, 75, 90 or 105 seconds. Convert b to units of minutes.

$$b = t_0 + (t_1 - t_0) \left(\frac{T - T_0}{T_1 - T_0} \right)$$

$$b = 7.25 + (7.50 - 7.25) \left(\frac{25.559 - 25.554}{25.780 - 25.554} \right)$$

$$b = 7.26 \text{ minutes}$$

Calculate the net corrected temperature rise, ΔT , using the following equation:

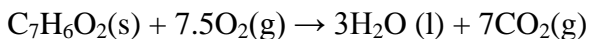
$$\Delta T_{\text{calorimeter}} = T_c - T_a - r_1(b - a) - r_2(c - b)$$

$$\Delta T_{\text{calorimeter}} = 26.534 - 26.534 - (-26.534) \times (7.27 - 6) - .27 - 647) \times (11 - 7.27)$$

$$\Delta T_{\text{calorimeter}} = 2.469 \text{ }^\circ\text{C}$$

The molar enthalpy of combustion of benzoic acid at 25 °C and 1 atm is -3228.0 kJ/mol and the specific enthalpy of combustion of nichrome wire is -5.858 kJ/g. For benzoic acid only, write the balanced combustion reaction equation, then calculate ΔU° using the following equation:

$$\Delta U = \Delta H - nRT$$



$$\Delta U_{BA} = -3228.0 \text{ kJ mol}^{-1} - (7 \text{ mol} - 7.5 \text{ mol})(8.3145 \times 10^{-3} \text{ kJ mol}^{-1} \text{K}^{-1})(297.246 \text{ K})$$

$$\Delta U_{BA} = -3226.8 \text{ kJ mol}^{-1}$$

For the nichrome wire, assume that $\Delta H^\circ = \Delta U^\circ$. Next, calculate the number of moles of benzoic acid using the mass of the pellet and its molar mass.

$$\text{moles}_{BA} = \frac{\text{mass}_{BA}(\text{g})}{\text{molar Mass}_{BA}(\text{gmol}^{-1})}$$

$$moles_{BA} = \frac{0.95829}{122.12}$$

$$moles_{BA} = 0.00785 \text{ mol}$$

Now calculate C_{cal} using the following equation:

$$C_{cal} = \frac{-[(n\Delta\bar{U})_{BA} + (m\Delta U)_{wire}]}{\Delta T}$$

$$C_{cal} = \frac{-[(0.00785 \times -3226.8)_{BA} + (0.00778 \times -5.858)_{wire}]}{2.469}$$

$$C_{cal} = 10.278 \text{ kJ}^\circ\text{C}^{-1}$$

Calculate ΔT for the gelatin capsule run in the same way as you calculated it for the calibration run (plotting a graph of T versus t). Then calculate ΔU_{gel} using the following equation:

$$\Delta U_{gel} = \frac{(C \cdot \Delta T)_{calorimeter} - (m \cdot \Delta U)_{wire}}{m_{gel}}$$

Calculate ΔT for the py-oil run in the same way as you calculated it for the calibration run (plotting a graph of T versus t). Then calculate ΔU_{oil} using the following equation:

$$\Delta U_{oil} = \frac{(C \cdot \Delta T)_{calorimeter} - (m \cdot \Delta U)_{wire} - (m \cdot \Delta U)_{cap}}{m_{oil}}$$

Water Content (Karl Fischer Coulometric Titration)

Location: C5009; contact Geraldine Kennedy. Maybe in C5016A during summer months (Helleur)

Add 100 mL of Hydranal to the beaker on top of the C30 titrator and turn it on. Make sure all openings are airtight to prevent air from interacting with the Hydranal solution. Log in with the username Eid, select the method saved with the ID “newM314”, and press start twice. The machine will then begin a pretitration.

Place a 20 mL glass scintillation vial on an analytical balance and tare (zero) the balance. Add approximately 0.1 g of py-oil to the vial, followed by approximately 3.9 g of methanol (a 40:1 ratio of methanol to py-oil). Record the exact masses used. Cap and shake the vial to ensure that the sample is well mixed.

Using an analytical balance, load approximately 3.0 g of the freshly prepared py-oil sample into the injection syringe and record the mass.

When pretitration is complete (the titrator is in standby mode), insert the needle through the rubber septum on top of the titrator. Press start sample and inject the sample into the beaker.

Weigh the empty syringe on the analytical balance, and determine by difference the amount of sample used. Enter this mass on the titrator and press OK.

The water content is recorded after the sudden drop and prior to the plateau of the graph (viewed on the titrator screen). This may take as long as 30 minutes and depends on how much water is present in the sample. This value is then used to calculate the water content of the py-oil sample.

Periodically run a blank by repeating steps 3 to 6 using only 3.0 g of pure methanol as the sample. This needs to be done only once a week (or each time the solvent is changed), and allows for the determination of the water content of the methanol used to dilute the py-oil.

Sample Calculations

Blank:

Parameter	Units	Equation	Symbol
Mass of Methanol	g	Recorded	A
Measured Mass of Water	g	Recorded	B
Mass of Water per g Methanol	None	B/A	C

Mass of Methanol (A): 3.2134 g

Mass of Water per g

Methanol (C):

Measured Mass of Water (B): 0.0021411 g

$$\frac{0.0021411\text{g}}{3.2134\text{g}} =$$

0.000666

Py-oil:

Parameter	Units	Equation	Symbol
Mass of Methanol	g	Recorded	D
Mass of Py-oil	g	Recorded	E
Total Sample Mass	g	D + E	F
Fraction of Methanol in Sample	None	D/F	G
Fraction of Py-oil in Sample	None	E/F	H
Mass of Sample Used	g	Recorded	I
Mass of Methanol Used	g	G × I	J
Mass of Py-oil Used	g	H × I	K

Measured Mass of Water	g	Recorded	L
Water due to Methanol	g	J × C	M
Water due to Py-oil	g	L-M	N
% Water Content of Py-oil	None	(N/K) × 100	O

Mass of Methanol (D): 3.9214 g

Total Sample Mass (F):

Mass of Py-oil (E): 0.1063 g

3.9214 g + 0.1063 g = 4.0277 g

Fraction of Methanol in Sample (G):

Fraction of Py-oil in Sample (H):

$$\frac{3.9214 \text{ g}}{4.0277 \text{ g}} = 0.973607766$$

$$\frac{0.1063 \text{ g}}{4.0277 \text{ g}} = 0.026392234$$

Mass of Sample Used (I): 3.1524 g

Mass of Methanol Used (J): $0.973607766 \times 3.1524 \text{ g} = 3.069201122 \text{ g}$

Mass of Py-oil Used (K): $0.026392234 \times 3.1524 \text{ g} = 0.083198878 \text{ g}$

Measured Mass of Water (L): 0.0341617 g

Water due to Methanol (M): $3.069201122 \text{ g} \times 0.000666 = 0.00204502 \text{ g}$

Water due to Py-oil (N): $0.0341617 \text{ g} - 0.00204502 \text{ g} = 0.03211668 \text{ g}$

% Water Content of Py-oil (O): $\frac{0.03211668 \text{ g}}{0.083198878 \text{ g}} \times 100 = 38.60229981 \% \cong 38.60 \%$

GC/MS

Location C5016A; contact R. Helleur

If the instrument is turned off, use the switch on the back right-hand side to power it on. If necessary, log on to the desktop computer that controls the GC/MS, with the password “040404”. Make sure the micro-furnace (attached vertically to the top of the GC injection port) is turned on, and that both the furnace and interface are set to 280°C. Use the



Windows 95-based laptop situated on the top of the GC for control.

Adjust the carrier gas (He) split flow rate to 60 mL/min (as close as possible). The rate is increased or decreased using the black knob labelled “total flow” on the left side of the instrument. The bubble flow meter attached

to the GC/MS is used to confirm the rate by squeezing the pipette bulb at the bottom to create bubbles and timing how fast they rise under the gas flow. It should take approximately 10 seconds for the bubble to move from the 1 mL line to the 10 mL line.

Select the software “MS Top” found on the desktop. In the main window click on “Methods” and select “Load and Run Method” from the drop down menu. Select the method saved as “1701-314.M” and click OK. The load method window will close and a second window will automatically open, titled “Start Run”.

Enter all of the necessary information, including:

Data File Name: C:\HPCHEM\1\DATA*File_Name.D*

Operator Name: *Your_Name*

Vial: 1

Sample Name: *Variable Field*

Misc Info: *Variable Field*

When all of the information has been entered, select “Run Method”. The information window will close and all of the parameters will automatically be uploaded to the main panel of the GC/MS. A new window titled “Acquisition – Prepare to Inject” will appear.

There is a black lab notebook located next to the computer labelled:

June 3, 2005

GC-MSD

Dr. Helleur’s Lab

LOG BOOK

Troubleshooting, Maintenance and Operation

Enter all of the necessary information in this book, including the date, file name, description of your sample, pyrolysis temperature/interface temperature, split flow and method. Now you are ready to prepare your sample.

Place a small metal sample cup on the micro-balance and zero it. Remove the cup and place it in its holder. Add approximately 0.75mg-1.00mg of py-oil to it using the tip of a

paper clip. Determine the exact mass of sample added using the micro-balance and record it. Return the cup to its holder and bring it to the GC/MS.

Located near the instrument is a removable plunger which is used to load the sample into



the external furnace at the top of the GC/MS. Fit the sample cup on to the hook at the bottom of the plunger by gently pressing the hook down into the cup.

Unscrew and remove the furnace cover and replace it with the plunger. The GC/MS will make a high-pitched beeping sound, which occurs when there is a leak and the pressure cannot be maintained inside the instrument. This is normal and should stop when the seal is restored.

NOTE: If the plunger is not screwed on properly, the frequency of the beeping will increase until the instrument shuts off automatically. This occurs to prevent damage to the column. If this occurs, check the seal then power off the GC/MS and power it back up again.

Loosen the screw on the side of the plunger, and leave it for approximately 10 seconds before tightening it again. This will flush the air out of the system with nitrogen, removing any oxygen that was trapped when the plunger was put in place. Again, you may hear the high-pitched beep, but it should stop when the screw is tightened.

Depress the plunger and turn to lock it. Press “Start” on the main GC/MS panel. The desktop screen will prompt you for a solvent delay. **DO NOT OVERRIDE THIS!** Your sample will run for about 47 minutes.

After the sample has finished running, lift the plunger, unscrew it and replace the cap.

The GC/MS can be purged by running a blank sample, but this is not always necessary

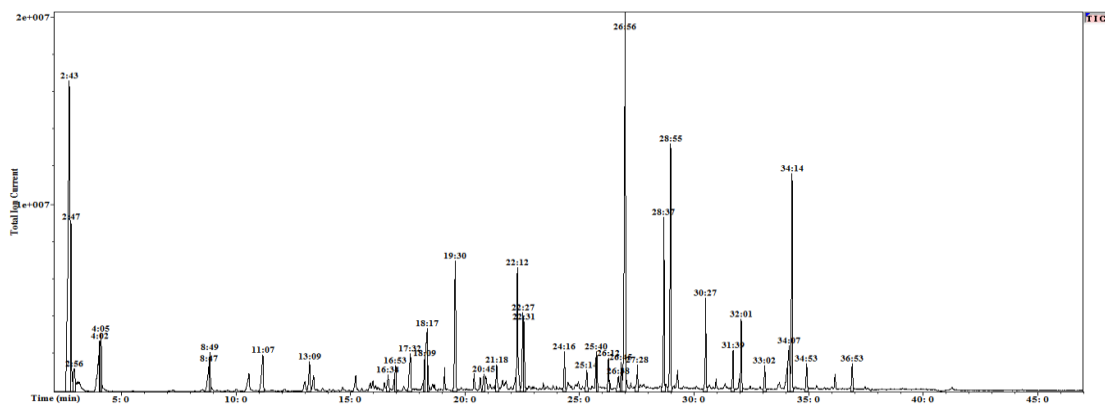
Data Work-Up

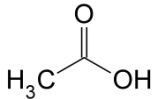
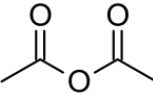
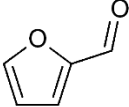
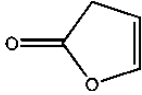
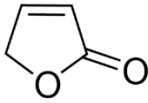
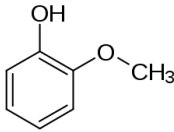
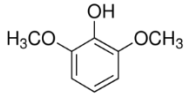
Each method will generate a MS file, *File_Name.D*, which may be found under the folder called “DATA” on the desktop. There is no integrated MS library, so you will need to use other software to properly analyze your data. The MS files can be transferred to a flash drive and opened on the Acer laptop which can be found opposite the GC/MS, on the other side of the lab bench. Data analysis is done as follows:

If necessary, log on to the “stand alone” laptop computer using the password “050505”.

Open the “wsearch32” software on the desktop. Click “File”, then “Open”, and select the appropriate MS file folder. The chromatogram will open in the main window.

Click “Chromatogram” and then “Auto Integrate”. The chromatogram should look similar to the one below.



2:42.88	Acetic Acid		43.5
4:4.91	Acetic Anhydride		14.8
11:6.38	Furfural		74.0
16:52.75	2(3H)-furanone		43.7
	2(5H)-furanone		42.0
19:29.39	2-methoxyphenol (Guaiacol)		70.9
26:55.30	2,6-dimethoxyphenol (Syringol)		79.6

Most light compounds will be acetals, furans and lactone-type compounds appearing in the first 12-15 minutes. Following this are phenolic compounds such as guaiacols and vanillin, usually around the 20 and 30 minute marks. The final compounds to elute will be the anhydro-saccharides and possibly hormone-steroidal compounds (the latter often varies depending on the amount of extractives present in the feedstock).

You must take the MS search results at “face value” as a significant number of matches will be wrong. Use common sense and use the literature on GC/MS of typical pyrolysis products to come to the right identification.

Dynamic Viscosity (units in cP)

Location: Bruneau centre; contact K. Hawboldt

Materials:

Brookfield DV-III ULTRA Programmable Rheometer

Eppendorf Pipette

Spindle Size #18

Set the temperature of the heater to 20°C and turn it on. Switch on the heating and cooling lines. Turn on the rheometer and use the “motor on/off” button to zero it. Once zeroed, any key – usually the “0” key – is used to start the rheometer.

An Eppendorf pipette set to a volume of 6.7 mL is used to sample the pyrolysis oil. Slowly fill the tip of the pipette, being careful not to suck the oil up into the filter. Discard the first aliquot and ensure that the walls of the tip are covered in oil, then refill it and use this as your sample.

Place the pyrolysis oil in the test cup and install it in the thermal jacket of the rheometer. Assemble the spindle and install it, using one hand to stabilize the pin of the motor, and the opposite hand to screw the spindle assembly in place.

Using the thermometer attached to the heater, ensure that the temperature of the py-oil in the test cup is uniformly 20°C.

Start the motor using the motor on/off key. The starting speed should be 10 rpm (rotations per minute). Record the readings for shear stress (D/cm^2), shear rate (1/sec), torque (%) and viscosity (cP).

Increase the speed in intervals of 10 rpm until a speed of 60 rpm is reached. Then, at 60 rpm, increase the speed in intervals of 20 rpm until a speed of 200 rpm is reached. Finally, increase the speed in intervals of 10 rpm until the maximum speed of the rheometer – 250 rpm – is reached. Record the four readings at each interval.

NOTE: For samples with a high viscosity, at lower temperatures (20°C and 40°C), the torque reading may eventually exceed 100%. When this occurs, an error message will be shown on the display, and then the run is over.

When the test is finished at 20°C, increase the heater temperature to 40°C. Repeat steps 2 to 6 and record all data. The same sample can be used again for this test.

When the test is finished at 40°C, increase the heater temperature to 60°C. A new sample must be used for this test. Discard the previously used oil, and use acetone to rinse the inside of the test cup and the surface of the spindle.

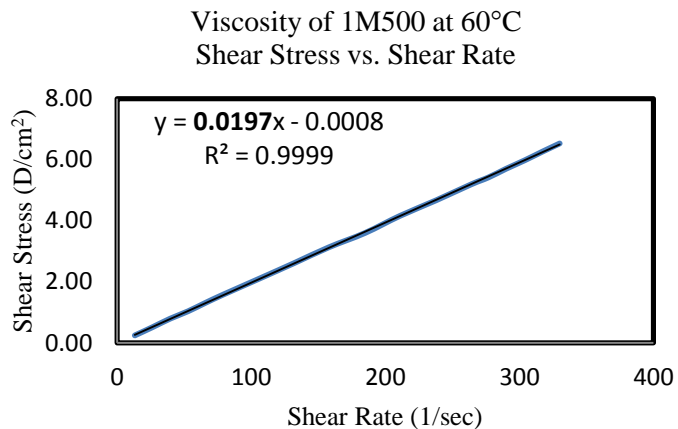
Sample Calculations

Rheometer Data: Viscosity of 1M500 at 60°C

rpm	Shear Stress (D/cm^2)	Shear Rate (1/sec)	Torque (%)	Viscosity (cP)
0	0.00	0.0	0.0	0.00

10	0.24	13.2	0.7	2.10
20	0.51	26.4	1.3	1.95
30	0.79	39.6	2.0	2.00
40	1.03	52.8	2.6	1.95
50	1.31	66.0	3.2	1.92
60	1.58	79.2	4.0	2.00
80	2.10	106	5.3	1.99
100	2.61	132	6.6	1.98
120	3.13	158	7.9	1.97
140	3.60	185	9.1	1.97
160	4.16	211	10.4	1.97
180	4.67	238	11.8	1.95
200	5.19	264	13.1	1.96
210	5.42	277	13.7	1.97
220	5.70	290	14.5	1.96
230	5.98	304	15.1	1.97
240	6.26	317	15.9	1.99
250	6.53	330	16.5	1.98

Plot shear stress (in D/cm^2) as a function of shear rate (1/sec). Perform a linear fit on the data and display the equation on the graph. This equation will be in $y = mx + b$ form, and the slope (m) of the data is the viscosity, given in poise (P). Multiply this value by 100 to get the viscosity in centipoise (cP).



Percent Suspended Solids (Bio-char) in Py-Oil

Can be done in the lab with a water aspirator and the necessary equipment. Helleur's lab is equipped.

Materials:

500 mL Suction Flask

Sintered Glass Crucible Filter

Rubber Adapter

Ring Stand

Thick Rubber Tubing

Clamp

Vacuum (Water aspirator works)

Glass Stirring Rod

Dry a clean sintered glass crucible in an oven – set at approximately 85-90°C – for one hour. Cool the crucible to room temperature in a desiccator, and then weigh it using an analytical balance. Record the mass to the nearest 0.1 mg.

Place a 20 mL glass scintillation vial on an analytical balance and tare (zero) the balance. Using a disposable pipette, weigh approximately 3.0 g of py-oil into the vial. Record the weight to the nearest 0.1 mg.

Add approximately 3.0 g of methanol to the vial. Cap the vial and shake the mixture vigorously to dissolve the py-oil in the solvent.

Clamp and secure the neck of the suction flask to the ring stand. Connect the side arm of the flask to the side arm of the aspirator using the thick rubber tubing. Place the rubber

adapter which holds the crucible in the top of the flask, ensuring that the joint is air tight. Turn on the water aspirator and place a hand over the top of the crucible to ensure that the system produces the necessary suction.

Slowly pour the py-oil/methanol mixture using a glass stirring rod to direct the solution and solids to the center of the crucible. When there is no more liquid in the vial, wash it thoroughly with a small amount of methanol and return the contents to the crucible. Wash the filtrand (solids/bio-char) with methanol until the filtrate runs clear.

Ensure that the edges of the crucible are clean of any pyrolysis solids. If needed, rinse any remaining solids onto the bottom of the crucible with methanol, ensuring that no sample is lost.

Turn off the aspirator, releasing the vacuum. Remove the crucible from the top of the suction flask and place it in the oven at 85-90°C for one hour.

Remove the crucible from the oven and cool to room temperature in a desiccator. Using an analytical balance, weigh the crucible and record the stabilized weight to the nearest 0.1 mg.

Repeat steps 1 to 8, obtaining duplicate results. Take the average of the two trials as the final result.

Sample Calculations:

The suspended solid content of the py-oil sample is calculated by dividing the mass of the solids retained in the crucible by the mass of the original py-oil sample used, and multiplying that value by 100%. The following equation may be used:

$$\text{Suspended solids (wt \%)} = \frac{m_s}{m_o} \times 100\%$$

where suspended solids is the solid content of the oil (wt %), m_s is the mass of the solids retained in the crucible and m_o is the mass of the original py-oil sample used. Each sample is run in duplicate, and the average of the two trials is accepted as the final result.

For example, the sample “Maple 470°C – Nov 2014” gave the following results:

Run #1:

mass of py-oil used: 1.0800 g

mass of empty crucible: 32.1315 g

mass of crucible and solids: 32.1461 g

mass of solids retained in crucible = mass of crucible and solids – mass of empty crucible

$$= 32.1461 \text{ g} - 32.1315 \text{ g}$$

$$= 0.0146 \text{ g}$$

$$\text{Suspended solids (wt \%)} = \frac{m_s}{m_o} \times 100\%$$

$$= \frac{0.0146 \text{ g}}{1.0800 \text{ g}} \times 100\%$$

$$= 1.351 \%$$

Run #2:

mass of py-oil used: 1.0327 g

mass of empty crucible: 31.3234 g

mass of crucible and solids: 31.3315 g

mass of solids retained in crucible = mass of crucible and solids – mass of empty crucible

$$= 31.3339 \text{ g} - 31.3234 \text{ g}$$

$$= 0.0105 \text{ g}$$

$$\text{Suspended solids (wt \%)} = \frac{m_s}{m_o} \times 100\%$$

$$= \frac{0.0105 \text{ g}}{1.0327 \text{ g}} \times 100 = 1.016 \%$$

$$\text{Average} = \frac{1.351 + 1.016}{2} = 1.1835 \% \approx 1.18 \%$$

Acidity (Total Acid Number)

Can be performed in any chemistry/process Eng. Lab with a meter and probe and in C5016 (Helleur).

Materials:

Two pH standards	pH/Voltmeter with probe	Dry Methanol
0.1000 M NaOH Solution	50 mL Burette	100 mL Beaker

Ring stand with 2 clamps

Stir plate

py-oil Sample

Stir bar

Calibrate the voltmeter using two standards of known pH. Clean all glassware with deionized water and acetone to remove any contaminants.

In a 100 mL beaker, combine 3.0 g of py-oil (record exact mass used) and 20 mL of dry methanol. Place a stir bar in the beaker, and position it on the stir plate. Set the stirrer to the lowest rpm, and leave the solution for about a minute to ensure good mixing.

Fill the burette with 0.1000 M NaOH solution, and clamp it over the beaker. Place the probe in the solution and clamp it in a position such that the tip of the probe is completely submerged, but is not in contact with the stir bar or the beaker.

Switch the voltmeter to mV, and record the initial voltage reading (we can easily use the pH reading as well).

Slowly add the NaOH solution from the burette to the beaker in 1 mL intervals. Record the reading from the voltmeter at each interval, and continue until the voltage is past the negative value of the original reading on the voltmeter (see Figure 1 below)

Sample Calculations:

Plot voltage measured (in mV) as a function of the volume of base used (in mL). The derivative of each point is calculated using the slope of this function, and is plotted on the

same axis. The volume of base on the derivative graph at which the voltage value is at its highest point is used to calculate the total acid number – mL NaOH/g – using the equation below.

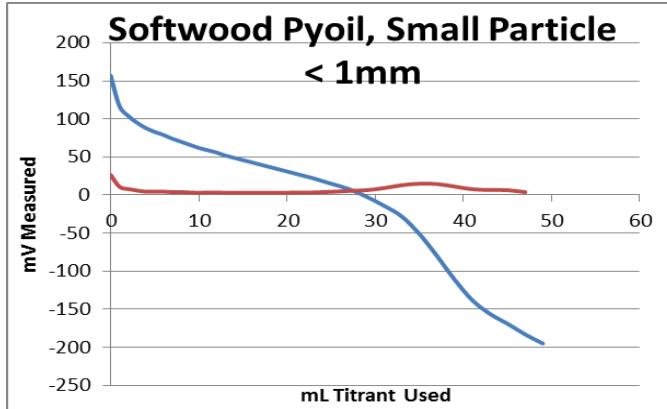


Figure 1: V vs mL of base used to titrate acid

Total Acid Number =

$$\frac{0.1 \times \text{mL Base Used}}{\text{Mass of Py - Oil}} \times 56.1$$

For example, the volume used for the calculation of the total acid number from Figure 1 is 37.0 mL.

$$\frac{0.1 \times 37.0 \text{ mL}}{3.002 \text{ g}} \times 56.1 = 69.14$$